Coordination Chemistry Reviews, 50 (1983) 109–208
Elsevier Science Publishers B.V., Amsterdam – Printed in The Netherlands

RHODIUM(II) CARBOXYLATES

ESTHER B. BOYAR and STEPHEN D. ROBINSON
Department of Chemistry, King's College, London WC2R 2LS (Gt. Britain)
(Received 18 August 1982)

CONTENTS

A. INTRODUCTION

A large number of binuclear coordination compounds of the platinum metals containing metal–metal bonds have been prepared in recent years, opening up the chemistry of new oxidation states including Ru(I), Os(I), Rh(II) and Pt(III); none is more important or has been more thoroughly investigated than the rhodium(II) carboxylates. The first reported binuclear rhodium compound containing four bridging carboxylate groups was synthe-

0010-8545/83/$30.00

sised in 1960 by Chernyaev and co-workers [1] who heated chlororhodic acid in formic acid. The compound was initially formulated as a rhodium(I) species $H[Rh(O_2CH)_2 \cdot 0.5H_2O]$ but was quickly shown to lack acid character [2]. X-ray diffraction studies on the analogous acetato compound of rhodium [3] indicated a dimeric "lantern" structure $[Rh_2(O_2CMe)_4(H_2O)_2]$ possessing a metal–metal bond [4] (Fig. 1) (M = Rh). Antsyskina subsequently showed the formato complex to possess a polymeric structure based on linked hydrated and anhydrous lantern units $\langle[Rh(O_2CH)_2 \cdot H_2O]_2[Rh(O_2CH)_2]_2\rangle_\infty$ [5], Fig. 2. The lantern structure which had previously been established for $[Cr_2(O_2CMe)_4(H_2O)_2]$ [6] and $[Cu_2(O_2CMe)_4 \cdot (H_2O)_2]$ [7] is now known to occur widely in the chemistry of transition metal complexes containing carboxylate anions and related bridging ligands. Rhodium(II) carboxylates of ca. 25 different carboxylic acids have been prepared. The compounds are very stable, but react with a wide variety of neutral ligands (L) or anions (X^-) to form adducts $[Rh_2(O_2CR)_4L_n]$ and salts $M^I_n[Rh_2(O_2CR)_4X_n]$ ($n = 1, 2$; M = alkali metal or protonated N-base) respectively, displaying varied and often brilliant colours. The bonds formed

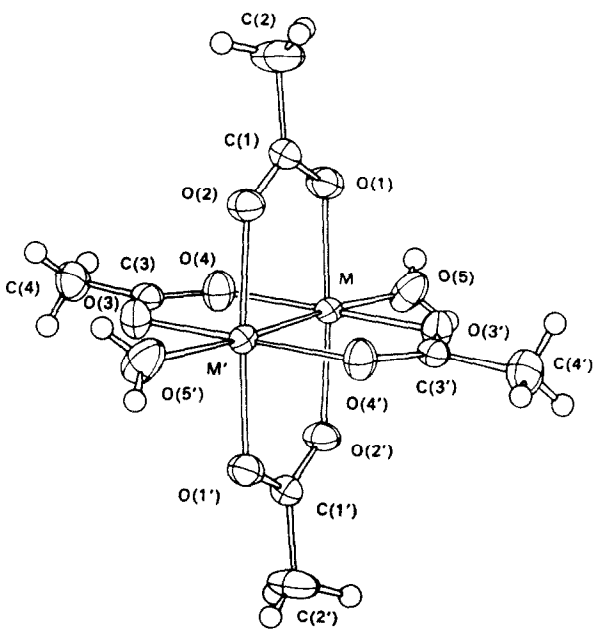

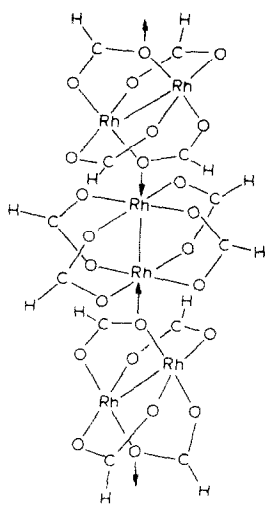

Fig. 1. The molecular structure of $Rh_2(O_2CMe)_4 \cdot 2H_2O$, $Cr_2(O_2CMe)_4 \cdot 2H_2O$ and $Cu_2(O_2CMe)_4 \cdot 2H_2O$ (with permission from ref. 11).

Fig. 2. $\langle[Rh(O_2CH)_2H_2O]_2[Rh(O_2CH)_2]_2\rangle_\infty$. This structure has only been reported in outline (Porai-Koshits et al., Coord. Chem. Rev., 17 (1975) 1). (H_2O ligands omitted.)

by the axial ligands with rhodium in the dimeric carboxylates are weak compared with Rh–L or Rh–X bonds in mononuclear complexes and this has been attributed to the *trans*-influence of the covalent Rh–Rh σ bond [8]. The diamagnetic character of these rhodium(II) (d^7) complexes is attributed to the presence of a metal–metal bond, however the nature of this bond has been the subject of much controversy [9,10]. The initial report on the crystal structure of $[Rh_2(O_2CMe)_4(H_2O)_2]$ gave a Rh–Rh distance of 2.45 Å and contained the proposal that a Rh–Rh single bond was present [4]. Cotton et al. performed more accurate X-ray crystallographic measurements and suggested that the short Rh–Rh distance (2.386(1) Å), which is considerably less than expected for a Rh–Rh single bond (2.7–2.8 Å) indicated the presence of a Rh≡Rh triple bond [11,12]. Theoretical calculations supported by electronic spectra and ESR data indicate a Rh–Rh single bond, but the shortness of the bond has still not been adequately explained [8]. Opposing views concerning the nature of the rhodium–axial ligand bonds remain unresolved.

The interest in rhodium(II) carboxylates has been maintained in recent years by their potential practical applications. In 1972 Bear and co-workers discovered the activity of rhodium(II) carboxylates as anti-tumour agents [13]. In vivo studies have shown that the rhodium(II) carboxylates are able to inhibit certain biological processes, in particular the cellular synthesis of DNA [14,15]. Rhodium(II) carboxylates are also used as catalysts in organic synthesis; examples include the homogeneous hydrogenation of alkenes [16] and the cyclopropanation of alkenes with alkyl diazoacetates [17].

Rhodium(II) carboxylates have been reviewed briefly [18–20] and have been discussed in general articles on platinum metal carboxylato complexes [21], metal carboxylates [22–24] and inorganic trifluoroacetates [25], however no attempt has been made to correlate the considerable amount of data which has been reported in the past two decades concerning their physical and chemical properties and their uses. This article will attempt to remedy this deficiency. *

B. SYNTHESIS

Rhodium(II) formate was originally synthesised by heating chlororhodic acid $H_3[RhCl_6]$ in formic acid, however some metallic rhodium was also formed since formic acid is a strong reducing agent [1]. Rhodium(II) acetate

* After this manuscript was completed a review of "The Chemistry, Structure and Metal–Metal Bonding in Compounds of Rhodium(II)" including rhodium(II) carboxylates appeared; T.R. Felthouse, Prog. Inorg. Chem., 29 (1982) 73.

was prepared by an analogous method [26]. Several variations to the original procedure are now employed for the preparation of the rhodium(II) carboxylates, the choice of method being influenced by the pK_a value of the acid. Rhodium(II) acetate is prepared by refluxing a mixture of rhodium trichloride trihydrate, sodium acetate trihydrate and glacial acetic acid in ethanol [27,28], while the rhodium(II) carboxylates of stronger acids such as trifluoroacetic acid are generally obtained by the interaction of rhodium trichloride with the appropriate sodium salt alone in ethanol [29,30]. Other preparative methods include heating rhodium(III) hydroxide with the appropriate acid under reflux in ethanol followed by extraction into acetone, treatment of hydrous rhodium(III) oxide with the acid in ethanol followed by extraction into dichloromethane [32], and exchange of the acetate ligands with the appropriate free acid [31,32]. The stepwise exchange of acetate for trifluoroacetate has been followed by ^{1}H NMR and mass spectrometry [33]; a more complete discussion of the exchange reaction is given on page 162.

The rhodium(II) carboxylates usually crystallise as solvates $[Rh_2(O_2CR)_4(solv)_n]$ but can be converted into non-solvated form by gently heating in vacuo [33]. Adducts of rhodium(II) carboxylates with neutral ligands (L) can be prepared by treatment of the anhydrous solid $[Rh_2(O_2CR)_4]$ with a solution of a solid ligand or a slight excess of neat ligand in liquid or gaseous form. Excess liquid ligand is removed in vacuo, while a gaseous ligand is passed over the finely ground solid until constant weight is achieved [31]. Salts of the rhodium(II) carboxylates are prepared by mixing alkali metal or protonated N-base salts (MX) with $[Rh_2(O_2CR)_4(H_2O)_2]$ yielding $M[Rh_2(O_2CR)_4X]$ or $M_2[Rh_2(O_2CR)_4X_2]$.

C. DIFFRACTION STUDIES AND STRUCTURAL FEATURES

The first X-ray diffraction crystal structure analysis on a rhodium(II) carboxylate was performed by Antsyskina on rhodium(II) acetate [5]. His estimate of 2.45 Å for the Rh–Rh bond length in $[Rh_2(O_2CR)_4L_2]$ R = Me, L = H_2O was based on the inspection of just two electron density projections and has subsequently been revised by Cotton et al. to 2.385(5) Å in the light of more accurate data from a full three dimensional analysis [11,34].

X-ray diffraction crystal analyses have been performed on over thirty rhodium(II) carboxylate adducts and salts, all of which possess the basic "lantern" structure: the rhodium–rhodium bond lengths vary from 2.371 Å in $[Rh_2(O_2CCMe_3)_4(H_2O)_2]$ [60] to 2.486(1) Å in $[Rh_2(O_2CCF_3)_4(PPh_3)_2]$ [35]. Since comparisons with related structures indicate that the short Rh–Rh distances (less than those in rhodium metal) are not imposed by the steric requirements of the bridging carboxylate ligands, they were originally taken by some authors to imply the presence of a rhodium–rhodium triple bond

[11,12]. However, a Rh–Rh bond order of one in these complexes is now generally accepted. X-ray crystallographic and structural parameters for rhodium(II) carboxylates and for rhodium(II) compounds where two of the carboxylates are replaced by other bridging ligands are given in Table 1. Rhodium–rhodium distances are dependent upon the nature of the axial donor ligands; replacement of axial nitrogen or oxygen donors by phosphorus donors increases the metal–metal bond distances in adducts of rhodium(II) acetate and trifluoroacetate significantly (ca. 0.05 Å). However replacement of PPh_3 by $P(OPh)_3$, a phosphorus donor ligand generally considered to possess greater π acceptor capacity, produces only small changes (2.4505 → 2.445 Å) and (2.486 → 2.470 Å) in the Rh–Rh bond distances of rhodium(II) acetate and trifluoroacetate respectively.

An X-ray crystal structure of the oxidised species $[Rh_2(O_2CMe)_4(H_2O)_2]$-$ClO_4 \cdot H_2O$ has been reported, Rh–Rh and Rh–OH_2 bond distances of 2.317(2) and 2.22(1) Å respectively are much shorter than in the neutral species $[Rh_2(O_2CMe)_4(H_2O)_2]$ where the corresponding values are 2.385(5) and 2.310(3) Å respectively [11,34]. Even after allowing for a decrease in the effective radius of the rhodium on oxidation, there is still a net reduction in bond length. For a more complete discussion of Rh–Rh and Rh–L bonding, see section J on Electronic Structure.

Complete substitution of D for H in axial dimethyl sulphoxide of $[Rh_2(O_2CCF_3)_4(Me_2SO)_2]$ has been shown to alter the crystal packing [37]. This is the first example of isotopic control of a structure in a transition metal complex. Cotton and co-workers have suggested that a "size" effect may be operating, since a CD_3 group has a smaller Van der Waals radius than a CH_3 group, but have voiced reservations about this explanation since the methyl groups constitute only a small fraction of the volume of $[Rh_2(O_2CCF_3)_4(Me_2SO)_2]$. They have also noted that the different structures for each compound may have arisen merely from slightly different conditions prevailing during crystallisation, or alternatively both types of crystals may have been present in each case, even though each batch of crystals appeared to be homogeneous.

Comparison of crystallographic data for $[Rh_2(O_2CCF_3)_4(EtOH)_2]$ and $[Rh_2(O_2CMe)_4(EtOH)_2]$ shows that withdrawal of electron density to the fluorine atoms leads not only to an increase in the length of the neighbouring CF_3–C bond but also to an increase in the angle between the C–O bonds. The resultant increase in the O · · · O distance (0.02 Å) is accompanied by a similar increase in the Rh–Rh distance, so that the displacement of the rhodium atom from the plane of the oxygen rectangle remains unchanged (Table 2). The two crystallographically independent forms of $[Rh_2(O_2CCF_3)_4(EtOH)_2]$ which exist are joined by hydrogen bonds to form chains. Each pair of complexes is joined by two hydrogen bonds, one

TABLE 1

X-ray crystal structure data for binuclear rhodium(II) carboxylates

$Rh_2(O_2CR)_4L_n$	Crystal system	Space group	Z	Rh–Rh (Å)	Rh–O (Å)	Rh–O (Å)	Rh–L (Å)	Ref.
$Rh_2(O_2CH)_4(H_2O)$	Triclinic		2		2.03			2
$Rh_2(O_2CMe)_4(H_2O)_2$	Monoclinic [a]	$C2/c$ (C_{2h}^6)	4	2.45				4
	Monoclinic	$C2/c$ (C_{2h}^6)	4	2.385(5)	2.036(3)	2.047(3)	2.310(3)	11
					2.029(3)	2.042(4)		34
$Rh_2(O_2CMe)_4(NHEt_2)_2$	Ortho-rhombic	$Pbcn$ (D_{2h}^{14})	4	2.402(0)	2.046(3)	2.038(3)	2.301	8
					2.031(3)	2.034(3)		57
$Rh_2(O_2CMe)_4(C_5H_5N)_2$	Monoclinic	$C2/c$ (C_{2h}^6)	4	2.3963 [b]	2.038	2.046	2.227(3)	8
				2.3994	2.041	2.043		58
$Rh_2(O_2CMe)_4(C_7H_8N_4O_2)_2 \cdot 2\ H_2O$ [c] Theophylline-$C_7H_8N_4O_2$	Monoclinic	$C2/c$ (C_{2h}^6)	4	2.412(6)	2.07(4) Average		2.23(3)	59
$Rh_2(O_2CMe)_4(C_8H_{10}N_4O_2)_2$ Caffeine-$C_8H_{10}N_4O_2$	Triclinic	$P\bar{1}$ (C_i^1)	1	2.395(1)	2.036(10) Average		2.315(9)	59
$Rh_2(O_2CMe)_4(C_4H_8S)_2$	Ortho-rhombic	$Pbcn$ (D_{2h}^{14})	4	2.413(1)	2.035(3)	2.036(3)	2.517	60
					2.046(3)	2.042(3)		
$Rh_2(O_2CMe)_4(Me_2SO)_2$	Ortho-rhombic	$Pbca$ (D_{2h}^{15})	4	2.406(1)	2.032(3)	2.035(4)	2.451	60
					2.042(3)	2.035(3)		
$Rh_2(O_2CMe)_4\{P(OMe)_3\}_2$	Monoclinic	$P2_1/c$ (C_{2h}^5)	2	2.4555(3)			2.437(5)	8
$Rh_2(O_2CMe)_4\{P(OPh)_3\}_2$	Monoclinic	$C2/c$ (C_{2h}^6)	4	2.445(1)	2.033(3)	2.043(2)	2.418(3)	8
					2.048(3)	2.033(2)		61
$Rh_2(O_2CMe)_4(PPh_3)_2$	Triclinic	$P\bar{1}$ (C_i^1)	1	2.4505(2)	2.054(1)	2.038(1)	2.4771(5)	61
					2.056(1)	2.031(1)		
$Rh_2(O_2CMe)_4(PF_3)_2$	Cubic	$I23$ (T^3)	6	2.430(3)			2.42(1)	8
$Rh_2(O_2CMe)_4(CO)_2$	Ortho-rhombic	$Pbca$ (D_{2h}^{15})	4	2.4196(4)			2.092(4)	8
$[GunH]_2[Rh_2(O_2CMe)_4Cl_2]$	Tetragonal	$I4$ (C_4^5)	4	2.397(2)	2.04(1)	2.05(1)	2.591(1)	62

$[NH_4]_2[Rh_2(O_2CMe)_4Br_2]2NH_4Br$	Ortho-rhombic [a]	*Pncm* (D_{2h}^7)	4	~ 2.4				63
$[GunH]_2[Rh_2(O_2CMe)_4Br_2]$	Tetragonal [a]	*I4* (C_4^5)	4					63
$[Rh_2(O_2CMe)_4(H_2O)_2][ClO_4]$	Triclinic	$P\bar{1}$ (C_i^1)	2	2.315(2)	2.014(13) 2.012(12)	2.013(11) 2.012(11)	2.228 [g]	35
				2.319(2)	2.015(12) 2.021(14)	2.022(12) 2.006(15)	2.222	36
$Rh_2(O_2CMe)_2(mhp)_2(C_3H_4N_2)$ [d] Imidazole = $C_3H_4N_2$	Monoclinic	*C2/c* (C_{2h}^6)	4	2.388(2)	2.027(8) 2.054(8)	2.015(7)	2.17(1)	44
$Rh_2(O_2CMe)_2(mph)_2(C_3H_4N_2)$ $\cdot 2\ CH_2Cl_2$ Imidazole = $C_3H_4N_2$	Monoclinic	*C2/c* (C_{2h}^6)	4		2.046(4) 2.027(4)	2.029(5)		44
$Rh_2(O_2CMe)_2(HOH\cdots O_2CMe)$- $(OH)(H_2O)(NH_3)_2$	Monoclinic	*Cc* (C_5^4) or *C2/c* (C_{2h}^6)	4					64 53
$Rh_2(O_2CMe)_2(dmg)_2(PPh_3)_2\cdot H_2O$ [c]	Monoclinic	$P2_1/b$ (C_{2h}^5)	4	2.618(5)			2.485(9) [f]	49
$Rh_2(O_2CCF_3)_4(EtOH)_2$	Triclinic	$P\bar{1}$ (C_i^1)	2	2.396(2)	2.02(1) 2.04(1)	2.03(1) 2.03(1)	2.28(1) [g]	38
				2.409(2)	2.04(1) 2.04(1)	2.04(1) 2.04(1)	2.26(1)	
$Rh_2(O_2CCF_3)_4(Me_2SO)_2$	Triclinic	$P\bar{1}$ (C_i^1)	1	2.419(1)	2.031(3) 2.022(3)	2.016(3) 2.029(3)	2.236(3)	65
$Rh_2(O_2CCF_3)_4(d_6Me_2SO)_2$	Triclinic	$P\bar{1}$ (C_i^1)	2	2.409	2.032(3) 2.026(3)	2.042(3) 2.040(3)	2.263(3) [g]	37
$Rh_2(O_2CCF_3)_4(Me_2SO_2)_2$	Triclinic	$P\bar{1}$ (C_i^1)	2	2.407	2.039(3) 2.033(3)	2.040(2) 2.029(3)	2.234(3)	66
				2.401(1)	2.029(3) 2.021(3)	2.038(3) 2.031(3)	2.291(3) [g]	
				2.399(1)	2.036(3) 2.036(3)	2.024(3) 2.031(3)	2.284(3)	
$Rh_2(O_2CCF_3)_4(P(OPh)_3)_2$	Triclinic	$P\bar{1}$ (C_i^1)	1	2.470(1)	2.047(5) 2.053(5)	2.040(5) 2.026(6)	2.422(2)	67

TABLE 1 (continued)

$Rh_2(O_2CR)_4L_n$	Crystal system	Space group	Z	Rh–Rh (Å)	Rh–O (Å)	Rh–O (Å)	Rh–L (Å)	Ref.
$Rh_2(O_2CCF_3)_4(PPh_3)_2$	Triclinic	$P\bar{1}$ (C_i^1)	1	2.486(1)	2.031(5) 2.057(5)	2.041(5) 2.051(5)	2.494(2)	67
$Rh_2(O_2CEt)_4(C_{13}H_9N)_2$ (Acridine = $C_{13}H_9N$)	Triclinic	$P\bar{1}$ (C_i^1)	1	2.417	2.040(3) 2.027(3)	2.041(3) 2.039(3)	2.413(3)	41
$Rh_2(O_2CEt)_4(C_7H_6N_2)_2$ (7-azaindole = $C_7H_6N_2$)	Ortho-rhombic	$Pbca$ (D_{2h}^{15})	8	2.403(1)	2.047(5) 2.043(5)	2.022(5) 2.043(5)	2.275(6)	41
$[Rh_2(O_2CEt)_4(C_{12}H_8N_2)]_n$ (Phenazine = $C_{12}H_8N_2$)	Triclinic	$P\bar{1}$ (C_i^1)	1	2.409(1)	2.046(3) 2.043(3)	2.033(3) 2.038(3)	2.362(4)	41
$[Rh_2(O_2CEt)_4(C_{10}H_{16}N_2)]_n$ (2,3,5,6-tetramethyl-*p*-phenylenediamine = $C_{10}H_{16}N_2$)	Triclinic	$P\bar{1}$ (C_i^1)	1	2.387	2.030(4) 2.028(4)	2.032(4) 2.031(4)	2.324(6)	41
$Rh_2(O_2CEt)_4(Me_2SO)_2$	Monoclinic	$P2/n$ (C_{2h}^5)	4	2.407	2.025(3) 2.026(3)	2.028(3) 2.027(3)	2.449(1)	65
$Rh_2(O_2CCMe_3)_4(H_2O)_2$	Triclinic	$P\bar{1}$ (C_i^1)	1	2.371	2.036(2) 2.036(2)	2.043(2) 2.044(2)	2.295(2)	60
$[Rh_2(O_2CCH_2CH_2NH_3)_4(H_2O)_2][ClO_4]\cdot 2\ H_2O$	Ortho-rhombic	$Pccn$ (D_{2h}^{10})	4	2.38	2.05		2.34	68

[a] Preliminary crystallographic analysis. [b] Uncorrected value. [c] Crystal structure in Fig. 13. [d] mhp = 2-oxy-6-methylpyridine (C_6H_6NO). [e] dmgH = dimethylglyoxime ($C_4H_8N_2O_2$). [f] Possesses Rh–O and Rh–N bonds. [g] Two crystallographic forms per unit cell.

TABLE 2

Average values of bond distances (Å) and bond angles (degrees) in $[Rh_2(O_2CMe)_4(EtOH)_2]$ and $[Rh_2(O_2CCF_3)_4(EtOH)_2]$

	C–CH_3	C–O	< OCO	Rh–O	O ··· O	Rh–Rh
$[Rh_2(O_2CMe)_4(EtOH)_2]$	1.498(2)	1.269(4)	124.8(3)°	2.039(3)	2.242(5)	2.3855(2)
$[Rh_2(O_2CCF_3)_4(EtOH)_2]$	1.527(7)	1.252(9)	128.7(8)°	2.034(5)	2.262(9)	2.4015(12)

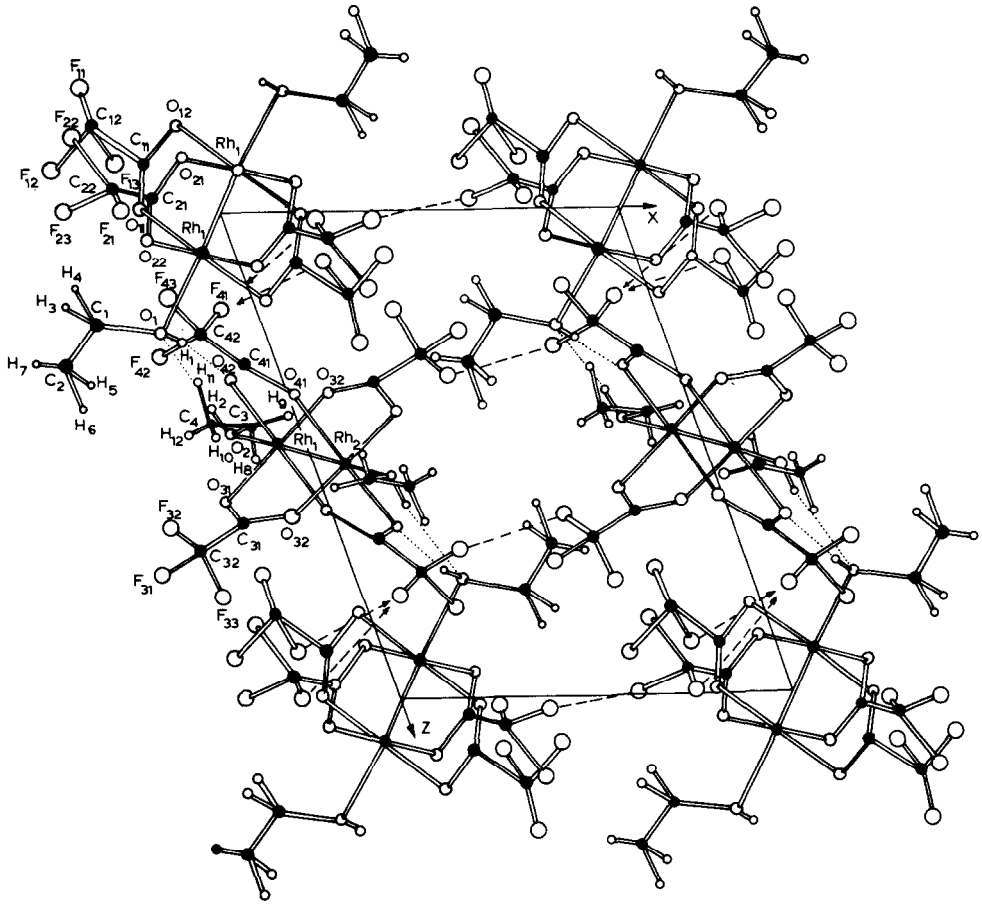

Fig. 3. The crystal packing of the two independent forms of $[Rh_2(O_2CCF_3)_4(EtOH)_2]$ (with permission from ref. 38).

between the hydroxyl group of ethanol and one of the oxygen atoms of the carboxyl group, and the other between the hydroxyl groups of ethanol. There are contacts between the chains via fluorines [38] (Fig. 3).

The use of potential linking ligands (N–N) to prepare adducts leads to formation of polymeric products $[Rh_2(O_2CR)_4(N–N)]_n$ (R = Me,Et; N–N =

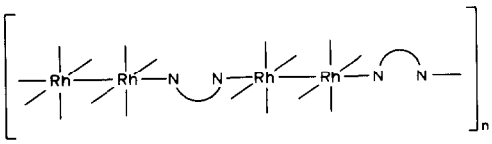

Fig. 4. Polymeric products with linking ligands (N–N).

cyanoguanidine [39], adenine [40], phenazine and durene-diamine [41]) (Fig. 4). The ambidentate thiocyanate and selenocyanate anions can also act as links between the lantern units [42,43].

The operation of *trans* influences and other electronic factors in bridging carboxylate exchange reactions leads to exclusive formation of di- and tetra-substituted products (further discussion of this phenomenon is given in Section L) [33]. Direct replacement of carboxylate by other bridging ligands is also possible. Thus treatment of $Rh_2(O_2CR)_4$ with mhpH = 2-hydroxy-6-methylpyridine or chpH = 2-hydroxy-6-chloropyridine yields a variety of partially or fully substituted lantern compounds, several of which have one or both axial sites blocked by the 6-methyl or 6-chloro groups (Figs. 5 and 6). Four asymmetric mhp or chp ligands are arranged in a 3 : 1 rather than the anticipated 2 : 2 conformation. Adoption of the 3 : 1 mode ensures axial ligation at least at one of the axial sites, while a 2 : 2 arrangement would probably prevent ligation at both axial sites. In order to minimise the repulsive forces between the three methyl groups or chlorine atoms at the crowded end of the molecule, the orientation of each bridging ligand is twisted by ca. 20° [44–46].

Compounds in which carboxylate anions are replaced by chelate ligands such as phenanthroline [47,48] and dimethylglyoxime [49–51] also occur (Figs. 7–9).

In addition to numerous complexes where the lantern structure has been confirmed there are a number of cases where the presence of the binuclear structure is supported by magnetic and spectroscopic evidence but has not been fully established. In many of these instances, crystallographic confirmation is desirable. Treatment of rhodium(II) carboxylates with β-diketones leads to formation of disubstituted products of uncertain structure. Spectroscopic evidence suggests adoption of the chelating mode by the β-diketonate

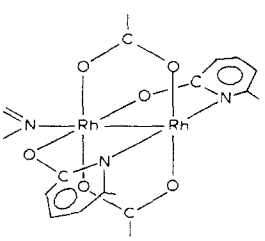

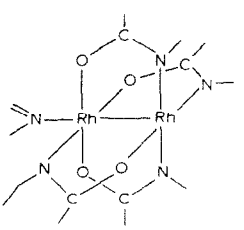

Fig. 5. Partially substituted compound $[Rh_2(O_2CMe)_2(mhp)_2(C_3H_4N_2)]$ with one axial site blocked, obtained by treatment of $[Rh_2(O_2CMe)_4]$ with mhpH.

Fig. 6. The four asymmetric chp ligands are arranged in a 3 : 1 configuration in $[Rh_2(chp)_4(C_3H_4N_2)\cdot 3H_2O]$.

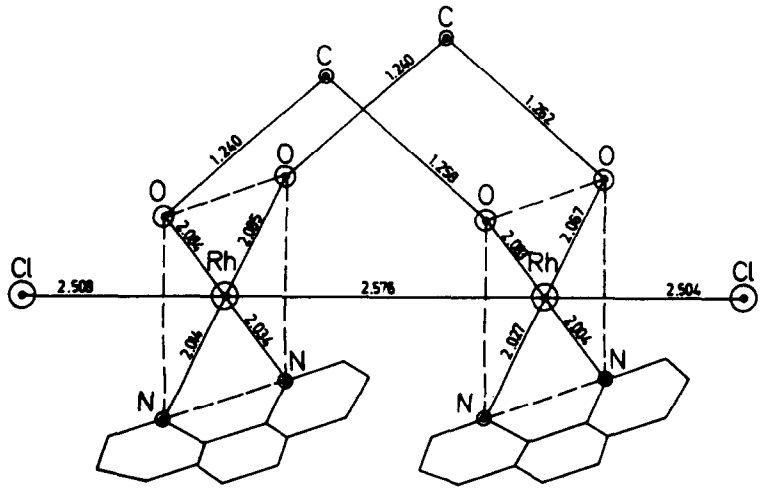

Fig. 7. Structure of $[Rh_2(O_2CH)_2(phen)_2Cl_2]$ (with permission from ref. 48).

anions (Fig. 10), but structures with bridging modes have also been proposed [52].

Modified lantern structures have been proposed for $[Rh_2(O_2CMe)_2(HOH \cdots O_2CMe)_2(NH_3)_2]$ and for $[Rh_2(O_2CMe)_2(HOH \cdots O_2CMe)(OH)(HOH)\text{-}(NH_3)_2]$ [53] (Figs. 11 and 12).

A green complex of stoichiometry $Rh(dpc) \cdot 3H_2O$ is formed when hydrated rhodium(II) acetate is treated with pyridine-2,6-dicarboxylic acid ($dpcH_2$). It is thought to be a true rhodium(II) complex with the $Rh_2(O_2C\text{–})_4$

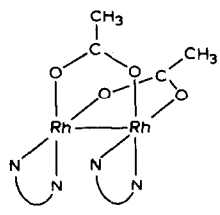

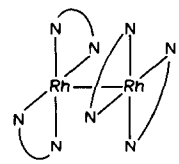

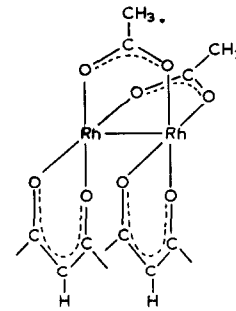

Fig. 8. $[Rh_2(O_2CMe)_2(dmg)_2]$ (N–N = dmg).

Fig. 9. $[Rh_2(dmg)_4]$ (N–N = dmg).

Fig. 10. $[Rh_2(O_2CMe)_2(acac)_2]$.

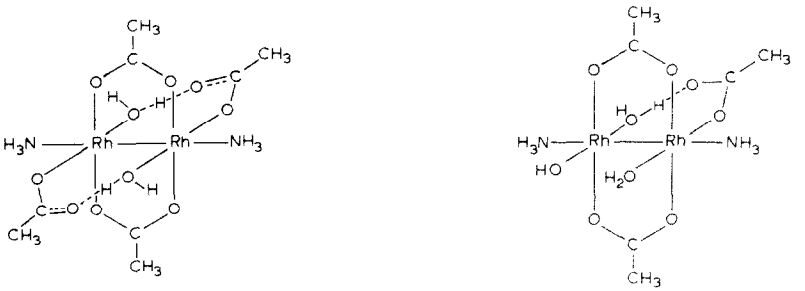

Fig. 11. Proposed structure of $[Rh(O_2CMe)(HOH \cdots O_2CMe)(NH_3)]_2^0$. In the original paper the figure captions are transposed (ref. 53).

Fig. 12. Proposed structure of $[Rh_2(O_2CMe)_2(HOH \cdots O_2CMe)(OH)(H_2O)(NH_3)_2]$.

unit preserved through linking dpc units in which the N-donor atom is not coordinated. However, it is difficult to visualise a molecular structure of this type which does not involve considerable distortion. It has been suggested that one of the three water molecules associated with each Rh(dpc) unit could be coordinated to the rhodium atom and the remaining two could be "lattice" water. $Rh3d_{3/2}$ and $Rh3d_{5/2}$ binding energies for a sample of this complex were located at 312.6 and 307.8 eV respectively which is in the range characteristic of other rhodium(II) compounds. ($Rh3d_{3/2}$ 312.2–313.4 eV, $Rh3d_{5/2}$ 307.8–310.0 eV [54]).

The rhodium(II) salicylates appear to possess a modified lantern structure.

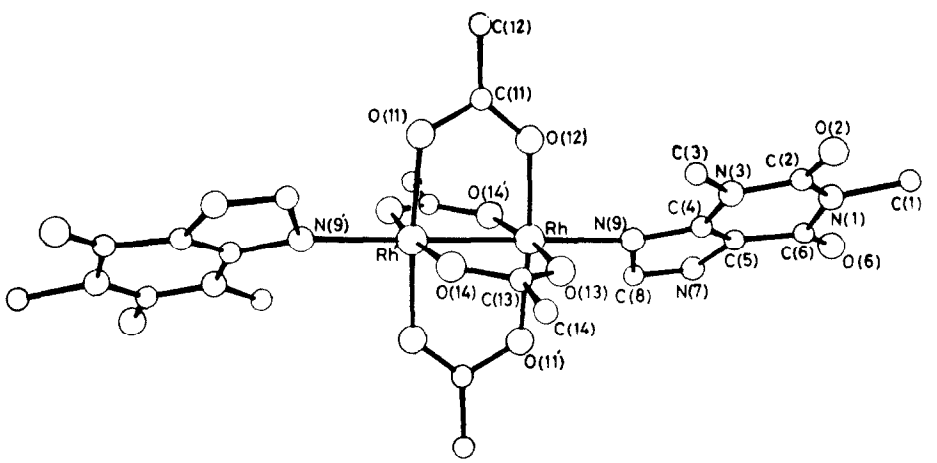

Fig. 13. The molecular structure of $[Rh_2(O_2CMe)_4(theophylline)_2]$ (with permission from ref. 59).

The IR spectra of these complexes are similar to those of copper(II) salicylates and have been taken to indicate coordination of salicylate by the oxygen of the carboxyl and phenoxy groups [55]: however, the X-ray crystal diffraction study on copper(II) salicylate indicates the molecule does not possess the lantern structure [56]. The whereabouts of the phenoxy proton has not been determined. Evidence concerning the structure of these molecules is discussed in Section E.

D. MAGNETIC MEASUREMENTS

The diamagnetic nature of the rhodium(II) carboxylates was one of the first pieces of evidence for a metal–metal bond. In 1965 Nazarova et al. reported that the magnetic susceptibility of diamagnetic anhydrous rhodium(II) acetate varies with temperature [69], however Kitchens and Bear [70] noted the variation was small (ca. $0.11 \rightarrow 0.30$ BM when measured by Faraday's method over the temperature range $-196°$ to $+188°$C) and may simply be due to the increase in error upon heating and cooling the sample. They pointed out that their results cannot be compared with those obtained earlier, since the latter did not include details of the method and the temperature range employed [70].

An investigation of the effect of the various axial substituents L on the magnetic susceptibilities of the acetato compounds of rhodium has been carried out. It was found that the substituents have only a small effect on the susceptibility of the basic acetate group $Rh_2(O_2CMe)_4$. An effective magnetic moment of ca. 0.5 BM per rhodium was also found with a variety of axial ligands and bridging carboxylate groups. Rhodium(II) salicylate, the structure of which is still unresolved, also has an effective magnetic moment of ca. 0.5 BM per rhodium [71].

A pale green rhodium glycinate ether adduct which was formulated as $[Rh(O_2CCH_2NH_2)_2\{(C_2H_5)_2O\}]$ on the basis of analytical data was found to be paramagnetic with $X_G = 2 \times 10^{-6}$ and an effective magnetic moment of 1.4 BM [71]. However, the exact constitution of this product remains uncertain. Magnetic moments in solution have been determined by Evans' NMR method for $[Rh_2(O_2CMe)_4]^+$ (see p. 135).

E. VIBRATIONAL SPECTROSCOPY

IR and Raman spectroscopic data have been recorded for many of the rhodium(II) carboxylate adducts and in several cases full coordinate analyses have been performed; references are given in Table 19 (p. 182). Some general trends and specific examples will be discussed in this section.

The ν(Rh–O) vibrations appear as an intense absorption band with other

TABLE 3

Selected IR data for $[Rh_2(O_2CR)_4L_2]$ and $[Rh_2(OSCR)_4L_2]$ [a]

Cpd. R	L	ν_{asym}(RhO) (cm^{-1})	ν_{sym}(RhO) (cm^{-1})	$\nu_{asym}(CO_2)$ (cm^{-1})	$\nu_{sym}(CO_2)$ (cm^{-1})	Ref.
$[Rh_2(O_2CR)_4L_2]$						
H	–	455, 450	498, 481	1589, 1529	1340, 1318	
				1541		72
	H_2O	460, 455	499, 483	1600, 1544	1343, 1319	
				1533		72
	NH_3	443	468	1592	1335	72
	$(NH_2)_2CO$	446	469	1586, 1535	1344	72
	$(NH_2)_2CS$	449	476	1590, 1542	1334	72, 39
	C_5H_5N	446, 420	477	1600	1337, 1315	72
	Me_2SO	460	480	1615, 1592	1340, 1318	72
	Cl^-	445	470	1579, 1530	1340, 1326	72
	NO_2^-	453	480	1598, 1545	1335, 1328	72
Me	–	395, 380	354	1584	1443	72
	H_2O	386, 375	342	1584	1450	72
	$(NH_2)_2CO$			1585	1442	72
	$(NH_2)_2CS$			1589	1435	73
	C_5H_5N	383	334	1594	1450	72
	Me_2SO	391	348	1585	1441	72
	EtOH			1585	1430	29
	PPh_3	374, 379	320			72, 74 [b]
	Cl^-	389	344	1579	1447	72

Et	–	436, 411	354			74 [b]
	H_2O	435	415	1580	1470	75 [b], 76 [b]
	Me_2SO		425	1590	1468	76 [b]
	Et_2SO	475	430	1591	1470, 1432	76 [b]
	Cl^-	380		1570	1455	39 [b]
CF_3	–	392	343	1660, 1645	1460	72
	H_2O	384	341	1670, 1650	1460, 1454	72
	Me_2SO	383	343	1665	1452	72
	C_5H_5N	381	339	1660	1454	72
	EtOH	386	342	1670, 1658	1455	72
Ph	PPh_3	415, 400	334			74
$[Rh_2(OSCR)_4L_2]$	L	ν(RhO)(cm^{-1})	ν(RhS)(cm^{-1})	ν_{asym}(CO)(cm^{-1})	ν_{sym}(CO)(cm^{-1})	Ref.
Me	–	317	288	1553, 1522 1538	1475	77
	H_2O	316, 301	290	1550, 1540 1500	1490	77
	Me_2SO	320	283	1550 1540	1498	77
	C_5H_5N	319	288	1554 1540	1488	77
	Cl^-	314	289	1550 1535	1489	77
Ph	H_2O	369		1555	1410	78
	Me_2SO	386		1563	1400	78
	C_5H_5N	355		1558	1400	78
	$(NH_2)_2CS$	370		1555	1400	78

[a] IR data source, Table 19. [b] Rh–O stretch vibrations given but are not assigned to ν_{sym} and ν_{asym}. N.B. For rhodium(II) acetate, propionate, benzoate and trifluoroacetate $\nu_{sym}(RhO) < \nu_{asym}(RhO)$; the reverse order is proposed for rhodium(II) formate but no explanation has been given.

low and medium intensity bands in the 500–420 cm^{-1} region for rhodium(II) formate, while for acetate and trifluoroacetate the ν(Rh–O) vibrations appear at 395–340 cm^{-1} generally as two bands of medium intensity. Although the reason for the marked difference is unclear it has been attributed "to the influence of the hydrocarbon group" or to a slight difference in the ionic character of the Rh–O bonds [72]. There is no obvious correlation between ν(Rh–O) and the mass of R in $[Rh_2(O_2CR)_4]$ (see Table 3).

The small values of $[\nu(OCO)_{asym} - \nu(OCO)_{sym}]$ are consistent with a bridging mode for the carboxylate ligands. Values of $\nu(OCO)_{sym}$ and $\nu(OCO)_{asym}$ for selected complexes are given in Table 3. Although changes in the nature of the axial ligands produce no significant trends in the vibrational frequencies recorded for the lantern structure $[Rh_2(O_2CR)_4]$, small axial ligand dependent shifts in $\nu(OCO)_{asym}$ and $\nu(OCO)_{sym}$ are obtained.

Raman active ν(Rh–Rh) bands can be related to the relative order of the Rh–Rh bonds under investigation; however the considerable complexity of the spectra in the ν(Rh–Rh) region combined with the low intensity expected for a band resulting from the stretching modes of these relatively weak metal–metal interactions prevents an unambiguous assignment of ν(Rh–Rh) [79] (Fig. 14). Following the earlier conclusions of Cotton et al., Ketteringham and Oldham assumed the Rh–Rh bond order to be 3, and they thus assigned an intense line in the Raman spectra at ca. 350 cm^{-1} to the Rh–Rh stretching mode; the value agreed with that calculated from the simple harmonic oscillator model for multiply bonded rhodium atoms [74]. This assignment has recently received fresh support [92,122] from Raman perturbation difference spectroscopy and single crystal polarised absorption spectra. However, other authors have pointed out that Raman active bands attributed to Rh–Rh single bonds in $Rh_6(CO)_{16}$ and $Rh_4(CO)_{12}$ occur at ca. 190 cm^{-1} and have concluded that since the Rh–Rh bond order in rhodium(II) carboxylates is now generally accepted to be one, it is more

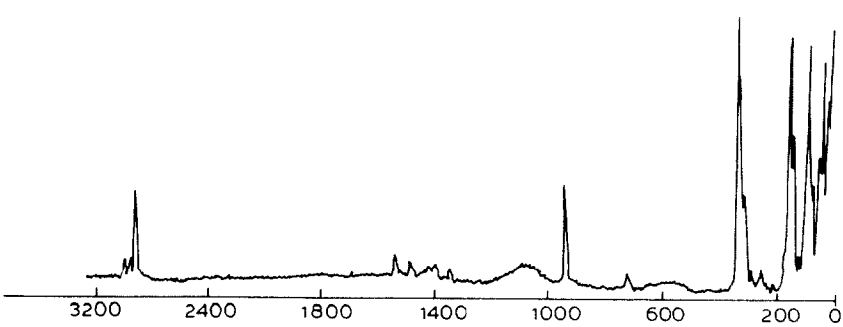

Fig. 14. Raman spectrum of $[Rh_2(O_2CMe)_4(MeOH)_2]$ (with permission from ref. 79).

logical to assign ν(Rh–Rh) to the strong Raman absorption which occurs at ca. 150 cm^{-1} [79,81]. Theoretical analysis of these vibrations has shown that they entail appreciable contributions from δ(O–Rh–Rh) and δ(C–O–Rh) modes in addition to ν(Rh–Rh) [81]. Using Rh–Rh distances of 2.550 and 2.386 Å for rhodium(II) thioacetate and acetate complexes, respectively, combined with the corresponding ν(Rh–Rh) values of 164 and 155 cm^{-1}, Shchelokov et al. calculated the force constants and found them to be in the generally accepted range for Rh–Rh single bonds (see Table 4) [80]. In view of the conflict in assigning ν(Rh–Rh) it would seem that more work is desirable in this area.

The coordination modes of ambidentate axial ligands have been investigated by IR spectroscopy. Bands occurring at ca. 1100 cm^{-1}, 950 cm^{-1} and 1100–950 cm^{-1} have been assigned to ν(SO) in S-bonded, O-bonded and S,O-linked DMSO adducts respectively; in the free ligand ν(SO) occurs at ca. 1100–1055 cm^{-1}. Thus $[Rh_2(O_2CCF_3)_4(DMSO)_2]$ (ν(SO) ca. 1019 cm^{-1}) and $[Rh_2(O_2CR)_4(DMSO)_2]$ (R = H, Me, Ph; ν(SO) ca. 1089 cm^{-1}, 1087 cm^{-1}, 1102 cm^{-1}) have been assigned O- and S-bonded structures respectively. The coordination of DMSO in $[Rh_2(OSCR)_4(DMSO)_2]$ (R = Me, Ph; ν(SO) ca. 1089 cm^{-1}, 1108 cm^{-1}) has also been assigned as S-bonded [72]. The mode of DMSO coordination has been confirmed for rhodium(II) acetate and rhodium(II) trifluoroacetate adducts by X-ray crystal diffraction studies [60,65]. In $[Rh_2(O_2CH)_4(DMSO)_{1.5}]$ DMSO acts as a link between lantern units (Me_2SO)–Rh–Rh–(Me_2SO)–Rh–Rh–$(OSMe_2)$ leading to the appearance of two ν(SO)bands in the IR spectrum at 1090 and 1058 cm^{-1} attributed to S-bonded terminal and S,O linking DMSO ligands respectively [76].

Axial coordination of amino pyridines, amido pyridines and benzamide has been investigated by IR spectroscopy. Coordination through the amino group is expected to produce a displacement of $\nu(NH_2)_{asym}$ and $\nu(NH_2)_{sym}$

TABLE 4

Rhodium–rhodium bond distances, vibrational stretching frequencies and force constants for selected rhodium(II) carboxylates

Compound	(Rh–Rh) (Å)	ν(Rh–Rh) (cm^{-1})	K(Rh–Rh) (mdyn $Å^{-1}$)	Ref.
$Rh_2(O_2CH)_4(H_2O)_2$		168	0.77	81
$Rh_2(O_2CMe)_4(H_2O)_2$	2.385(5)	155	0.67	4, 81
$Rh_2(O_2CMe)_4(MeOH)_2$		170		79
$Rh_2(OOCMe)_4$	2.386	155	0.67	80
$Rh_2(OSCMe)_4$	2.550	164	0.61	80

to lower wavenumbers (ca. 140–60 cm^{-1} and 100–20 cm^{-1} respectively). Thus the shift of $\nu(NH_2)$ (ca. 60–25 cm^{-1}) to higher wavenumbers (ca. (3474, 3331 cm^{-1}), (3472, 3358 cm^{-1}) and (3488, 3370 cm^{-1})) respectively on coordination of 2-, 3- and 4-amino pyridine is taken to indicate bonding through the aromatic (pyridine) nitrogen. Similarly coordination of benzamide through the amido oxygen is indicated by a small displacement of $\nu(CO)$ to lower wavenumbers (1668 → 1658 cm^{-1}) and a larger shift of $\nu(NH_2)$ to higher wavenumbers (3381, 3185 → 3429, 3350 cm^{-1}). Spectroscopic data for diethylnicotinamide (a small displacement of $\nu(CO)$ to lower wavenumbers (1645 → 1622 cm^{-1})) indicates coordination via oxygen; however the pink colour of the complex suggests coordination through the less sterically hindered (pyridine) nitrogen [82,83].

A small decrease in the $\nu(CO)$ (ca. 40–10 cm^{-1}) and an increase in the $\nu(C-NH_2)$ frequency indicates that urea and related amido compounds are coordinated via oxygen. For semicarbazide and 1,5-diphenylcarbonohydrazide the IR data available do not allow an unambiguous conclusion about the mode of coordination, however a shift of $\nu(CO)$ to higher wavenumbers (ca. 10 and 8 cm^{-1}) and $\delta(NH_2)$ to lower wavenumbers (ca. 29 cm^{-1}) has been taken to indicate coordination of the amido nitrogen to rhodium and this conclusion is supported by the red and violet colours of the compounds concerned [84]. Thiourea is coordinated through sulphur as indicated by the decrease in $\nu(CS)$ wavenumber (733 → 645 cm^{-1}) [73].

The cyanate anion usually coordinates through nitrogen, and IR data for $K_2[Rh_2(O_2CCH_3)_4(NCO)_2 \cdot 2H_2O]$ ($\nu(CN) = 2185$ cm^{-1}, $\nu(CO) = 1328$ cm^{-1} and $\delta(NCO) = 623$, 643 cm^{-1}) compared with the "free" ion values

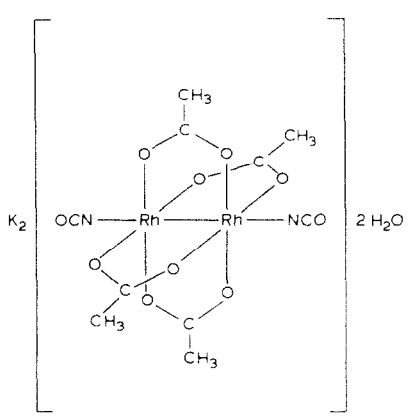

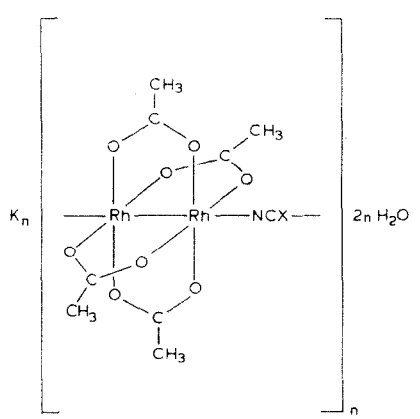

Fig. 15. Proposed structure of $K_2[Rh_2(O_2CMe)_4(NCO)_2] \cdot 2\ H_2O$.

Fig. 16. Proposed structure for $K_n[Rh_2(O_2CMe)_4(NCX)]_n \cdot 2nH_2O$.

(ν(CN) = 2165 cm^{-1}, ν(CO) = 1254 cm^{-1} and δ(NCO) = 637, 628 cm^{-1}) are considered to be consistent with this arrangement [42,43,85]. The appearance of ν(OH) frequencies at 3560 and 3480 cm^{-1} (cf. 3518 and 3400 cm^{-1} in $[Rh_2(O_2CMe)_4(H_2O)_2]$) is taken to indicate the presence of lattice water in the cyanate adduct, which is therefore formulated as a dihydrate (Fig. 15).

In contrast IR data for the complexes $[Rh_2(O_2CMe)_4(KNCX)]_n \cdot 2nH_2O$ (X = S, ν(CS) = 760 cm^{-1}, ν(CN) = 2126 cm^{-1} and δ(NCS) = 458 cm^{-1}; X = Se, ν(CSe) = 590 cm^{-1}, ν(CN) = 2137 cm^{-1} and δ(NCSe) = 425 cm^{-1}) are consistent with the presence of linking NCX ligands and have been taken as evidence for the presence of polymeric structures (Fig. 16) [42,43].

There have been attempts to distinguish axial cyanide ligands bound in terminal and linking modes by their IR spectra. The orange complexes $[Rh_2(O_2CR)_4 \cdot 2\ KCN]$ (R = Me, Et, ^{n}Pr) and $[Rh_2(O_2CCF_3)_4 \cdot 2\ KCN \cdot 0.5\ H_2O]$ all show bands at ca. 2105–2095 cm^{-1}, 530–515 cm^{-1} and 470–450 cm^{-1} corresponding to ν(CN), ν(Rh–C) and δ(Rh–CN) respectively for terminal C-bonded cyanide, and are thus formulated as salts $2K[Rh_2(O_2CR)_4(CN)_2]$. In contrast the complexes $[Rh_2(O_2CR)_4 \cdot 0.5\ KCN \cdot H_2O]$ and $[Rh_2(O_2CR)_4 \cdot 1.5\ KCN]$ show bands attributable to linking cyanide (ν(CN) = 2127 cm^{-1}, 2140 cm^{-1}) and are formulated as $[H_2O–Rh–Rh–CN–Rh–Rh–OH_2]^-$ and $[NC–Rh–Rh–CN–Rh–Rh–CN]^{3-}$ respectively [86]. A displacement of ν(C≡N) to higher wavenumbers for cyclohexyl isocyanide in $[Rh_2(O_2CR)_4(C_6H_{11}NC)_2]$ (R = H, CH_3, C_2H_5, ν(C≡N) at 2182, 2170 and 2172 cm^{-1} respectively compared with 2148 cm^{-1} in the free ligand) confirms axial coordination through carbon [75].

A shift of ca. 10 cm^{-1} in ν(C=NH) to lower wavenumber combined with an unchanged ν(C≡N) value has been taken to indicate coordination of guanidine and its derivatives through the >C=NH rather than the CN group. Changes in ν(C=NH) and ν(C≡N) for $[Rh_2(O_2CR)_4Gu–CN \cdot m\ H_2O]$ (R = Me, Et; m = 1, 2) are too small to be conclusive; therefore the structure of these compounds must be open to doubt [39].

A structure for rhodium(II) salicylates has been postulated with salicylate bound via phenolic and/or carboxylate oxygens on the basis of IR evidence [55]. The absence of high frequency bands ν(CO) ca. 1730–1680 cm^{-1} and the presence of ν_{asym}, ν_{sym} ca. 1590, 1390 cm^{-1} respectively, indicate a rhodium–carboxylate oxygen bond. Similarly the absence of the intense bands ca. 1350–1310 cm^{-1}, usually indicative of phenolic δ(OH) bending modes, suggests that the oxygen atom of the phenoxy group is not joined to the proton, and hence forms a bond with the rhodium atom. Copper(II) and rhodium(II) salicylates have almost identical IR spectra; thus conclusions reached for the rhodium compounds have been based on the established structure of the copper compounds [56] for which the terminal and bridging salicylate ligands are bound to copper via the carboxylate and phenolic

oxygens in a chain. Conceivable structures for the rhodium compound include those given in Figs. 17a and b; however these structures do not explain the absence of δ(OH) or vibrations characteristic of protonated ligand L. To emphasise this structural ambiguity the original authors employed the formulation $[Rh_2(O_2CC_6H_4O)_4(H)_4(L)_2]$ for these compounds [55].

For $[Rh_2(O_2CR)_2(N{-}N)_2X_2]$ (where N–N = 1,10-phenanthroline or 2,2′-bipyridyl and X = Cl, Br) the lower ν(Rh–O) frequencies are consistent with the longer Rh–O distances found by diffraction methods [47].

The IR spectra of $[Rh_2(O_2CMe)_2(acac)_2]$ (acacH = $CH_3COCH_2COCH_3$) are complex in the 1600–1200 cm^{-1} region owing to overlap of absorptions due to the acetate and β-diketonate groups. The assignments reported were made on the basis of the shift to higher frequencies of the bands due to the β-diketonato moiety when a methyl group is substituted by a trifluoromethyl group, and by comparison of the spectra of $[Rh_2(O_2CMe)_2(acac)_2]$ and $[Rh_2(O_2CMe)_4]$. The asymmetric $\nu(CO_2)$ stretching of the acetato group (1570–1560 cm^{-1}) is at a lower frequency than that found for $[Rh_2(O_2CMe)_4]$ (1588–1580 cm^{-1}), and the difference $\Delta(\nu_{asym} - \nu_{sym})$ is smaller than that found in rhodium(II) acetate, i.e. 145–130 cm^{-1} compared with 162–150 cm^{-1}. These data confirm that the acetato group is still symmetrically bound as a bidentate ligand, however they do not distinguish clearly between chelate and bridging modes for the acac ligands [52]. Numerous structures involving chelating and/or bridging acac have been considered [52]. However, on the basis of the IR spectra and given the tendency for acac to chelate, the structure given in Fig. 10 seems the most likely.

A study of the IR absorption spectra of rhodium(II) thioacetates and thiobenzoates has shown that, as with the corresponding carboxylates, the

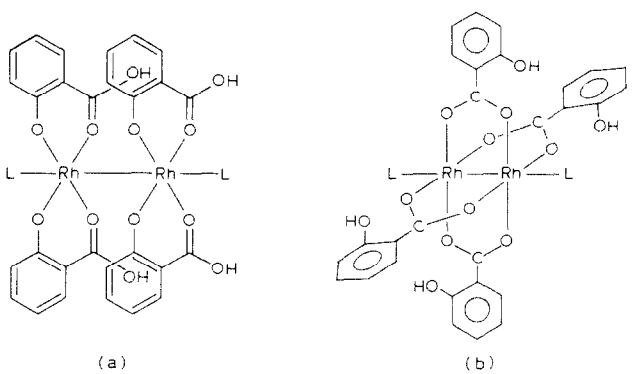

Fig. 17. (a) and (b): Conceivable structures for $[Rh_2(O_2CC_6H_4O)_4(H)_4(L)_2]$. These structures do not, however, explain the IR spectra.

nature of the axial ligand does not significantly affect the vibrational frequencies of the binuclear lantern structure. An intense absorption band ca. 970 cm^{-1} which is present in all IR spectra of thiobenzoate complexes, but absent in the spectra of the corresponding benzoate compounds, has been tentatively assigned to a complex deformation vibration of the CS bond [78].

Oxidation of $[Rh_2(O_2CMe)_4]$ gives mixed valence species, e.g. $[Rh_2(O_2CMe)_4Cl]$ in which the acetate bridge structure is maintained. A band at 231 cm^{-1} has been assigned to Rh–Cl stretching modes and two other bands in the low frequency region of the spectra (330, 405 cm^{-1}; see diagram in ref. 87) have been assigned to ligand modes consisting mainly of metal–oxygen stretch vibrations and deformations. The fact that there are the same number of such bands in the mixed valence compound as in the rhodium(II) compound has been taken to imply that on the IR time scale the valencies are equivalent and not localised as Rh(II), Rh(III) [87] (see Table 3).

F. ELECTRONIC SPECTROSCOPY

The colour of the rhodium(II) carboxylate adducts varies with the nature of the axial donor ligands; blue or green products are usually obtained with oxygen, red or pink with nitrogen and burgundy or orange with sulphur or phosphorus donors [31].

Solution spectra have been recorded for many of the more soluble adducts and in some cases reflectance spectra or single crystal polarised absorption spectra have been obtained.

The electronic spectrum of rhodium(II) acetate in water consists of two weak bands in the visible region, band I (ca. 600 nm), and band II (ca. 450 nm), with two stronger bands, III and IV, in the UV (ca. 250 nm (shoulder) and 220 nm respectively) [88,89]. Whereas band II remains constant, band I is strongly influenced by changes in the axial ligand [89,90] and shifts to lower wavelengths in the following sequence according to the donor atom.

$$O < S < N_{sp^3} < N_{sp^2} \approx As < \rangle S{=}O \text{ (S bonded)} \; [40,88]$$

Dubicki and Martin [89] found an almost linear correlation of Dq (cm^{-1}) values of axial ligands L ($L = I^-$, Br^-, Cl^-, H_2O, NCS^-, NH_3), obtained from data on Cr(III) compounds, with variation of band I energy. The position of other axial ligands was found to be consistent with the spectrochemical series, with the soft-acid character of Rh(II) being demonstrated by the high energy of band I for NO_2^-, Me_2SO and SO_3^{2-} adducts. Bands III and IV shift to higher wavelengths, the former more than the latter [89]. Figure 18 illustrates the change in the UV spectrum on replacing water by ammonia.

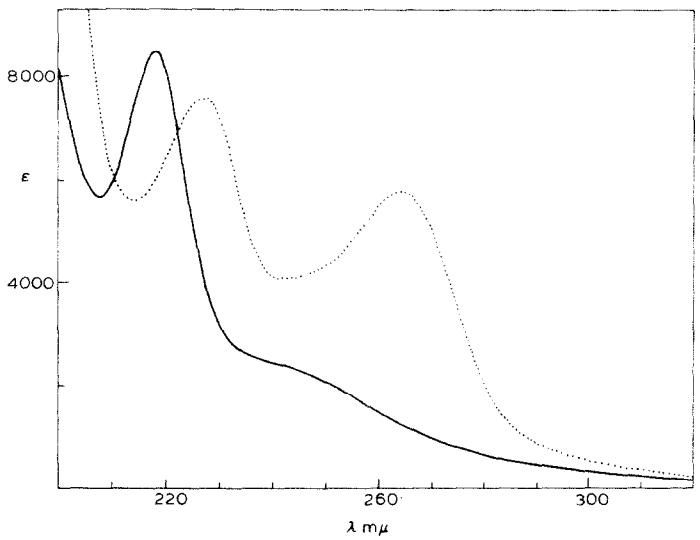

Fig. 18. The UV spectrum of rhodium(II) acetate monohydrate (full line) and its ammonia adduct (dotted line) in water. (The extinction coefficient ϵ is the "molar" extinction coefficient per monomer) (with permission from ref. 89).

Norman and Kolari have assigned bands I and II in the visible spectrum to the allowed transitions $\pi^* \rightarrow \sigma^*$ and $\pi^* \rightarrow$ Rh–O σ^* on the basis of the close match between calculated and experimental energies, and the observed axial ligand dependence of the band energies [9]. Norman et al. then performed explicit spin-polarised transition-state calculations of the excitation energies [10]. A comparison of experimental and calculated data is given

TABLE 5

Electronic spectral data for $[Rh_2(O_2CR)_4(H_2O)_2]$

D_{2h} transition	Type [a]	$[Rh_2(O_2CH)_4(H_2O)_2]$	$[Rh_2(O_2CMe)_4(H_2O)_2]$
		Calc. μm^{-1} (nm) [b,c]	Exp. μm^{-1} (nm) [d]
$6b_{3g}, 6b_{2g} \rightarrow 8b_{1u}$	$\pi^* \rightarrow \sigma^*$	1.97 (508)	1.71 (584)
$6b_{3g}, 6b_{2g} \rightarrow 5a_{1u}$	$\pi^* \rightarrow$ Rh–O σ^*	2.47 (405)	2.27(441)

[a] π^* and σ^* denote the Rh–Rh character of mainly Rh orbitals. Rh–O σ^* is Rh orbital of δ^* symmetry with respect to the Rh–Rh bond. [b] All spin and D_{4h} symmetry dipole-allowed transitions between 0.5 μm^{-1} (2000 nm) and 2.8 μm^{-1} (375 nm). [c] Ref. 10. [d] Ref. 91.

in Table 5. These assignments are supported by single-crystal polarized spectra of $[Rh_2(O_2CMe)_4(H_2O)_2]$ [92,93] (Figs. 19a and b).

The location of the Rh–Rh δ^* orbital just above the π^* implies that there should be a dipole-forbidden vibronically allowed transition just below the Rh–Rh $\pi^* \rightarrow$ Rh–Rh σ^* transition at 17300 cm^{-1} (578 nm) assigned to $\delta^* \rightarrow \sigma^*$ [10]. Martin et al. [92] were unable to extend their measurements below 15500 cm^{-1} (645 nm) because of the decrease in sensitivity of the detector in their spectrophotometer, but they suggested that there is evidence for such a weak transition in the diffuse-reflectance spectrum of rhodium(II) butyrate, where a weak shoulder appears at 14300 cm^{-1} (699 nm) on a peak at 16500 cm^{-1} (606 nm).

Band II also contains a weaker *z*-polarized component at a slightly lower energy than the *xy* polarized maximum; this has been assigned to $\delta^* \rightarrow$ Rh–O σ^* or $\delta \rightarrow \sigma^*$ [10].

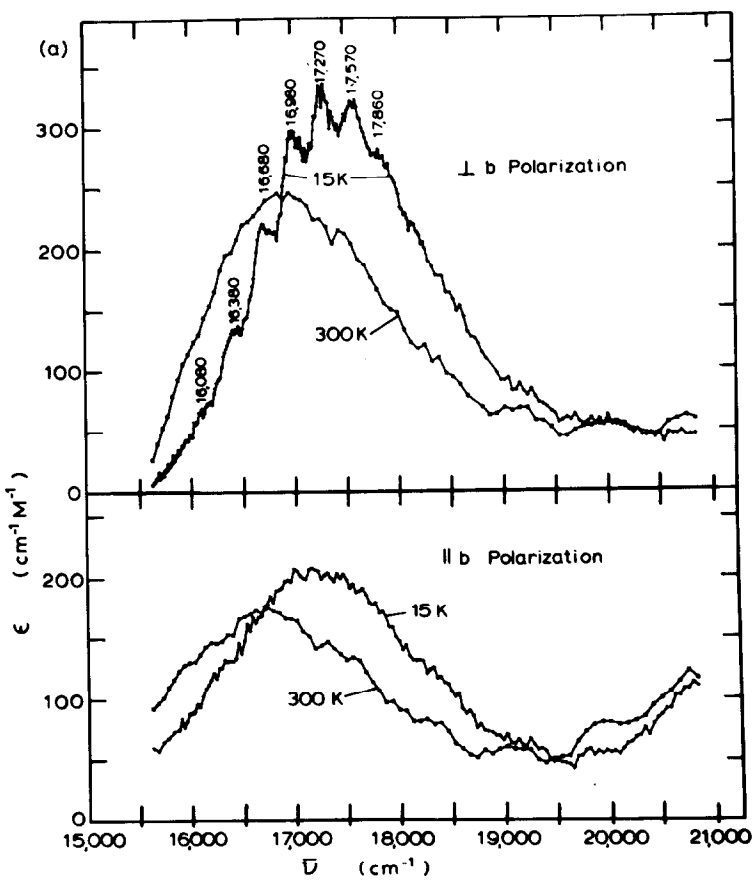

Fig. 19. (a) Polarized crystal spectra for the 17000 cm^{-1} (588 nm) band of $[Rh_2(O_2CMe)_4(H_2O)_2]$, crystal thickness (5.2 nm) (with permission from ref. 92).

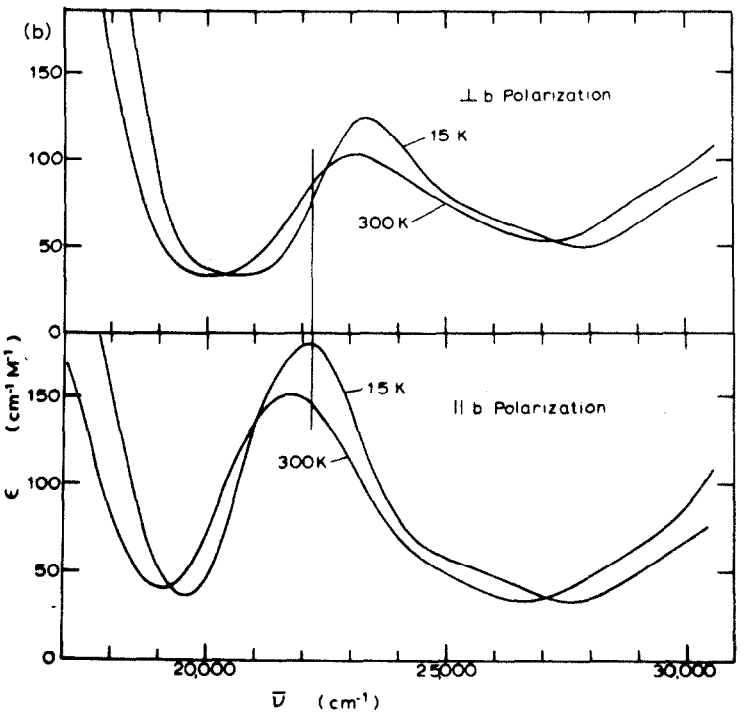

Fig. 19. (b) Polarized crystal spectra for the 22000–23000 cm^{-1} (455–435 nm) bands of $[Rh_2(O_2CMe)_4(H_2O)_2]$ crystal thickness (32 μm) (with permission from ref. 92).

Nine allowed transitions have energies fairly close to those of bands III and IV. However, only two of these should show the observed red shift as axial donor strength increases since it is only Rh–Rh σ type orbitals which are significantly elevated in energy by axial donors. Norman and Kolari [9] have thus assigned band III to $8a_g \rightarrow 8b_{1u}$ and band IV to $7a_g \rightarrow 8b_{1u}$. As expected from the considerable ligand to metal charge transfer in the predicted transitions, more for the second than the first, the intensities of bands III and IV are greater than for bands I and II, band IV being stronger than band III. The ground state energy difference for $7a_g \rightarrow 8b_{1u}$ (43800 cm^{-1}) is close to the experimental energy of band IV (45900 cm^{-1}). The low ground state value for $8a_g \rightarrow 8b_{1u}$, 29000 compared to 40000 cm^{-1} for band III is not surprising since this is essentially the Rh–Rh σ–σ^* transition, and thus should show very great ground to transition state relaxation [9]. These assignments of bands I, II and III parallel those of Dubicki and Martin [89]. There have been numerous reports on the electronic spectrum of $[Rh_2(O_2CMe)_4(H_2O)_2]$, Table 6.

TABLE 6

λ_{max} values (nm) for $[Rh_2(O_2CMe)_4(H_2O)_2]$ (aq)

I	II	III	IV	Ref.
587	447			31
584	441			88
ca. 600	ca. 450	250	218	89
585	440			91, 94
587	447			95

The electronic spectrum measured in aqueous or ethanolic solution has been found to be pressure dependent; shifts of 2 nm/1000 atm to higher energies have been recorded for the band near 600 nm [96].

Kitchens and Bear have studied the reflectance spectra of $[Rh_2(O_2CMe)_4L_n]$ (L = DMSO, Et_2S, $n = 2$, 1, 0) as a function of temperature and have correlated spectral changes with thermogravimetric data [70]. Spectroscopic data for the anhydrous rhodium(II) acetate and its mono and bis adducts obtained in this manner are given in Table 7.

The solution spectrum of $[Rh_2(O_2CMe)_4]^+$ has two bands analogous to those observed for the neutral species but shifted to slightly higher energies in accord with the comparative orbital and excitation energies calculated for $[Rh_2(O_2CH)_4(H_2O)_2]$ and $[Rh_2(O_2CH)_4(H_2O)_2]^+$. There is also an additional low-energy band at 12300–13100 cm^{-1} [9,10], which has been tentatively assigned to a $\delta \rightarrow \delta^*$ transition ($9a_g \rightarrow 7b_{1u}$), made possible by the removal of one δ^* electron upon ionization [9,10]. Another possible assignment is $7b_{2,3u} \rightarrow 6b_{2,3g}$ ($\pi \rightarrow \pi^*$), if π^* rather than δ^* is the HOMO [9]. Norman and Kolari pointed out that an unambiguous prediction of the HOMO for the neutral rhodium(II) acetate or its monopositive cation is not

TABLE 7

λ_{max} values (nm) for $[Rh_2(O_2CMe)_4L_n]$

L_n	$\lambda_{I\,max}$	$\lambda_{II\,max}$
$(DMSO)_2$	497	sh
(DMSO)	555	ca. 437
$(Et_2S)_2$	541	ca. 425
(Et_2S)	555	ca. 425
–	617	442

possible due to the close spacing of the energy levels involved, and the difficulty in accurately defining the δ^* position [9].

Two bands in the electronic spectrum of the mixed acetate-β-diketonate compounds $[Rh_2(O_2CMe)_2(\beta\text{-diketonate})_2(H_2O)_2]$ are analogous to those in $[Rh_2(O_2CMe)_4(H_2O)_2]$ (ca. 600–550 and 420 nm); an additional band at ca. 360 nm has been assigned to a charge transfer transition between the metal and the β-diketonato ligand [52]. The electronic spectra of $[Rh_2(O_2CR)_2(N\text{–}N)_2L_2]$ (N–N = 1,10 phenanthroline, 2,2′-dipyridyl; L = Cl, Br) are also similar to that of rhodium(II) acetate in the visible region. Band I has been assigned to π^* $(5e_g) \rightarrow \sigma^*$ $(5a_{2u})$; the $\sigma^*(5a_{2u})$ orbital is directed to the outside of the molecule along the metal–metal bond; thus the position of this band is axial ligand dependent. The UV bands result mainly from transitions occurring within the N–N ligands [97].

The principal features of the electronic absorption spectra of the rhodium(II) salicylato complexes are broadly similar to those of other rhodium(II) carboxylates, with two weak absorption bands in the visible range of the spectrum at 16000–19000 cm^{-1} (625–526 nm) and ca. 22000 cm^{-1} (455 nm) and a distinct maximum at 45000 cm^{-1} (222 nm) with a shoulder at ca. 40000 cm^{-1} (250 nm) in the UV region. However, a distinctive feature of the electronic spectra of the rhodium(II) salicylates is the presence in the near UV range of an additional very intense band having a maximum at 32000–33000 cm^{-1} (313–303 nm). This extra absorption band has tentatively been assigned to a charge transfer transition between the rhodium and oxygen atom of the phenol group on the salicylate ligand [55]. However this assignment must be treated with caution since, as noted above, there is still uncertainty concerning the constitution of rhodium(II) salicylates.

The spectra of $[Rh_2(CO_3)_4]^{4-}$ and $[Rh_2(SO_4)_4]^{4-}$ are similar to that of rhodium(II) acetate [91,94] and analogous assignments have been proposed [9].

G. NUCLEAR MAGNETIC RESONANCE

Although the rhodium(II) carboxylates and many of their adducts are amenable to study by NMR, very little work has been reported in this area to date. The exchange of rhodium(II) acetate with excess trifluoroacetic acid has been followed by ^1H NMR spectroscopy with the intermediate compounds being identified by mass spectrometry [33] (see p. 162; see also p. 180, ref. 177). ^1H NMR has also been used to identify the donor site in ambidentate ligands; the coordination sites of the 1 : 1 adducts of adenine and adenosine have been investigated in this manner. On coordination the ligand proton situated adjacent to the metal binding site shows a downfield

shift relative to other protons present in the ligand; thus the large downfield shift observed for H(8) of adenosine upon coordination has been taken to indicate binding of the N(7) site to the metal. The adenine adduct was too insoluble for ^{1}H NMR data to be obtained, however the similarity of its properties to those of the adenosine adduct, suggests that here also bonding occurs through the N(7) atom (Fig. 20) [59].

In a similar ^{1}H NMR study, Pneumatikakis and Hadjiliadis [40] observed that both H(8) and H(2) shifted downfield on coordination of adenine derivatives and took this to indicate that both N(1) and N(7) sites are bound to rhodium(II) in a polymeric linking structure. In contrast, these authors noted that tetraacetyladenosine forms 1 : 2 adducts with rhodium(II) carboxylates (Fig. 21), presumably for steric reasons, in which both H(2) and H(8) show a single resonance at 8.93 ppm (cf. H(2) 8.76 ppm, H(8) 8.42 ppm for the uncomplexed ligand). Since H(8) shifted downfield by 0.51 ppm while H(2) shifted only by 0.17 ppm on coordination, they concluded that bonding occurs solely through the N(7) site.

Evans' NMR method [99,100] has been used to measure the magnetic susceptibility of $[Rh_2(O_2CMe)_4]^+$ at 35°C [91]. Values obtained are $\mu = 2.6 \pm 0.3$ BM (5.24×10^{-3} M solution in trifluoromethylsulphonic acid), $\mu = 2.1 \pm 0.4$ BM (7.22×10^{-3} M solution in trifluoromethylsulphonic acid).

A multinuclear NMR study of the rhodium(II) carboxylate–trimethylphosphite adducts indicates that at ambient temperature the complexes are partially dissociated and that there is rapid exchange of dissociated and bound trialkylphosphite leading to loss of internuclear coupling in the ^{1}H, ^{13}C and ^{31}P spectra. On cooling the mixture the exchange processes are frozen and spin-spin splitting patterns consistent with the presence of mono- and bis-adducts develop. Thus the ^{31}P{^{1}H} spectra of the species

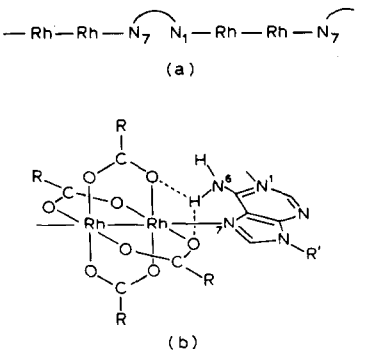

Fig. 20. (a) The proposed polymeric structure of rhodium(II) acetate–adenine complex. (b) Proposed intramolecular H bonding between the amino N at C(6) and the acetato oxygen in the monoadduct of adenine (with permission from ref. 59).

"$[Rh_2(O_2CMe)_4\{P(OMe)_3\}_2]$" obtained at 213 K consists of the X portion of an AMX pattern attributable to the mono-adduct $[Rh_2(O_2CMe)_4\{P(OMe)_3\}]$and the XX' part of an AA'XX' pattern due to the

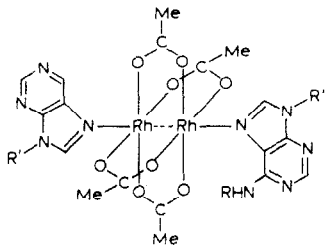

R = acetyl
R' = 2,3,5,-*O*-triacetyl-β-D-*ribo*-furanosyl,

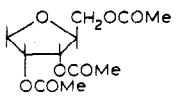

Fig. 21. Proposed structure for rhodium(II) acetate tetraacetyladenosine (with permission from ref. 40).

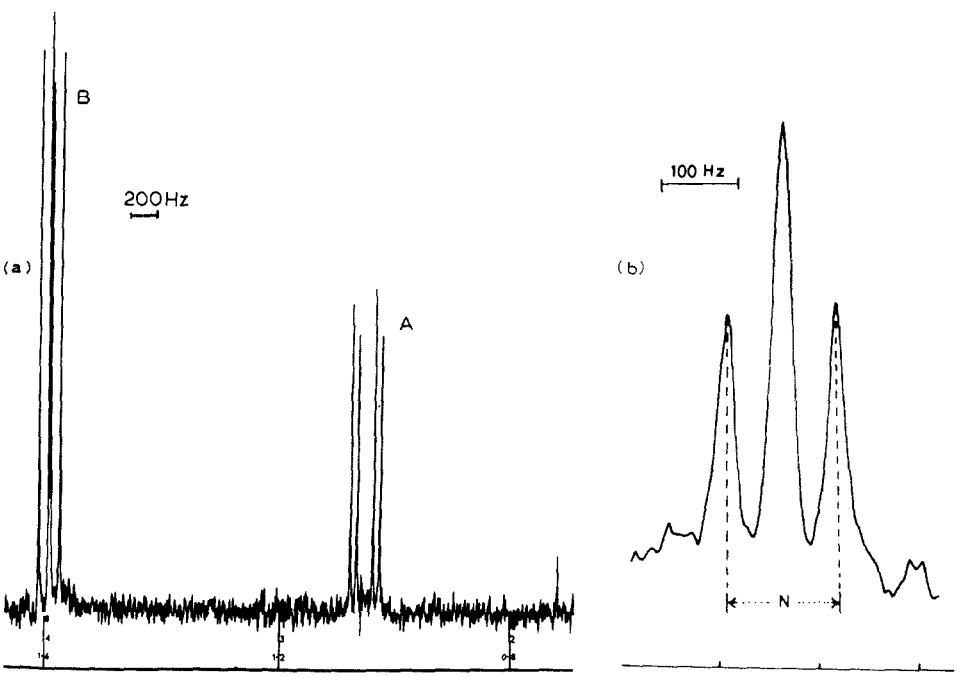

Fig. 22. (a) ^{31}P NMR spectrum of "$[Rh_2(O_2CMe)_4\{P(OMe)_3\}_2]$" (36.4 MHz) in CD_2Cl_2 at 213 K; signals A and B are attributed to mono- and bis-adducts respectively. (b) ^{103}Rh NMR spectrum (12.6 MHz) of $[Rh_2(O_2CMe)_4\{P(OMe)_3\}_2]$ in CD_2Cl_2 at 213 K.

bis adduct [A,A',M = ^{103}Rh; X, X' = ^{31}P] (Fig. 22a). The possibility that a water molecule occupies the second coordination site in the mono-adduct has not been excluded. Direct observation of the ^{103}Rh signal from $[Rh_2(O_2CMe)_4\{P(OMe)_3\}_2]$ has also been achieved (Fig. 22b). Analysis of these spectra gives the coupling constants $^1J(^{31}P, ^{103}Rh)$ 151.4 Hz and $^2J(^{31}P, ^{103}Rh)$ 43.9 Hz for the mono-adduct (signs of J unknown) and $^1J(^{31}P, ^{103}Rh)$ 134.1 Hz, $^2J(^{31}P, ^{103}Rh)$ −1.5 Hz, $^3J(^{31}P, ^{31}P)$ 853.7 Hz, and $^1J(^{103}Rh, ^{103}Rh)$ 7.9 Hz for the bis-adduct (signs of J are relative) [101a].

The large chemical shift difference of ca. 50 ppm between ^{31}P resonances of mono- and bis-adducts, prompted a study of the mixed products $[Rh_2(O_2CMe)_4\{P(OMe)_3\}L]$. These species were prepared in solution by mixing a 1 : 1 mole ratio of $[Rh_2(O_2CMe)_4\{P(OMe)_3\}_2]$ and axial ligand L in the NMR solvent and their NMR spectra were recorded at 213 K to eliminate ligand exchange phenomena. Data collected for a variety of neutral ligands L gave a good linear plot for δ(P) against $^2J(^{103}Rh, ^{31}P)$, Fig. 23; the ligand sequence arising from this plot appears to constitute a *trans*-influence series [101b]. A systematic change in the ^{31}P chemical shift as a function of

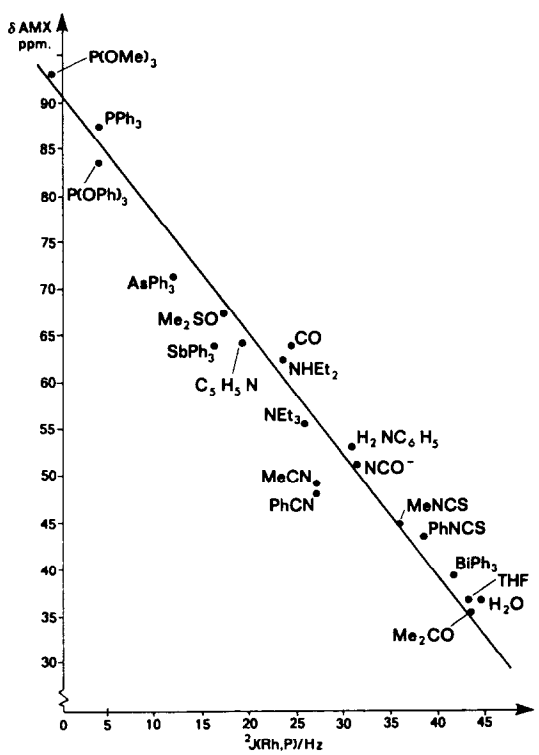

Fig. 23. Plot of ^{31}P chemical shift δ(AMX) ppm of $[Rh_2(O_2CMe)_4\{P(OMe)_3\}L]$ vs. ^2J(RhP) Hz.

the *trans* ligand L has previously been noted for mononuclear complexes (for examples see ref. 103) but to the best of our knowledge the rhodium system mentioned here provides the first example of a *trans* influence series operating across a binuclear metal centre.

H. ELECTRON SPIN RESONANCE

ESR has been used to study the electronic structure of the rhodium(II)/(III) species $[Rh_2(O_2CR)_4L_2]^+$ and the nitroxide radical adducts of rhodium(II) trifluoroacetate $[Rh_2(O_2CCF_3)_4L]$ L = 2,2,6,6-tetramethylpiperidine-*N*-oxyl (TMPNO), Fig. 24. An attempt to study the anion radicals, i.e. the Rh(I)/(II) species $[Rh_2(O_2CR)_4L_2]^-$, by ESR was unsuccessful [104] since the anions generated electrochemically proved too susceptible to further reduction [105]. The cation radicals $[Rh_2(O_2CR)_4(PR'_3)_2]^+$ (R = Et, CF_3; $PR'_3 = PPh_3$, $P(OPh)_3$, $P(OCH_2)_3CEt$) are readily generated electrochemically [35,36,106] and their ESR spectra have been reported [104,107] (see Table 8). A comparison of fluid and solid phase spectra of $[Rh_2(O_2CEt)_4(PPh_3)_2]^+$ shows that the anisotropic couplings of 15.1 ($\perp$ component) and 21.7 mT ($\parallel$ component) are due to a pair of equivalent nuclei of $I = \frac{1}{2}$ and that they have the same sign which is tentatively assumed to be positive. The isotropic and anisotropic parts of the couplings are $a = 17.3$ and $2b = 4.4$ mT, respectively. The coupling anisotropy is greater than that of ^{103}Rh with a $4d$ spin density of $\frac{1}{2}$ [108]. The largest triplet splitting has therefore been assigned to the pair of ^{31}P nuclei. The high unpaired spin density on the phosphorus atoms (total 53%) and the inequality of $a_{\parallel}(P) > a_{\perp}(P)$ are consistent with the odd electron orbital being assigned to the a_{1g} (in D_{4h}) orbital. This orbital has Rh–Rh $d\sigma$–$d\sigma$ bonding and Rh–P σ antibonding characteristics and corresponds to the $8a_g$ MO of

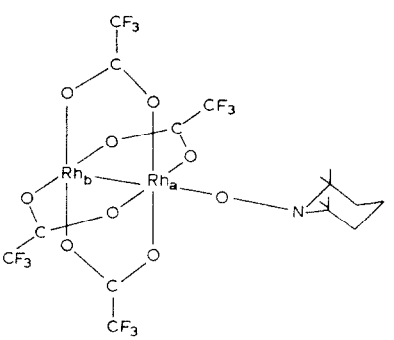

Fig. 24. Proposed structure for the rhodium(II) trifluoroacetate-TMPNO adduct (with permission from ref. 109).

TABLE 8

ESR data for $[Rh_2(O_2CR)_4(PR'_3)_2]^+$ species [104]

R	PR'_3	$g_{\parallel}$	$g_{\perp}$	$10^4 A_{\parallel}$(P) (cm^{-1})	$10^4 A_{\perp}$ (P) (cm^{-1})	$10^4 \lvert A_{\parallel}(Rh)\rvert$ (cm^{-1})	$10^4 \lvert A_{\perp}$(Rh)$\rvert$ (cm^{-1})
Et	PPh_3	1.996	2.148	(+) 205	(+) 152	13	a
Et	$P(OPh)_3$	2.001	2.174	(+) 342	(+) 309	17	a
Et	ETPB [c]	1.995	2.203	(+) 346	(+) 315	20 ± 2	a
CF_3	PPh_3	2.003	2.088	(+) 212	(+) 142	13.3	a
CF_3	$P(OPh)_3$	2.002	2.127	(+) 342	(+) 294	17.6	< 8 [a,b]
CF_3	ETPB [c]	2.003	2.154	(+) 373	(+) 324	20.3	< 8 [a,b]

[a] Not resolved. [b] Estimated from the line width. [c] ETPB = 4-ethyl-2,6,7-trioxa-1-phosphabicyclo[2.2.2]octane.

$Rh_2(O_2CH)_4(H_2O)_2$ calculated by Norman and Kolari using SCF–Xα–SW methods [9]. The ESR results are thus consistent with a single Rh–Rh bond, with the *trans* effect of the axial ligand on the Rh–Rh bond arising from interactions between σ lone pairs on the axial ligands and σ Rh–Rh and σ^* Rh–Rh molecular orbitals [9].

The ESR spectra of $[Rh_2(O_2CCF_3)_4L]$ (L = TMPNO) [109] have been observed at *X*- and *Q*-band frequencies, Fig. 25. In the X-band spectrum (Fig. 25a) the intense triplet at $g = 2.005$ has been assigned to uncomplexed TMPNO, while the doublet at lower field is thought to be due to two of the three lines for the complexed radical, the third line being hidden under the central line of the free nitroxide. The *Q*-band spectrum is of more use since the two species give well separated signals (Fig. 25b). Three sets of 1 : 1 : 1 triplets are evident; the intense high field triplet $g = 2.0052(1)$ is assigned to

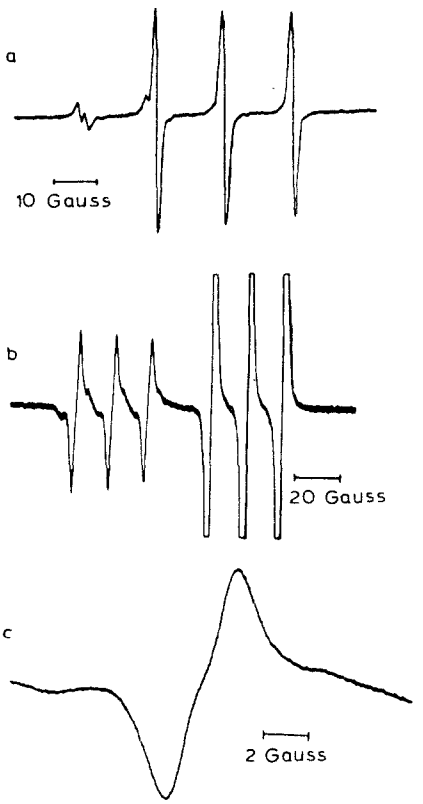

Fig. 25. (a) *X*-band and (b) *Q* band ESR spectra of toluene solution saturated in rhodium trifluoroacetate and ca. 10^{-3} M in TMPNO. Magnetic field increases to the right. (c) Expansion of the lowest-field *Q*-band line of bound nitroxide showing the hyperfine splitting assigned to Rh ($I = \frac{1}{2}$). (with permission from ref. 109).

free TMPNO, the second most intense triplet ($g = 2.0150$) is assigned to the nitroxide in the rhodium–trifluoroacetate adduct, and an additional weak broad line triplet in the same region as the bound nitroxide is thought to be due to some precipitated rhodium trifluoroacetate nitroxide adduct. The g-value shift calculated from $\Delta g = g(\text{bound}) - g(\text{free}) = -(\Delta H/H)g$ (free) using free nitroxide as an internal reference is given as 0.00984(1). The observed shift has been attributed to both spin-orbit coupling with the rhodium and to electron redistribution within the nitroxide upon complexation. Using $\Delta g_{obs} = 0.00984$ and $\Delta g_{NO} = -0.0004$, a value of 0.0102 is obtained for the g shift due to spin orbit coupling with the rhodium. The spectrum also features a rhodium hyperfine coupling (1.7 ± 0.2 G) to one of the rhodium nuclei (Fig. 25c), of which ca. -0.4 G has been assigned to the nuclear spin-orbit interaction and the rest (2.1 G) to Fermi contact coupling via spin polarisation. The results have been interpreted in terms of σ donation from a lone pair on the nitroxide oxygen into the Rhd_{z^2} orbital with back donation from the Rhd_{xz} orbital into the π^* nitroxide orbital containing the unpaired electron: the authors noted that the observed rhodium hyperfine coupling arises from a single rhodium atom, although the σ^* orbital is equally composed of both in the parent trifluoroacetate complex. A hyperfine splitting from a second non-equivalent rhodium about one-third the size of that observed for the first would not be detected. Setting a limit of this order indicates substantially different contributions

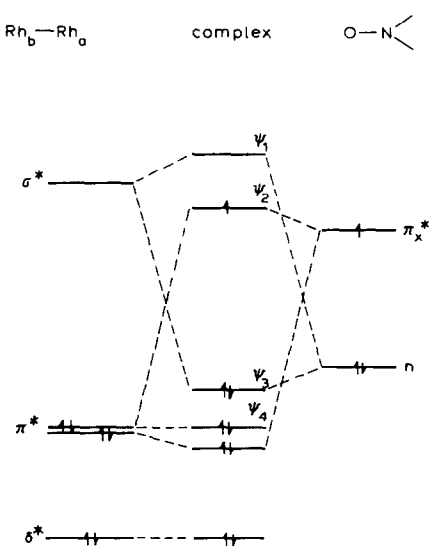

Fig. 26. Qualitative MO diagram of $[Rh_2(O_2CCF_3)_4TMPNO]$. MOs ψ_1 through to ψ_4 make the major contributions in the analysis (with permission from ref. 109).

TABLE 9

Rh3$d_{5/2}$ binding energies (eV) for selected rhodium(II) carboxylates and related compounds

	$Rh_2(O_2CR)_4L_2$				
L	R = H	Me	t-Bu	Ph	CF_3
		308.2 [110]		309.3 [78]	
		308.5 [111]			
H_2O	309.1 [112]	309.2 [112,113]			
C_5H_5N	309.1 [112]	309.2 [77,112,113]	308.8 [112]	309.0 [78]	309.6 [112]
		308.5 [110]		309.2 [112]	
NH_3		309.2 [55,113]			
$(H_2N)_2CS$	309.2 [112]	309.3 [113]		309.0 [78,112]	
		308.4 [110]			
		309.0 [112]			
Me_2SO	309.1 [112]	308.5 [110]		309.1 [78,112]	310.1 [112]
		309.2 [112]			
C_2H_5OH			309.2 [112]		
PPh_3		309.1 [112]			310.2 [112]
		308.0 [110]			310.0 [112]
Cl	309.3 [55,112]	309.3 [112]			

L	$Rh_2(O_2CR)_4L_2$			$Rh_2(OSCR)_4L_2$	
	R = CCl_3	o-$C_6H_4O(H)$	o-$C_6H_4S(H)$	R = Me	Ph
–				308.9 [77]	308.8 [78,112] 308.9 [77]
H_2O		309.7 [55]	309.6 [113]	308.7 [77] 308.8 [112]	
C_5H_5N	309.4 [112]	309.3 [55]		308.4 [77,112]	308.7 [112]
NH_3		309.6 [55]			
$(H_2N)_2CS$		309.3 [55]		308.5 [77,112]	308.6 [78,112]
Me_2SO				308.7 [77,112]	308.8 [78,112]
C_2H_5OH	309.7 [112]		309.5 [113]		
PPh_3					
Cl				308.7 [77,112]	

from the two rhodium atoms in the acceptor molecular orbital of the very weak adduct formed with the nitroxide. This result has been explained in terms of a molecular orbital diagram for the 1 : 1 adduct (Fig. 26). The result indicates a larger contribution from Rh(a) leading to a doublet, with the contribution from Rh(b) being too small to be observed. A greater overlap of Rh(a) than Rh(b) with the nitroxide lone pair yields non equivalent rhodium atoms in the MO ψ_3. Likewise the orbital on the ligand containing the unpaired electron is mainly N–O π^* but is mixed slightly with $4d_{xz}$. The overlap of the oxygen p_x with the rhodium(a) d_{xz} orbital leads to non-equivalent rhodium contributions to MO ψ_2. This places the odd electron directly into a metal d orbital which is reported [108] to give rise to a negative coupling constant. This rhodium character gives the unpaired electron some orbital angular momentum, which is responsible for the shift in the g value and the nuclear spin-orbital contribution to the rhodium hyperfine.

I. X-RAY PHOTOELECTRON SPECTROSCOPY

Much effort has been expended in the collection of X-ray photoelectron spectroscopy (ESCA) data, particularly by Russian workers, but interpretation of the results has been largely restricted to the confirmation of the oxidation state of the rhodium by an investigation of the 3d core electron binding energies [110] (Fig. 27). The Rh3$d_{5/2}$ binding energy in all simple aliphatic carboxylates studied is ca. 309.2 eV and lies midway between the

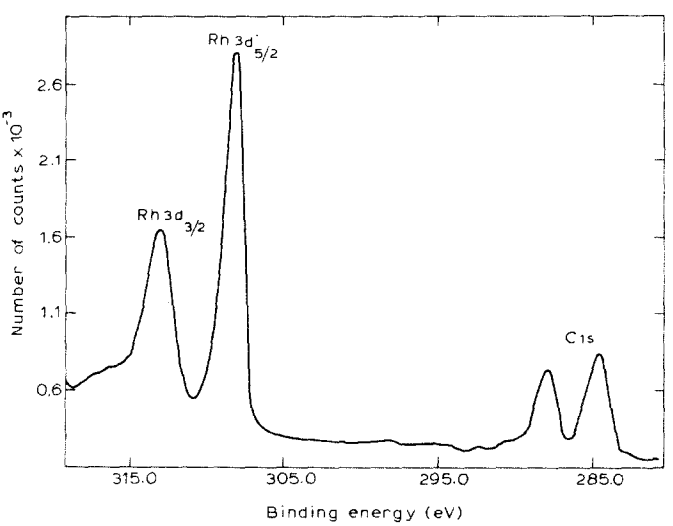

Fig. 27. X-ray photoelectron spectra of $Rh_2(O_2CMe)_4$ between 280 and 320 eV (with permission from ref. 111).

values typical of complexes of rhodium(I) (ca. 308.5 eV) and rhodium(III) (ca. 310.7 eV). Attempts to use ESCA data as a means of measuring axial ligand donor strength have failed, due to the relative insensitivity of the Rh3$d_{5/2}$ binding energy to the nature of the axial ligand, L, [112,113]. From Table 9 it can be seen that the variation of the binding energy with L is within the experimental error.

ESCA data have yielded information on the *trans* influence of the Rh–Rh bond [113,114]. The metal–metal bond in d^7–d^7 complexes of Rh(II) weakens the rhodium axial ligand bond, in turn decreasing the inner shell electron binding energies of the axial ligands. For neutral donor ligands this weakening of axial metal–ligand bonding is revealed by a decrease in electron density transfer from ligand to metal; thus the inner binding energies for the ligand donor atom are lower for these Rh(II) complexes than for mononuclear rhodium compounds (Table 10). Likewise for anionic ligands the ionic character of metal–axial ligand is enhanced and the binding energies of ligand inner electrons decrease tending to values which are characteristic of ionic salts [113,114] (Table 11). Similar results have been found for rhodium(II) thioacetate adducts [77].

The Rh3$d_{5/2}$ value (ca. 309 eV) for $[Rh_2(O_2CR)_4]$ does not vary significantly with changes of the hydrocarbon group R. However, halogen-substituted groups withdraw electron density from the rhodium atoms; thus for rhodium(II) trifluoroacetate the Rh3$d_{5/2}$ value approaches the values for rhodium(III) complexes. This marked increase in the Rh3$d_{5/2}$ value (ca. 1 eV) is not matched by changes in the Rh–Rh bond length (which is approximately the same for rhodium(II) acetate and trifluoroacetate), but is reflected in significant differences in the properties of the trifluoroacetate relative to other rhodium(II) carboxylates; e.g. DMSO is coordinated through

TABLE 10

Inner binding energies (eV) for axial ligand donor atoms in $[Rh_2(O_2CR)_4L_2]$(L = Py, DMSO or thiourea) [114]

Compound	Ligand L and energy level		
	Py N 1*s*	DMSO [a] S 2*p*	Thiourea S 2*p*
Ligand in Rh(III) complex	400.2	167.1	163.1
$[Rh_2(O_2CH)_4L_2]$	399.7	166.5	162.4
$[Rh_2(O_2CMe)_4L_2]$	399.8	166.5	162.4

[a] S coordination.

TABLE 11

Inner binding energies (eV) for axial ligand donor atoms in $M_2[Rh_2(O_2CR)_4X_2]$ (X = Cl, Br, NO_2) [112,114]

Compound	Ligand X and energy level		
	Cl Cl 2*p*	Br Br 3*d*	NO_2 N 1*s*
Ligand in Rh(III) complex	198.8	69.4	404.3
$M_2[Rh_2(O_2CMe)_4X_2]$	198.1	68.9	403.6
$M_2[Rh_2(O_2CH)_4X_2]$	198.1	68.9	403.5

O in $[Rh_2(O_2CCF_3)_4$ (DMSO)] and through S in other carboxylates and thiocarboxylates [112].

X-ray and X-ray photoelectron spectra have been used to investigate the electronic structure of the anion $[Rh_2(O_2CMe)_4Cl_2]^{2-}$. Correlation between data for this anion and $RhCl_6^{3-}$ has been taken to indicate a structure with a rhodium–rhodium bond order close to unity, with weak Rh–Cl interactions and a large negative charge on the chloride atoms [115,116].

The oxidised complex $[Rh_2(O_2CMe)_4]^+ClO_4^-$ shows only a single $Rh3d_{5/2}$ peak [111], which implies the rhodium atoms are identical within the time scale of X-ray photoelectron spectroscopic measurements. The increase in $Rh3d_{5/2}$ binding energy (310.1 eV) compared with that for the neutral compound $[Rh_2(O_2CMe)_4]$ (308.5 eV) is consistent with the increase in positive charge in converting Rh(II) to Rh(II)/(III). A single O 1*s* peak [111] indicates equivalent oxygen atoms, implying equivalency of the two rhodium atoms to which they are bound, and a shift of 0.5 eV of the O 1*s* binding energy from 531.7 eV for $[Rh_2(O_2CMe)_4]$ to 532.2 eV for the oxidised species, indicates a stronger interaction of the bridging carboxylates with the two rhodium atoms.

J. ELECTRONIC STRUCTURE

There has been much controversy concerning the nature of the axial rhodium–rhodium and rhodium–ligand bonds in d^7–d^7 rhodium(II) carboxylates. The initial report of the crystal structure of $[Rh_2(O_2CMe)_4(H_2O)_2]$ proposed a single rhodium–rhodium bond [4], however, Cotton and co-workers felt that the unusually short rhodium–rhodium distance revealed by their more accurate structure determination indicated a triple bond [34,117] with electronic configuration $\sigma^2\pi^4\delta^2\sigma_n^2\sigma_n'^2\delta^{*2}$ [12], where rhodium

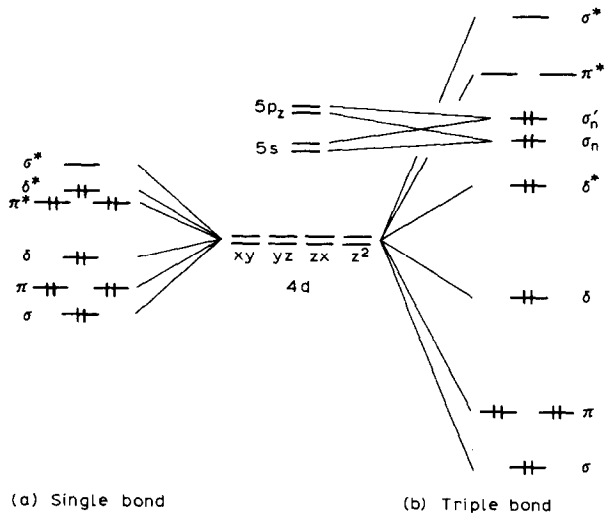

Fig. 28. A schematic description of the single and triple bond models for Rh–Rh in $[Rh_2(O_2CR)_4]$ (with permission from ref. 104).

lone pair orbitals (σ_n and σ_n') directed away from the intermetallic bonding zone and consisting mainly of $5s$ and $5p_z$ atomic orbitals * are embedded among the $4d$ levels [104]. Extended Hückel calculations by Dubicki and Martin which gave an electronic configuration of $\sigma^2\pi^4\delta^2\delta^{*2}\pi^{*4}$, were consistent with the single bond, and with the changes in the electronic spectrum observed upon replacing the axial water molecules with stronger donor ligands [89]. Norman and Kolari [9] reported SCF–Xα–SW calculations for $[Rh_2(O_2CH)_4(H_2O)_2]$ and found the electronic configuration $\sigma^2\pi^4\delta^2\pi^{*4}\delta^{*2}$ (Fig. 28a) in which d–d bonding interactions are not as large as the energy separation between $4d$ and $5s$–$5p$ levels, and π^* MOs are occupied [104]. In this model the σ_n and σ_n' orbitals, which are described as essentially non-bonding $p_z d_{z^2}$ hybrids, are much too high in energy to be occupied [10]. This configuration is indicative of a single metal–metal bond (Fig. 29); moreover the calculated ordering of levels appeared to be completely consistent with the experimental electronic spectrum. More recently Kawamura and co-workers have calculated the electronic structures of $[Rh_2(O_2CR)_4L_2]$ by an ab initio SCF–MO method with an STO–3G basis set and have concluded the electronic configurations are $\pi^4\delta^2\pi^{*4}\delta^{*2}\sigma^2$ for L = free, H_2O, NH_3 and $\delta^2\pi^4\pi^{*4}\delta^{*2}\sigma^2$ for L = PH_3 [122]. Likewise, Bursten and Cotton [118] con-

* The non-bonding orbitals (σ_n and σ_n') have also been described as $p_z d_{z^2}$ hybrids (see below).

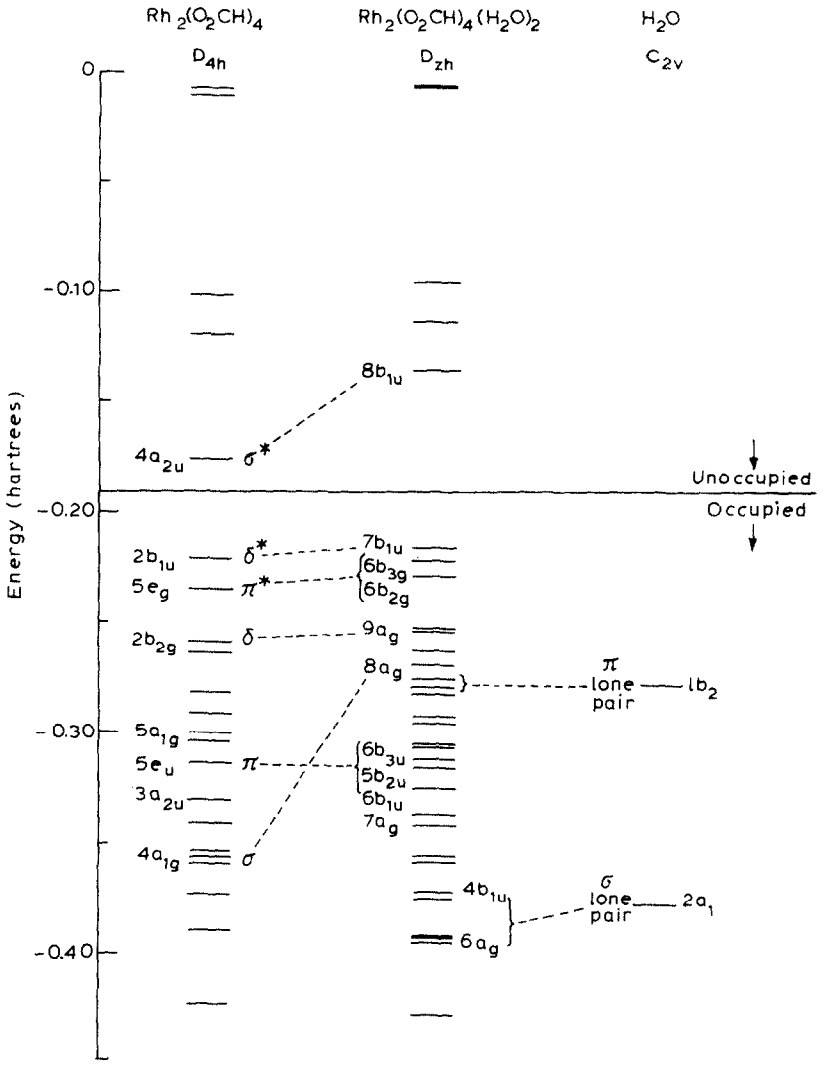

Fig. 29. SCF energy levels calculated by Norman and Kolari [9] for $[Rh_2(O_2CH)_4]$, $[Rh_2(O_2CH)_4(H_2O)_2]$ and H_2O above -0.49 Hartree (with permission from ref. 9).

cluded that the HOMO is σ for $L = PH_3$. It is now widely accepted that the metal–metal bond is single; however this conclusion does not adequately explain the shortness and strength of the Rh–Rh bond. To overcome this problem Christoph and Koh have suggested that the Rh–Rh bond is strengthened by extensive mixing of rhodium and bridging ligand orbitals and by mixing of higher lying empty orbitals into the ground state MOs for

the complex [8]. The total energy of the assembly is lowered by interaction of the filled orbitals with the higher empty levels (Rundle interactions); the levels are rehybridized so as to make the antibonding orbitals more diffuse and the bonding orbitals more concentrated in the region between the rhodium atoms (Fig. 30). Such effects have prompted Christoph and Koh to comment that the formal bond order does not necessarily reflect the true nature of the bonding in such compounds, and is thus probably not a useful index of the metal–metal interaction [8]. Norman and Kolari have noted the increase in Rh–Rh bond lengths for the series of closely related complexes $[Rh_2(O_2CMe)_4(PPh_3)_2]$, $[Rh_2(O_2CMe)_2(dmg)_2(PPh_3)_2]$ and $[Rh_2(dmg)_4(PPh_3)_2]$ (2.45, 2.62 and 2.94 Å respectively), in which bridging acetate ligands are progressively replaced by chelating dmg ligands (Fig. 31) and suggested that the constraints of the carboxylate bridging ligands may

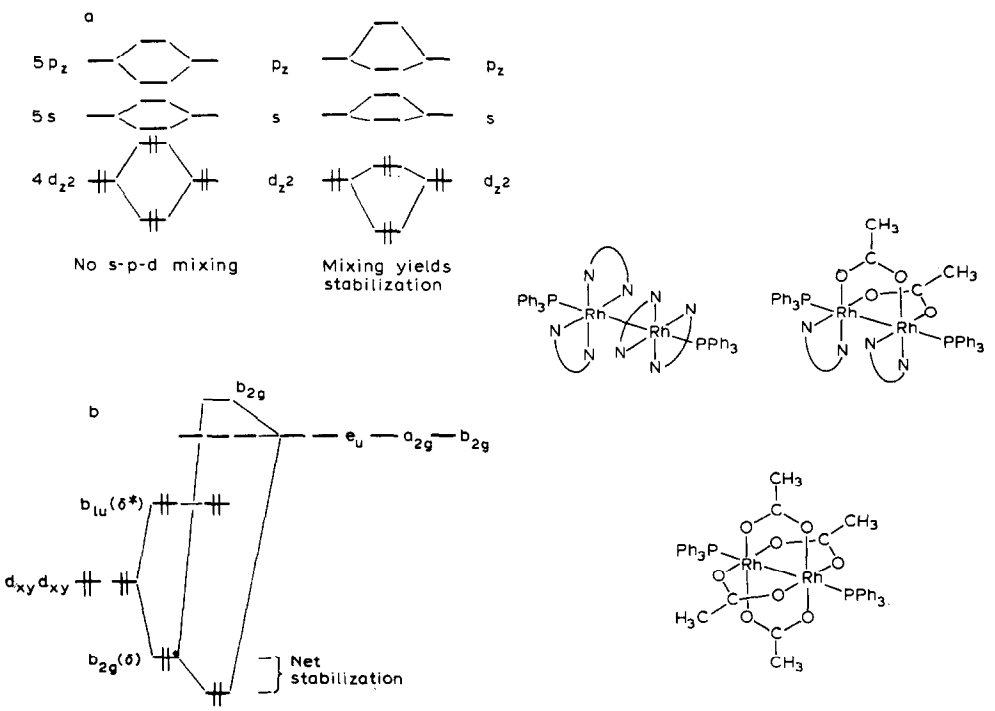

Fig. 30. (a) Rundle interactions or configuration mixing of empty higher lying *s* and *p* orbitals into filled valence levels stabilizes the metal–metal bond even when no formal bond exists. (b) Similar mixing of empty ligand levels with metal–metal valence levels can also lead to bond stabilization in a formal no-bond situation (with permission from ref. 8).

Fig. 31. $[\{Rh_2(dmg)_4\}(PPh_3)_2]$, $[\{Rh_2(dmg)_2(O_2CMe)_2\}(PPh_3)_2]$ and $[\{Rh_2(O_2CMe)_4\}(PPh_3)_2]$.

have a major influence in reducing the Rh–Rh bond length [9]. However, the presence of metal–metal bond lengths between 2.09 and 2.72 Å in carboxylates of the form $[M_2(O_2CR)_4]$ indicates that this is unlikely to be the case [8,9].

A similar discrepancy exists for the cations; the short rhodium–rhodium distance found by X-ray diffraction studies for $[Rh_2(O_2CMe)_4(H_2O)_2][ClO_4]$ (2.3165 Å) [36] was taken to indicate a bond order of 3.5 for the cation, on the basis of Cotton and co-workers' original electronic configuration for the neutral species $[Rh_2(O_2CMe)_4(H_2O)_2]$ [34,117]. The half-filled antibonding δ^* orbital only partially nullified the bonding effects of the δ orbital and the Rh(II)/Rh(III) bonding set of orbitals was given by $a_{1g}{}^2(\sigma)$, $e_u^4(\pi)$, $b_{2g}{}^2(\delta)$, $b_{1u}^1(\delta^*)$ [36]. Norman and Kolari [9] calculated an electron configuration of $\sigma^2\pi^4\delta^2\pi^{*4}\delta^{*1}$ for $[Rh_2(O_2CMe)_4(H_2O)_2]^+$, however a recent ESR study by Kawamura and co-workers [104,107] has shown that the singly occupied orbitals of the cation with phosphorus axial donor ligands have σ symmetry and the Rh–Rh bond is essentially single. Electronic configuration calculations by these authors are consistent with this result.

The nature of the axial metal–ligand bond is still a matter of controversy [44,118]. It is generally accepted that the Rh–Rh bond exerts a considerable *trans* influence which gives rise to unusually long axial Rh–L bonds. Thus the values of 2.310(3) Å and 2.418(3) Å for the Rh^{II}–OH_2 and Rh^{II}–$P(OPh)_3$ are ca. 0.28 Å longer than the comparable Rh–L bonds in mononuclear rhodium(I) and rhodium(III) complexes (Table 12). The *trans* influence of the Rh–Rh bond has been attributed by Norman and Kolari to the exceptionally strong σ-component of the Rh–Rh bond which means that the ligand lone pair must go into the high lying Rh–Rh σ^* orbital [9]. The energy match between the donor and acceptor levels is poor; thus weak and inefficient Rh–L interactions leading to abnormally long Rh–L bonds result. As the ligand donor levels approach that of the Rh–Rh σ^* level, the energy match and the orbital mixing improves, resulting in stabilization and shortening of Rh–L and destabilization and lengthening of the Rh–Rh bond [8]. Christoph and Koh [8] looked at the variation of the Rh–Rh distance along the series $[Rh_2(O_2CMe)_4L_2]$ (L = H_2O, Py, $NHEt_2$, CO, PF_3, $P(OPh)_3$); they proposed an energy level scheme (Fig. 32) with both π^* and π orbitals filled, but with $\pi(6e_u)$ higher than $\pi^*(5e_g)$ in energy; thus the ordering of the Rh–Rh bond distances required significant back donation to CO and PR_3 from Rh–Rh π orbitals. In a more recent publication [61] they have compared structural data for the complexes $[Cr(CO)_5L]$ and $[Rh_2(O_2CMe)_4L_2]$ (L = $P(OPh)_3$ and PPh_3) and have noted that bond lengths in the latter complexes cannot be rationalised in terms of Rh–P π-bonding interactions. Data for the chromium complexes (L = $P(OPh)_3$; Cr–P = 2.309(1) Å, Cr–CO(*trans*) = 1.861(4) Å: L = PPh_3; Cr–P = 2.422(1)

TABLE 12

Structural parameters for binuclear dirhodium and mononuclear Rh(I) or Rh(III) complexes

L	pK_b	Rh–Rh (Å)	Rh–L [b] (Å)	Rh(I)–L [a] (Å)	Rh(III)–L [a] (Å)
OH_2	15.7	2.3855(5)	2.310(3)		2.03(1)
Py	8.6	2.3963(2)	2.227(3)	2.107(8)	2.06(1)
					2.09(2)
					2.12(1)
$NH(Et)_2$	2.9	2.403(3)	2.308(3)		2.07(1)
C≡O		2.4196(4)	2.092(4)	1.82(2)	1.89(1)
PF_3		2.430(3)	2.42(1)	2.155(9)	
$P(OPh)_3$ [c]		2.445(1)	2.418(3)	2.142(3)	
PPh_3 [c]	11.3	2.449(2)	2.479(4)	2.290(4)	2.338(4)
					2.378(2)
					2.375(5)
$P(OMe)_3$	~10.5	2.4555(3)	2.437(5)		2.199(5)

[a] Ref. 8 and references therein; details of the selection of Rh(I) and Rh(III) values given in ref. 8. Where possible, the values given for Rh(I)–L and Rh(III)–L, are for complexes in which L is bonded *trans* to L. [b] In all cases the Rh–L bond in the dirhodium complexes is at least 0.1 Å greater than in the corresponding mononuclear Rh(I) or Rh(III) compounds, however this *trans* influence is less marked than in the quadruply bonded dimolybdenum system. [c] Rh–Rh, Rh–L distances are from preliminary X-ray diffraction measurements [8]; see ref. 61 for refined data.

Å, Cr–CO(*trans*) = 1.844(4) Å) are qualitatively consistent with the expectation that $P(OPh)_3$ is a better π-acceptor ligand than PPh_3. However, for the rhodium complexes (L = $P(OPh)_3$; Rh–P = 2.412(1), Rh–Rh = 2.4434(6) Å: L = PPh_3; Rh–P = 2.477(1), Rh–Rh = 2.4505(2) Å) the situation is more ambiguous. The Rh–P bonds show the expected lengthening (ca. 0.15–0.25 Å) due to the *trans* influence of the Rh–Rh bond, but the differences in the Rh–Rh bond distance cannot be explained in terms of Rh–P π bonding effects. To counter the difficulty Christoph et al. [61] have suggested that the extraordinarily long Rh–P bonds have reduced the magnitude of the Rh–P π overlap to a level where the σ-component of the Rh–P bond is dominant. They then rationalise the differences in Rh–Rh bond lengths in terms of phosphorus ligand σ donor capacity and go on to suggest that a new explanation, which relies only upon σ-donor effects, must now be sought to account for the differences in Rh–Rh bond length found in the general class of compounds $[Rh_2(O_2CR)_4L_2]$ (L = hard or soft donor ligands). Norman et al. [10] propose the L $\sigma \rightarrow$ Rh–Rh σ^* donation to be stronger than the π-back donation for all the ligands and stronger for L = CO and PR_3 than

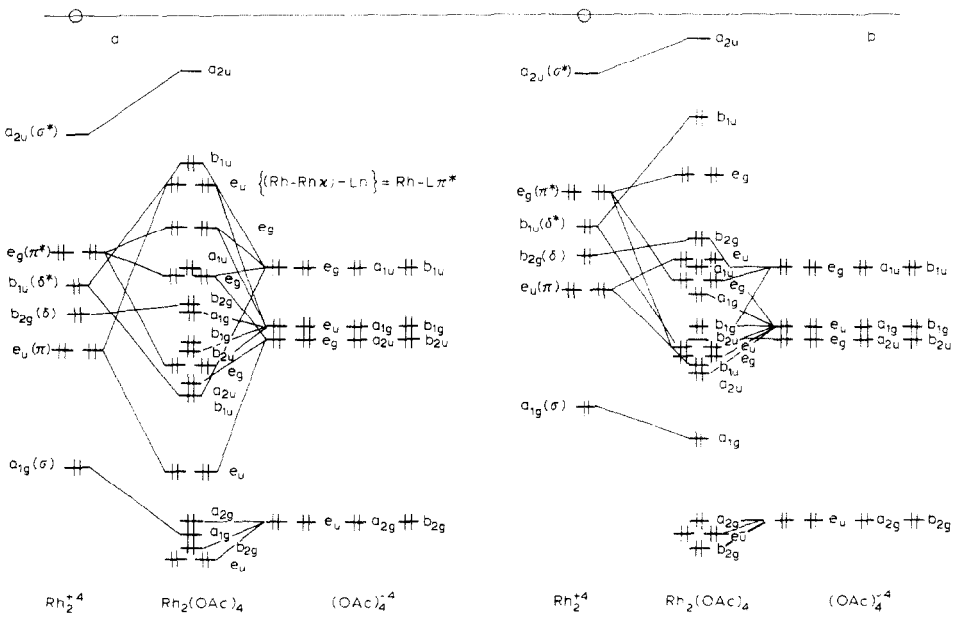

Fig. 32. Qualitative MO diagram showing the extensive mixing possible of the bridging carboxylate orbitals with those of the binuclear d^7–d^7 manifold. Carboxylate levels are indicated on the right in both (a) and (b) which have only the relative positions of the dimetal levels changed with respect to those of the carboxylate. The changes in position and ordering of the resultant MOs are illustrative of the great importance of the relative positioning of the contributing metal and ligand levels (with permission from ref. 8).

for $L = H_2O$, py and $NHEt_2$. They assigned $\pi < \pi^*$; thus the increasing rhodium–rhodium distance follows the order of increasing Rh–L σ covalent bond strength. The existence of the Rh–Rh bond requires that the Rh–Rh π^* orbital has more π donor ability and the Rh–Rh π orbitals less than normal. The π bonding orbital will have charge concentrated between the metals and thus away from the axial ligands, while its antibonding counterpart will have charge projected towards the ligands.

Drago et al. claim that metal–metal π interactions lead to π^*-back

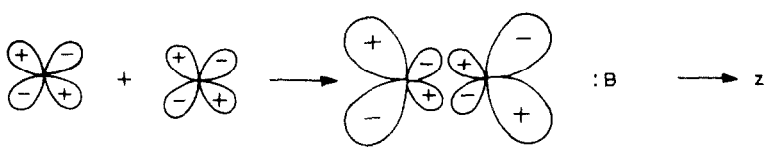

Fig. 33. Metal–metal π interactions leading to π^* interactions.

bonding (see Fig. 33) [106,119,120]. These authors measured ΔH_f for

$$[Rh_2(O_2CR)_4] + 2\ L \rightarrow [Rh_2(O_2CR)_4L_2]$$

where $R = C_3H_7$, in solution and by separating a "σ-only" component of ΔH_f using E and C * parameters, they were able to determine when a significant π-component is present. Even for L = Py, not normally a π-acceptor, some extra stabilization over the "σ-only" ΔH_f is found due to the hybridization of the Rh–Rh π^* orbital towards the ligands. σ-Inductive effects provide an efficient mechanism for decreasing π back-bonding stabilization by weakening the acidity of the metal centre and probably lengthening the metal–ligand bond [106,119].

Support for the presence of a significant measure of Rh–L π bonding in adducts of aromatic nitrogen donors is provided by the experimentally determined stability trend isonicotinic acid > pyridine ≃ niacin ≫ picolinic acid which parallels the expected order of π-bonding capacity [121] (see Section L).

Cotton [118] has criticised the extensive Rh–L π back-bonding proposed by Drago et al. [106]; his Xα–SW–MO calculations on $[Rh_2(O_2CH)_4(PH_3)_2]$, chosen as a model of the structurally characterised $[Rh_2(O_2CR)_4(PR_3)_2]$ species, do not support the presence of back-bonding. He states that no new interactions have been introduced by the axial phosphine ligands, but the magnitudes of the Rh–L interactions have been altered. It is expected that a continuum of electronic structures could be produced for $[Rh_2(O_2CR)_4L_2]$ by variation of the ligand L and that at some intermediate donor strength, a crossover of the HOMO from Rh–Rh δ^* to Rh–Rh σ, Rh–Lσ^* would be observed. Drago [120] has expressed surprise at Cotton's [118] results, but in the absence of experimental data on $[Rh_2(O_2CH)_4(PH_3)_2]$ sees no direct basis for comparison with his own.

As noted on p. 147, the ab initio SCF–MO calculations of Kawamura et al. led to σ as HOMO for all the complexes including L = PH_3, which is in accord with ESR experimental results [104,107]. All the MO levels are raised by addition of axial ligands (in agreement with ligand field theory). The effect on the σ^* orbital is dominant and is followed by the effect on the σ orbital (HOMO). The net gross charge of Rh was obtained by a Mulliken

---

* An empirical four parameter equation has been used to describe bond strengths of adducts in which the interaction involves σ-bond formation. The enthalpy of interaction (ΔH) measured in a poorly basic, non polar solvent can be predicted using

$$-\Delta H = E_A E_B + C_A C_B \qquad (1)$$

where subscripts A and B represent the Lewis acid and bases and E and C approximate the qualitative assignment of tendencies of acids and bases to undergo electrostatic and covalent interactions.

population analysis and was found to be +0.70 (ligand free), +0.61 (L = H_2O), +0.57 (L = NH_3), +0.41 (L = PH_3) with $d(\xi = 0.43)$, showing charge transfer from axial ligands to Rh. The difference between their result and that of Norman et al. [9,10] has been noted, but no explanation has been given.

The structural differences between $[Rh_2(O_2CMe)_4(H_2O)_2]$ (Rh–Rh 2.385(5) Å, Rh–OH_2 2.310(3) Å) [34] and the oxidised species $[Rh_2(O_2CMe)_4(H_2O)_2]ClO_4 \cdot H_2O$ (Rh–Rh 2.317(2) Å, Rh–OH_2 2.22(1) Å) [35,36] have been rationalised by Bursten and Cotton [118] assuming the electron configuration of Norman et al. [10] to be correct. The shortening of the Rh–OH_2 bond upon removal of a δ^* electron localised on the rhodium atoms is attributed to the now smaller energy difference of the water lone pairs and the acceptor orbital of the $[Rh_2(O_2CMe)_4]$ framework. The decrease in the Rh–Rh bond length has been attributed to the antibonding nature of the electron involved [118,123], although the impact of the antibonding character in a δ^* MO has come under question. Bursten and Cotton [118] state that much more pronounced changes in the Rh–Rh and Rh–L bond lengths would be expected upon oxidation of $[Rh_2(O_2CMe)_4(PPh_3)_2]$ to the corresponding cation. The Rh–P bond is expected to shorten on removal of an electron from the strongly Rh–P antibonding $17a_g$ MO; this will be accompanied by increased donation from the phosphine lone pairs into the Rh–Rh σ^* orbital. The Rh–Rh bond would be expected to lengthen as electron density is removed from the Rh–Rh σ framework. Thus upon oxidation of the system a partial charge transfer from the σ to σ^* orbital will occur. If the Rh–P bond shortens upon oxidation then the overlap of the Rh–Rh π^* and phosphorus $3d$ orbitals would increase despite the higher formal oxidation state of the Rh atoms, and thus more back bonding is predicted to occur in the oxidised cationic species than in the neutral molecule [118].

Drago et al. [106] have however performed electrochemical studies to measure the stabilization of the base coordinated to the cation relative to the base coordinated to the neutral dirhodium(II) butyrate. They conclude that as the metal–ligand σ bond strength increases the metal–orbital non-bonding electrons are driven higher in energy and the adduct is more readily oxidized. The cation will be less effective at π back-bonding than neutral compounds.

K. THERMAL DECOMPOSITION

Thermal decomposition of rhodium(II) carboxylate adducts usually occurs in several stages with stepwise elimination of the axial ligands, followed at much higher temperatures by complete decomposition of the lantern struc-

TABLE 13

Thermal decomposition temperatures (°C) for some rhodium(II) carboxylates [a,b]

Compound	L	Elimination of 1st ligand		Elimination of 2nd ligand	Disruption of lantern	Ref.
$Rh_2(O_2CH)_4L_2$	Me_2SO	100		150	200	76
	Et_2SO		135			76
	$C_6H_{11}NC$		110		220	75
	C_5H_5N		115		145	78
$Rh_2(O_2CMe)_4L_2$	Me_2SO	140		185	270	76
	Me_2SO	136		165	262/264 [c]	125
	C_5H_5N		180		280	126
	$(NH_2)_2CS$		160		320	73
	$2\text{-}NH_2\cdot C_5H_4N$		185		230–300	83
	$3\text{-}NH_2\cdot C_5H_4N$		225		250–300	83
	$4\text{-}NH_2\cdot C_5H_4N$		210		310	83
	$C_6H_{11}NC$		125		370	75
$Rh_2(O_2CC_2H_5)_4L_2$	Me_2SO	130		152	236/264 [c]	125
	Et_2SO		130			76
	$C_6H_{11}NC$		150		350	75
	C_5H_5N	172		204	255/269 [c]	125
$Rh_2(O_2CC_3H_7)_4L_2$	Me_2SO	105		152	236/258 [c]	125
	C_5H_5N		133		262/267 [c]	125

[a] Table 19 p. 182 contains references to all papers on thermal analysis. [b] The data in Table 13 appear in numerical form in the original papers; however many papers present data solely in the form of TGA/DSC plots. [c] Onset of decomposition of lantern structure in N_2/air.

ture to yield rhodium(III) oxide (in air) or rhodium metal (in vacuo). Thermal analysis data for some rhodium(II) carboxylates are given in Table 13.

The loss of axial substituted BTD (2,1,3-benzothiadiazole) from $[Rh_2(O_2CMe)_4(BTD)_2]$ and collapse of the lantern occur simultaneously. The thermal stabilities of the rhodium(II) acetate complexes of substituted benzothiadiazoles changes sharply with the nature of the substituent in the following order [124]

$$4\text{-}NH_2BTD > 4\text{-}NO_2BTD > 4\text{-}CH_3OBTD > 4\text{-}CH_3BTD > BTD$$
$$260°C \qquad 210°C \qquad 195°C \qquad 190°C \qquad 130°C$$

Irrespective of the position of the amino group (1, 2 or 3), aminopyridines coordinate to rhodium via the pyridine nitrogen; comparison of the thermal stabilities shows that the metal–axial ligand bond strengths are practically the same as for the pyridine adduct [83].

Thermal analysis results for complexes $[Rh_2(O_2CMe)_4L_2]$ (L = RR'CO) indicate that the nature of R and R' groups on the axial ligands have an appreciable influence on the stability of the rhodium axial ligand oxygen bond. The decomposition temperature decreases in the following sequence;

L = formaldehyde > urea > benzamide > acetamide [84].

For the complexes $[Rh_2(O_2CMe)_4L_2]$ (L = Et_2SO, Me_2SO, $AsEt_3$ and $NHEt_2$) thermal gravimetric analysis (TGA) studies have shown that the

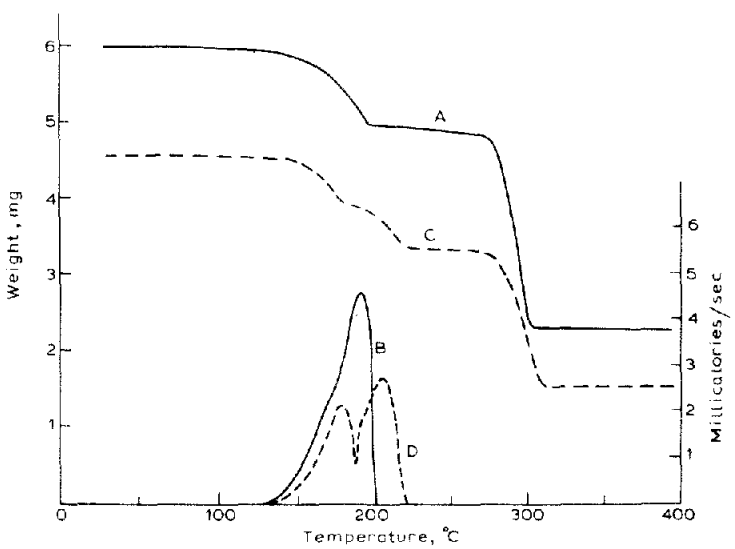

Fig. 34. A,B $[Rh_2(O_2CMe)_4(Me_2NH)_2]$ thermogram and DSC curve; C, D $[Rh_2(O_2CMe)_4(Me_2SO)]$ thermogram and DSC curve (with permission from ref. 88).

axial ligands are completely dissociated prior to lantern breakdown [88,125] (Fig. 34). In the corresponding rhodium(II) propionate and butyrate series only Me_2SO is removed prior to lantern breakdown. Differential scanning calorimetry (DSC) and TGA curves for rhodium(II) butyrate adducts show a small endothermic peak at ΔT_{min} of 218°C, immediately prior to the onset of lantern breakdown, which is thought to be due to nucleation. Small peaks occurring at 164°C and 171°C where no mass change or melting is evident are probably due to a solid state phase change [125].

Rhodium(II) trifluoroacetate sublimes before it decomposes. Mass spectrometry studies indicate the presence of the dimeric structure in the gaseous form, with the highest m/e value of 658 corresponding to the parent ion $[Rh_2(O_2CCF_3)_4]^+$ [30]. The lantern breaks down by stepwise loss of carboxylate groups to form $[Rh_2(O_2CCF_3)_3]^+$ ($m/e = 545$), $[Rh_2(O_2CCF_3)_2]^+$ ($m/e = 432$) and $[Rh_2(O_2CCF_3)]^+$ ($m/e = 319$).

A mechanism of thermal decomposition has been proposed for the aliphatic carboxylates $[Rh_2(O_2CR)_4L_2]$ on the basis of products identified by mass spectrometry [30]. Rhodium(II) acetate decomposes to give CO, acetic acid and rhodium metal according to Scheme 1.

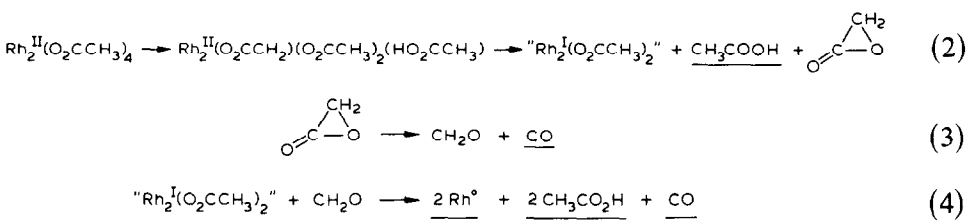

Scheme 1. Thermal decomposition of rhodium(II) acetate

Where dissociation $[Rh_2(O_2CR)_4L_2](s) \rightarrow [Rh_2(O_2CR)_4](s) + 2\ L(g)$ occurs, the heat measured should be the sum of two prominent factors, bond dissociation energy and change in crystal structure; however if the latter is small then the heats measured should correlate with the donor ability of the ligand, provided that only σ-bonding is involved. This hypothesis has been tested with axial nitrogen donor ligands; the expected Lewis basicity would be $NH_3 < NH_2R < NHR_2 < NR_3$ (R = Me, Et). This general order is found to hold, except for the tertiary amines where steric effects must be significant [88].

L. REACTIONS

(i) Adduct formation

Rhodium(II) carboxylates possessing a strong rhodium–rhodium single bond are resistant to chemical disruption but readily form adducts in which the axial sites are occupied by donor solvents or ligands. The contrasting tendency of $[Ru_2(O_2CMe)_4Cl]$ to give mononuclear products under similar conditions has been attributed to delocalisation of electron density away from the metal–metal bonding orbitals leading to weakening of the bond [127].

Preparative methods for formation of rhodium(II) carboxylate adducts have been mentioned in Section B.

In an attempt to throw fresh light on the nature of the rhodium–axial ligand bond, Bear et al. [121] determined stability constants, and forward and reverse rate constants for adduct formation reactions of rhodium(II) acetate, propionate and methoxyacetate with the ligands pyridine, picolinic acid, niacin and isonicotinic acid. The experimentally observed stability trend is: isonicotinic acid > pyridine ≃ niacin ≫ picolinic acid. Since the basicity of the ligands alone would not give this order, they concluded this was not the only factor controlling complex formation. Since electron withdrawal by a carboxylate substituted at the *para* position of a pyridine ring is more effective at lowering the energy of the π^* orbital than one at a *meta* position, the π acceptor ability should be isonicotinic acid > niacin > pyridine. From Table 14 it can be seen that isonicotinic acid does form significantly more stable complexes than niacin or pyridine, but the similarity of the stabilities of the latter two ligands suggests that the decreased π-acceptor capacity of pyridine is offset by the increased σ-bonding effects [121].

The mode of coordination of the ambidentate sulphoxide ligand can be controlled by changing the nature of the bridging carboxylate groups. The more electron-donating substituents, Me, Et, cause the rhodium to bond to DMSO via sulphur, while the strongly electron-withdrawing substituent CF_3 induces bonding via oxygen [65]. The competing donor properties of nitrogen and oxygen atoms in nicotinamide, *N*,*N*-diethylnicotinamide and benzamide have been investigated; benzamide bonds via oxygen although the carbamido nitrogen is not sterically hindered, while diethylnicotinamide and nicotinamide bond via the pyridine nitrogen [83]. *

---

* It is unclear from the original text whether diethylnicotinamide is bound to the rhodium(II) carboxylate via O or N. The pink colour indicates an N bonded adduct.

TABLE 14

Formation constants for $[Rh_2(O_2CR)_4L_n]$ ($n = 1, 2$) in aqueous solution, pH ca. 7.4

L	$K_1(\log K_1)$ [a]	$K_2(\log K_2)$ [a]
	$[Rh_2(O_2CCH_2(OMe))_4L_2]$	
Niacin	10700 ± 400	340 ± 10 [121]
Pyridine	11300 ± 400	490 ± 10 [121]
Pyridine	(4.52 ± 0.02)	(2.81 ± 0.04) [128]
Isonicotinic acid	14800 ± 400	420 ± 10 [121]
Imidazole	8776 ± 500	250 ± 22 [129]
Imidazole	6791 ± 241	120 ± 15 [b]
Imidazole	(3.94 ± 0.03)	(2.40 ± 0.04) [128]
Histidine	(4.38 ± 0.02)	(2.79 ± 0.03) [128]
AMP	1510 ± 50	158 ± 6.0 [131]
AMP	(3.45 ± 0.03)	(2.70 ± 0.06) [128]
	$[Rh_2(O_2CMe)_4L_2]$	
Niacin	8300 ± 300	310 ± 10 [121]
Isonicotinic acid	12300 ± 600	480 ± 10 [121]
Imidazole	10500 ± 300	300 ± 64 [129]
Imidazole	6826 ± 265	171 ± 15 [b]
Imidazole	14210 ± 610	249 ± 12 [130]
Imidazole	(4.02 ± 0.07)	(2.48 ± 0.08) [128]
N-Methylimidazole	19620 ± 1175	377 ± 17 [130]
Histidine	(4.05 ± 0.02)	(2.69 ± 0.02) [128]
Histidine	6880 ± 335	220 ± 15 [130]
Glycylglycine	471 ± 12	16 ± 2.3 [130]
Glycylglycine	488 ± 13	24 ± 2.4 [130]
D-L-Alanylalanine	247 ± 9	13 ± 3.7 [130]
Histidylhistidine	5990 ± 260	266 ± 21 [130]
Alanylhistidine	6400 ± 300	150 ± 40 [130]
Histidylglycine	7400 ± 400	220 ± 25 [130]
3,4-py-Dicarboxylate	8820 ± 320	267 ± 11 [130]
AMP	1893 ± 99	202 ± 14 [131]
AMP	(3.66 ± 0.03)	(2.66 ± 0.07) [128]
ADP	1152 ± 50	110 ± 14 [131]
ATP	1883 ± 103	128 ± 15 [131]
	$[Rh_2(O_2CEt)_4L_2]$	
Niacin	10600 ± 500	360 ± 10 [121]
Isonicotinic acid	14600 ± 700	550 ± 10 [121]
Imidazole	11660 ± 400	447 ± 52 [129]
Imidazole	7792 ± 267	156 ± 17 [b]
Imidazole	(4.07 ± 0.03)	(2.65 ± 0.07) [128]
Histidine	(4.14 ± 0.03)	(2.71 ± 0.02) [128]
AMP	4235 ± 267	344 ± 20 [131]
AMP	(3.78 ± 0.04)	(2.57 ± 0.04) [128]
ATP	4488 ± 267	329 ± 24 [131]

[a] Data in parentheses expressed in log form.

[b] Data appear in ref. 129, and are from unpublished work by J. Whileyman, University of Houston; all other K obtained by spectrophotometric methods for aqueous solutions at pH ca. 7–9 and 22–23°C.

Mixed rhodium(II) carboxylate adducts containing two different axial ligands have also been prepared. $[Rh_2(O_2CMe)_4KNCX \cdot DMF]$ (X = S or Se) is formed when a solution of KNCX in water is added to a concentrated solution of rhodium(II) carboxylate aquo adduct in DMF [42].

Formation of mixed adducts $[Rh_2(O_2CMe)_4\{P(OMe)_3\}L]$ in solution has been detected by NMR (see Section G).

Equilibrium studies on $[Rh_2(O_2CR)_4L_2]$ (L = N-, O- and P-donors) reveal a high K_1/K_2 ratio which cannot be explained solely by statistical factors. Bear et al. [121] attributed the large K_1/K_2 ratio to π bonding effects and concluded that once π-bonding has occurred between the metal and the first axial ligand, there is insufficient electron density in the π^* orbitals of the other metal atom to allow formation of a second axial metal ligand π bond. Therefore the thermodynamic stability of the bis adducts $[Rh_2(O_2CR)_4L_2]$ is determined primarily by the basicity of the coordinating donor atom [121].

Drago et al. [119] measured equilibrium constants and enthalpy of coordination for various axial ligands (Table 15). The earlier experiments were performed in benzene and indicated a greatly decreased acceptor capability for coordination of the second base relative to the first, while enthalpies for coordination of the first and second base were the same. Competition from benzene solvent molecules for axial sites was proposed to explain the unexpectedly large entropy effects. The experiments were repeated in methylene chloride and the results indicated a decreased acceptor capability and decreased enthalpy of coordination of the second base. In agreement with

TABLE 15

Thermodynamic and enthalpy data for the formation of 1:1 and 2:1 base adducts of rhodium(II) butyrate in benzene and methylene chloride solutions (with permission from ref. 119; data in the preliminary communication by the same authors are slightly different [106])

Base	C_6H_6 soln.			
	K_1	K_2	$-\Delta H_{1:1}$ (kcal mol^{-1})	$-\Delta H_{2:1}$ (kcal mol^{-1})
CH_3CN	$1.7(0.2)\times10^3$	$2.7(0.2)\times10$	5.1(0.2)	8.3(0.4)
C_5H_5N	$1.6(0.2)\times10^8$	$2.4(0.2)\times10^4$	11.2(0.2)	11.2(0.3)
N-Me imidazole	ca. 1×10^9	8×10^4	12.4(0.7)	10.5(0.5)
Piperidine	ca. 1×10^9	6×10^4	13.2(0.3)	12.5(0.4)
Tetrahydrothiophene	$1.7(0.1)\times10^7$	$1.9(0.3)\times10^4$	11.0(0.3)	10.3(0.4)
Caged phosphite	$9.1(0.7)\times10^7$	$2.6(0.1)\times10^4$	12.9(0.2)	11.3(0.2)
4-Picoline *N*-oxide	$2.4(0.3)\times10^5$	$2.9(0.3)\times10^2$	ca. 7.0	ca. 8.0
Me_2SO	$1.1(1.0)\times10^5$	$5.5(0.3)\times10^2$	6.6(0.2)	6.5(0.4)

Bear et al. [121], these results have been taken to indicate a σ-inductive effect which provides an efficient mechanism for decreasing π back-bonding stabilization by reducing the acidity of the metal centre and probably lengthening the metal–ligand bond [119]. Christoph et al. have interpreted their results similarly and have concluded that the rhodium–phosphorus π-interactions in phosphine and phosphite adducts of the rhodium(II) carboxylates should be weaker than usual, because of the unusually long Rh–P distances [61]. Bursten and Cotton however, have concluded that ligands of the general type PR_3 do not π back bond to rhodium in these systems [118]. Drago [120] sees no direct basis for comparison of his results with the $X\alpha$ calculations of Bursten and Cotton [118] on $[Rh_2(O_2CH)_4(PH_3)_2]$, since these authors have no experimental data on PH_3 as a ligand.

The variation of the stabilities of the adducts formed from different rhodium(II) carboxylates and a given ligand has been related to the inductive effect and lipophilicity of the carboxylate side chain [121,128]. The more hydrophobic character of the propionate species exerts a desolvating effect at the two axial positions, resulting in a more rapid ligand exchange.

(ii) Replacement of carboxylate bridges

By other bridging ligands

In a limited number of cases involving carboxylic acids of suitable boiling point, exchange of the carboxylate ligands can be performed by heating the

CH_2Cl_2 soln.

K_1	K_2	$-\Delta H_{1:1}$ (kcal mol^{-1})	$-\Delta H_{2:1}$ (kcal mol^{-1})
$1.15(0.05)\times10^3$	$1.1(0.1)\times10$	7.8(0.6)	6.8(1.5)
$1.115(0.001)\times10^7$	$9.88(0.05)\times10^3$	14.6(0.2)	8.5(0.2)
ca. 1×10^8	2.1×10^3	13.7(0.4)	9.9(0.5)
ca. 1×10^8	1.2×10^3	13.2(0.2)	8.9(0.2)
$8.2(0.3)\times10^4$	$1.89(0.045)\times10^2$	8.6(0.3)	5.7(0.5)

rhodium(II) carboxylate $[Rh_2(O_2CR)_4]$ under reflux in the appropriate neat carboxylic acid R'COOH. The stepwise exchange of acetate in $[Rh_2(O_2CMe)_4]$ by trifluoroacetate has been followed by NMR and intermediates have been identified using mass spectrometry [33] (Scheme 2).

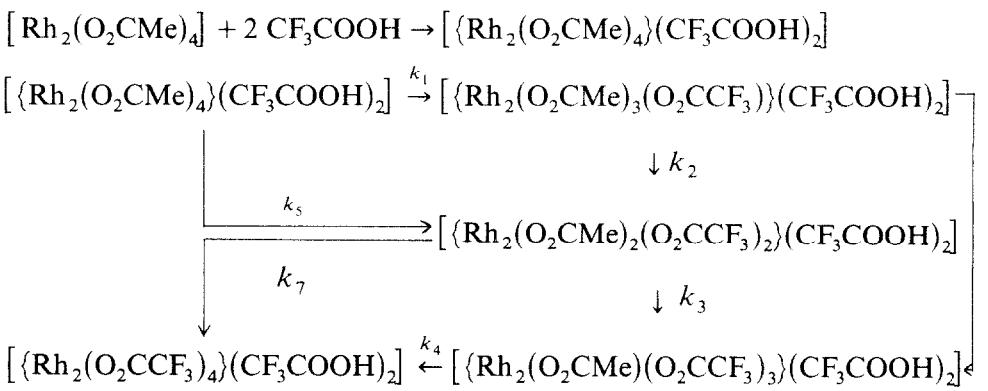

Absolute rate constants (sec^{-1}): $k_1 = 7.2 \times 10^{-4}$, $k_2 = 1.4 \times 10^{-3}$, $k_3 = 6 \times 10^{-5}$, $k_4 = 2 \times 10^{-5}$, $k_5 = k_6 = k_7 = 0$.

Scheme 2

Since each substitution involves essentially the same process all rates should be similar after allowing for statistical factors; however a considerable variation is observed. Assuming there is no change in metal–acetate bond energies upon trifluoroacetate substitution, the ratio should statistically be 1.0 : 0.75 : 0.50 : 0.25; however k_2 (1.4×10^{-3}) is found to be twice as large as k_1 (0.72×10^{-3}) and k_3 and k_4 are much smaller (6×10^{-5} and 2×10^{-5} respectively) than expected. These results indicate that a *trans* effect is operating in the second step of the reaction and dominates over the σ-bond strengthening which should occur as each successive trifluoroacetate group increases the effective positive charge on the metal. The third and fourth substitutions are progressively more difficult with no evidence of a labilizing *trans* effect in the fourth stage, and with the thermodynamic stabilization of the metal–acetate bonds being the controlling factor. As the reaction proceeds the concentration of free acid builds up to a significant level thus helping to suppress the final substitution step.

When rhodium(II) formate is heated with an excess of concentrated sulphuric acid at 80°C for 1 h, the bridging formate groups are replaced by sulphates to yield $[Cs_4\{Rh_2(SO_4)_4(H_2O)_2\} \cdot 2\ H_2O]$. The brown solution which forms is cooled with ice and treated with a concentrated aqueous solution of caesium sulphate to precipitate a dark green crystalline solid. When rhodium(II) acetate is used the reaction proceeds more slowly; after

4 h at 100°C a considerable amount of mixed rhodium sulphate–acetato complex $[Rh_2(O_2CMe)_2(SO_4)_2]^{2-}$ is formed [132].

A similar procedure is used to synthesise rhodium(II) phosphate $[Rh_2(H_2PO_4)_4(H_2O)_2]$. Heating rhodium(II) acetate in concentrated phosphoric acid at 150°C for several hours followed by dissolution of the mixture in water, filtering the solution and evaporating at 110–150°C, yields a mixture of $[(Rh_2(H_2PO_4)_4)(H_2O)_2]$ and $[(Rh_2(O_2CMe)_2(H_2PO_4)_2)(H_2O)_2]$ as dark green rhombic crystals. To obtain the pure orthophosphate the finely ground crystals may be treated once or twice more with phosphoric acid. The compound can be precipitated from the aqueous solution by concentrated perchloric acid as the tetrahydrate $[Rh_2(H_2PO_4)_4(H_2O)_2] \cdot 4\ H_2O$ which loses the crystallization water at 100–110°C [133]. X-ray diffraction studies and other physical measurements have been used to characterise these compounds [134,135].

Rhodium(II) carbonate $Na_4[Rh_2(CO_3)_4]_2 \cdot 2.5\ H_2O$ is formed when rhodium(II) acetate suspended in sodium carbonate solution is heated to near boiling for 10–15 min [94]. The rhodium(II) bicarbonato complex is believed to be formed when slightly more than an equivalent amount of perchloric acid is added for complete protonation of $[Rh_2(CO_3)_4]^{4-}$ and the solution is quickly evaporated to dryness [94].

Products which include fully and partially exchanged complexes are prepared by fusing rhodium(II) acetate with α-pyridone at 160°C under argon for 15 min, then removing excess ligand by vacuum sublimation at 110°C. Separation of the various complex products is achieved by crystallisation from acetonitrile or methylene chloride [44,45].

All four carboxylate ligands can be exchanged by thioacetate or thiobenzoate when rhodium(II) formate is treated with thioacetic acid and thiobenzoic acid respectively [77,136].

It has been reported that when $[Rh_2(O_2CCCl_3)_4]$ in butanol is treated with the ligand 2,4-dithiouracil (dtuH) at 60–70°C for 3 h, the carboxylates exchange with the ligand yielding the diamagnetic $[Rh_2(dtu)_4(H_2O)_2]$ species; a lantern structure is proposed but has not been confirmed [137]. However, attempts to introduce bridging diaryl triazene [101c] and pyridine-2-thiol (LH) groups [138] by anion exchange led only to formation of axial adducts $[Rh_2(O_2CR)_4(LH)_2]$.

By chelating ligands

Heating of $[Rh_2(O_2CMe)_4]$ with dimethylglyoxime (dmgH) in alcohol under nitrogen leads to replacement of two or four acetate groups by dimethylglyoxime ligands to yield *cis*-$[Rh_2(O_2CMe)_2(dmg)_2]$ and $[Rh_2(dmg)_4]$ respectively, each of which contains chelating dmg ligands [49–51].

The carboxylates can also be partially exchanged by β-diketones such as acetylacetone, trifluoroacetylacetone and hexafluoroacetylacetone yielding the mixed complexes $[\{Rh_2(O_2CMe)_2(\beta\text{-diketonate})_2\}(H_2O)_2]$ [52].

In most cases however, direct replacement of carboxylate by chelating ligands is not observed. Instead the compounds are prepared from $[Rh_2X_2(allyl)_4]$ (X = Cl, Br) by treatment with a suitable heterocyclic compound and a carboxylic acid in absolute ethyl alcohol in an inert atmosphere at 100°C [47,48]. The products $[Rh_2(O_2CR)_2(N{-}N)_2X_2]$ have binuclear structures with bridging carboxylate, chelating N–N ligands and axial ligands. The structure of these products (where N–N = 1,10 phenanthroline or 2,2′-bipyridyl; X = Cl, Br) has been discussed earlier (Section C, Figs. 7–10).

(iii) Destruction of the lantern

The strong rhodium–rhodium bond of the rhodium(II) carboxylates is fairly resistant to chemical attack, but some chemistry of these dimeric species leading to disruption of the lantern structure has been reported.

The observation by Bear and co-workers that reaction of cysteine with rhodium(II) carboxylates causes breakdown of the carboxylate cage liberating acetate ions [139,140], led Pneumatikakis and Psaroulis to attempt isolation of the products from this and related reactions [90]. The amino acids L-cysteine, L-cysteine methylester and L-penicillamine, all of which contain free –SH groups were used. When the rhodium(II) carboxylate is mixed with aqueous solutions of the ligands LH at a molar ratio of 1 : 4 at room temperature, dark red solutions result, from which the complexes analysing for RhL_2 can be isolated on addition of excess acetone. Infrared, magnetic moment measurements (1.8–1.9 μB) and ESR results [$g_1 = 1.955$, $g_2 = 2.020$ and $g_3 = 2.035$ for $[Rh(O{-}MeCys^-)_2]$ indicate that the products are mononuclear low spin rhodium(II) compounds with a square planar configuration. Mononuclear products $[Rh(MNT)_2]^{2-}$ are also observed when rhodium(II) carboxylates are treated with maleonitriledithiolate dianion (MNT) $[(CN)_2C_2S_2]^{2-}$ [141]. Treatment of rhodium(II) formate with thioxine (quinoline-8-thiol) also leads to a mononuclear rhodium(II) product $[Rh(C_9H_6NS)_2]$ [142]. In contrast the reaction of rhodium(II) carboxylates with the thioether amino acids, *S*-methylcysteine, *S*-ethylcysteine and methionine leads to simple adduct formation [90].

It was originally believed that treatment of rhodium(II) carboxylate with a strong non-complexing acid such as trifluoromethylsulphonic, perchloric or *p*-toluenesulphonic acid afforded "Rh_2^{4+} (aq)". Despite attempts to precipitate the cation with a wide variety of anions of various sizes and charges, and to obtain crystals by various cooling or evaporation techniques in different solvents, a simple salt could not be isolated [27]. Later studies have shown

that the aquation products of acid hydrolysis of rhodium(II) acetate are $[Rh_2(O_2CMe)_n](aq)^{(4-n)+}(n = 2,3)$ [91,143]. The formation of mixed compounds $[Rh_2(O_2CMe)_2(OC_6H_4CO_2(H))_2]$ by treatment of solutions of this type with salicylic acid has been taken to indicate the presence of these partial hydrolysis products [144]. The true hydrated Rh_2^{4+} species can be generated by the reaction of $Cr^{2+}(aq)$ with $[Rh(H_2O)_5Cl]^{2+}$ [145] and is believed to be $[Rh_2(H_2O)_8(H_2O)_2]^{4+}$ in which two of the water molecules, presumably axial, are more labile and can be replaced by entering ligands such as acetate or sulphate ions giving $[Rh_2(H_2O)_8(SO_4)_2]$ and $[Rh_2(H_2O)_8(O_2CMe)_2]^{2+}$ [146]. Elution of Rh_2^{4+} on a cation exchange column with 2 M $(NH_4)_2SO_4$ leads to $[(NH_4)_4Rh_2(SO_4)_4 \cdot 4.5\ H_2O]$ [94].

(iv) Redox reactions

Chemical oxidation—reduction

The action of dilute (1 : 1) HCl on the amine adducts of the rhodium(II) carboxylates and thiocarboxylates merely leads to the removal of the amine with the formation of the corresponding hydrated or anhydrous carboxylates or thiocarboxylates; however, concentrated HCl slowly converts the rhodium(II) carboxylates into red $[RhCl_6]^{3-}$ [77,78]. Treatment of the carboxylato compounds with HCl or HBr(g) in acetone or ethanol produces an insoluble residue of rhodium metal and a solution from which a rhodium(III) compound formulated as "$(Ph_4As)RhX_4 \cdot 2\ H_2O$" (X = Cl, Br) is precipitated on addition of $Ph_4AsCl \cdot n\ H_2O$ [147,148].

The oxidation of rhodium(II) acetate by ozone in acetic acid gives the trinuclear basic rhodium(III) acetate $[Rh_3O(O_2CMe)_6(H_2O)_3]^+$ [149]. When chlorine gas, lead dioxide or cerium(IV) sulphate are added to a blue-green solution of rhodium(II) acetate, oxidation products of unknown constitution, orange or violet in colour are produced, e.g. an orange solid is obtained when chlorine gas is bubbled through a solution of rhodium(II) acetate in methanol. The solution reverts back to its original colour with time but can be more quickly restored by addition of a piece of amalgamated mossy zinc [91].

The reaction of rhodium(II) acetate with arene sulphinic acids RSO_2H (R = Ph, $C_6H_4CH_3$-*p*) [150] in refluxing THF or methanol under aerobic conditions leads to cleavage of the rhodium–rhodium bond with formation of $[Rh(O_2SR)_3]$; when $Na^+O_2SR^-$ is used the unstable adduct $Na_2[Rh_2(O_2CMe)_4(RSO_2)_2]$ initially formed reacts further to give $Na_2[Rh_2(OH)_2(H_2O)_2(RSO_2)_6] \cdot 4\ H_2O$ for which two dimeric structures have been proposed (Fig. 35). Both structures are consistent with the IR spectrum, conductivity measurements, analytical and molecular weight data; in the absence of an X-ray structure determination it has not proved possible to distinguish between them [150].

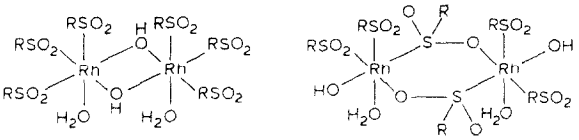

Fig. 35. Proposed structures for $Na_2[Rh_2(OH)_2(H_2O)_2(RSO_2)_6]\cdot 4\ H_2O$ (with permission from ref. 150).

When dithioacetic acid reacts with rhodium(II) acetate, a rhodium(III) complex $[Rh(CH_3CS_2)_3]$ [151] contaminated with other products is obtained. It has been suggested that the Rh–Rh bond is broken as a result of the reaction of dithioacetic acid leading to an extremely unstable rhodium(II) complex or a rhodium(I) species which is then auto-oxidised to a rhodium(III) compound. Reactions with sodium dithiocarbamates NaS_2CNR_2 yield analogous rhodium(III) complexes [18].

Rhodium(II) acetate reacts with organomagnesium compounds MgR_2 ($R = CH_3$, CH_2SiMe_3) in the presence of trimethylphosphine at 0°C with the formation of monomeric rhodium(III) complexes $[Rh(CH_3)_3(PMe_3)_3]$ and $[Rh(CH_2SiMe_3)\{(CH_2)_2SiMe_2\}(PMe_3)_3]$; a metal-containing ring is formed in the latter complex as a result of removal of hydrogen from a methyl group of a CH_2SiMe_3 ligand [152].

Treatment of a methanolic solution of "Rh_2^{4+}" * with a slight excess of triphenylphosphine, followed by a stoichiometric amount of the ligand LH (L = diethyldithiocarbamate; LH = 2-mercaptobenzothiazole, 2-mercaptopyridine, and toluene-3-thiol) leads to formation of $[Rh^{III}L_2(PPh_3)_2]BF_4$ [153]. These products probably arise by initial reduction of Rh(II) to Rh(I) by triphenylphosphine. Since the reactions are accompanied by the formation of triphenylphosphine oxide, an extra two moles of triphenylphosphine per "Rh_2^{4+}" are required to complete the reduction (the oxygen is thought to arise from water in the methanolic solvent); and this is followed by oxidation to rhodium(III) in the presence of the anionic ligands [153].

Neutral rhodium(III) complexes of stoichiometry $RhL_3(PPh_3)_n$ ($n = 1, 2, 3$) have been obtained from "Rh_2^{4+}", triphenylphosphine and an excess of ligand LH (LH = diphenylphosphorodithioic acid $[Ph_2PS_2H]$, diethoxyphosphorodithioic acid $[(EtO)_2PS_2H]$; or $L^- =$ thiocyanate $[SCN^-]$) in methanol [153].

Rhodium(I) carboxylates of stoichiometry $Rh(OCOR)(PPh_3)_3$ (R = alkyl, aryl or substituted alkyl) have been obtained by the interaction of the dirhodium(II) cation "Rh_2^{4+}" with a stoichiometric amount of triphenyl-

* "Rh_2^{4+}" is now known to be $[Rh_2(O_2CMe)_n]^{(4-n)+}$ ($n = 1, 2$).

phosphine and an excess of the lithium salt of the appropriate carboxylic acid [153]. On addition of a saturated methanolic solution of triphenylphosphine to the protonated solution "Rh_2^{4+}", the colour changes from green to red and after standing for some hours an orange solid precipitates. The IR spectrum of the solid indicates the presence of BF_4^- and PPh_3 and the elemental analysis is consistent with the formula $Rh(PPh_3)_3BF_4$ [27]. Further evidence for this formulation is provided by a quantitative reaction with LiCl to afford $RhCl(PPh_3)_3$. An alternative formulation preserving the rhodium(II) oxidation state and involving loss of an αH atom from one of the phenyl rings to give a Rh–C bond has been considered, but is not supported by the experimental evidence [27]. Interaction of $Rh_2(O_2CMe)_4$ with Ar_2Mg (Ar = Ph, $MeOC_6H_4$) and PMe_3 in diethylether produces the rhodium(I) compounds $Rh(Ar)(PMe_3)_3$, for which a distorted four coordinate planar structure (Ar = Ph), and a five coordinate geometry involving coordination of the methoxy group oxygen to rhodium (Ar = $MeOC_6H_4$) have been proposed [102a]. The interaction of $[Rh_2(O_2CMe)_4]$ with sodium amalgam in THF in the presence of an excess of PMe_3, under H_2 (3 atm), leads to the decomposition of the carboxylate [102b].

Wilkinson and co-workers reported that although bubbling carbon monoxide through the protonated green methanolic solution of rhodium(II) acetate caused no colour change, the subsequent addition of excess triphenylphosphine to this solution produced an orange colour and crystals of $[Rh(CO)(PPh_3)_3]BF_4$ precipitated [27]. In contrast, James et al. report the destruction of the lantern by carbonylation of rhodium(II) propionate in the presence of aqueous fluoroboric acid under relatively mild conditions (atmospheric pressure and 75°C) to give $Rh_6(CO)_{16}$ in very high yield [154a]. Reaction of $[Rh_2(O_2CMe)_4(MeOH)_2]$ with 20 atm. of CO in 1-butanol results in the appearance of a strong band in the IR at 2083 cm^{-1} which suggests simple adduct formation $[Rh_2(O_2CMe)_4(CO)_2]$ [154b]; more vigorous treatment (300 atm. of CO and 120°C) results in the formation of $Rh_6(CO)_{16}$.

Electrochemical oxidation—reduction

A potentiometric titration of rhodium(II) acetate with ceric sulphate indicates that 1.03 equivalents were consumed per dimer, while in a similar spectrophotometric titration, 1.05 equivalents were required [91]. Cyclic voltammetric experiments confirmed the existence of a redox process. A chloride ion associates with the oxidised Rh(II)/(III) species to give $[Rh_2(O_2CMe)_4Cl]$; saturation with respect to absorption changes is reached in 0.1 M NaCl and the change in the spectrum is much more marked than for the parent rhodium(II) acetate where concentrations of the order of 2 M NaCl are needed to produce a significant effect. The oxidised species can be

held by a cation-exchange resin from which it can be quickly removed by a strong non-complexing acid or salt. The species is unstable and disproportionates to rhodium(II) acetate and a yellow rhodium(III) species [91].

The redox reactions of a series of rhodium(II) carboxylates have been investigated in both aqueous and non-aqueous media at platinum and mercury electrodes. A typical cyclic voltammogram of $[Rh_2(O_2CC_2H_5)_4]$ oxidation at a platinum electrode in H_2O–0.1 M KCl is shown in Fig. 36. Both peak shape and current dependence on scan rate are indicative of a diffusion controlled one electron transfer. Potential separations between the anodic peak $U_{p,a}$ and the cathodic peak potential $U_{p,c}$ were in the range of 60 to 90 mV at 20 to 100 mV s^{-1} but increased with sweep rate. The ratio of the cathodic to the anodic peak current $I_{p,c}/I_{p,a}$ was unity at all scan rates indicating the absence of coupled chemical reactions. Diffusion controlled one-electron oxidation of the species $[Rh_2(O_2CR)_4]$ containing a variety of R groups produces the binuclear cations $[Rh_2(O_2CR)_4]^+$ which disproportionate to rhodium(II) carboxylate and rhodium(III) products. In contrast, the controlled reduction appears to involve several slow steps yielding an extremely stable monomeric rhodium(I) complex [155]. Cyclic voltammetry at a hanging mercury electrode gave a separation between the cathodic peak, and half-peak potential, $U_p - U_{p/2}$, of 125 mV. The absence of a reverse reduction peak and the cathodic shift of peak potential with increase in scan rate confirmed the irreversibility of the reaction. Using the experi-

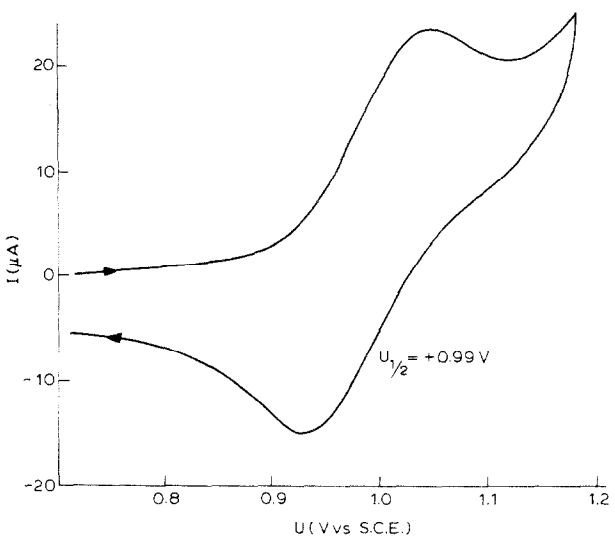

Fig. 36. Cyclic voltammogram showing oxidation of 8.8×10^{-4} M $Rh_2(O_2CC_2H_5)_4$ in H_2O/0.1 M KCl at a platinum electrode. Scan rate = 0.05 V s^{-1} (with permission from ref. 155).

mental $U_p - U_{p/2} = 125$ mV, a value of 0.38 for αn_a was obtained from which it may be inferred that $\alpha = 0.38$ and $n_a = 1$, i.e., the initial reduction step involves a rate determining single electron reduction

$$[Rh_2(O_2CR)_4]^+ \overset{e}{\rightleftharpoons} [Rh_2(O_2CR)_4] \overset{e}{\rightarrow} [Rh_2(O_2CR)_4]^- \overset{ne}{\rightarrow} \text{reduction product}$$

The shape of the polarographic wave indicates an irreversible charge transfer ($U_{3/4} - U_{1/4} = 120$ mV) (Fig. 37) [155].

Oxidation of $[Rh_2(O_2CR)_4L_2]$ becomes more favourable as the interaction of the axial group L becomes stronger which indicates that the HOMO levels are destabilized with increasing ligand binding ability [105,106]. Drago et al. [106] found that $[Rh_2(O_2CC_3H_7)_4L]$ (L = σ donors, piperidine, *N*-methyl imidazole and 4-picoline *N*-oxide) were stabilized by 6–7 kcal upon oxidation, while significantly less stabilization of adducts of π acceptor bases (L = acetonitrile, dimethylsulphoxide and phosphite) was observed. They interpreted this result in terms of π back-bonding; the oxidised adduct of a π-acceptor base has lost an electron involved in π back-bonding, thus rendering it less stable than the neutral adduct.

The half-wave potentials are dependent on the nature of the substituent R for $[Rh_2(O_2CR)_4]$ [105]. The Taft polar substituent constants bear a linear relationship with the half-wave potentials which indicates the expected stabilization of the higher oxidation state by electron donating substituents.

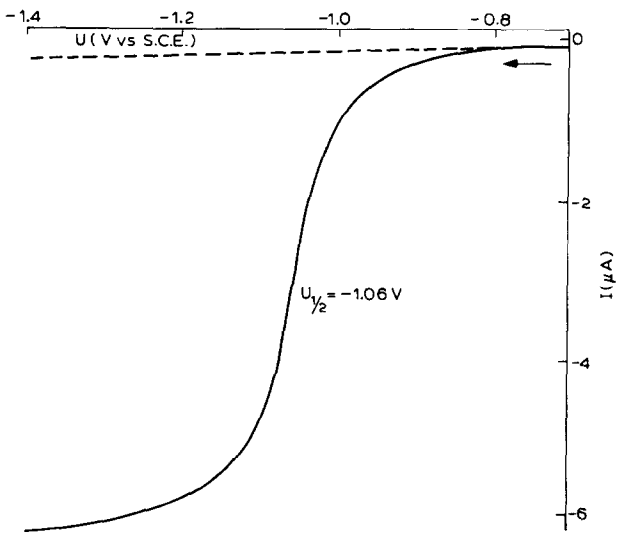

Fig. 37. Polarogram showing reduction of 8.8×10^{-4} $Rh_2(O_2CC_2H_5)_4$ in H_2O/0.1 M KCl (with permission from ref. 155).

With the strong electron withdrawing group CF_3, the lower oxidation state is stabilized to such an extent that oxidation of rhodium(II) trifluoroacetate is not observed up to the positive end of the potential limit of the solvent.

In order to verify the overall number of electrons involved in each step, Bear and co-workers oxidized and re-reduced $[Rh_2(O_2CR)_4]$ at controlled potentials [155]. The lack of pH dependence and spectroscopic evidence indicate that the lantern structure remains intact in the one-electron reversible process. Spontaneous reduction of $[Rh_2(O_2CR)_4]^+$ was found to be facilitated by anions such as halides which have axial coordinating ability towards the rhodium(II) lantern structure. The relatively high potential associated with the oxidation (ca. +1.0 V with respect to the standard calomel electrode) indicates that the neutral species is thermodynamically more stable than its oxidation product.

Mechanisms have been proposed for anation of $[Rh_2(O_2CMe)_4]^+$ by Cl^-, reduction of $[Rh_2(O_2CMe)_4Br]$ by Br^- and oxidation of $[Rh_2(O_2CMe)_4]$ by Cl_2, (Schemes 3–5 respectively) [87,156]. Detection of short-lived mixed valence bromide adducts have been performed by rapid-scanning stopped flow spectrometry.

Scheme 3. Anation of $[Rh_2(O_2CMe)_4]^+$

$$[Rh_2(O_2CMe)_4]^+ + Cl^- \rightleftharpoons [Rh_2(O_2CMe)_4Cl]^0 \quad (5)$$

$$[Rh_2(O_2CMe)_4Cl]^0 + Cl^- \rightleftharpoons [Rh_2(O_2CMe)_4Cl_2]^- \quad (6)$$

The "vacant" axial coordination sites on the rhodium atoms are probably occupied by water.

Scheme 4. Reduction of $[Rh_2(O_2CMe)_4Br]$

$$[Rh_2(O_2CMe)_4]^+ + Br^- \rightleftharpoons [Rh_2(O_2CMe)_4Br]^0 \quad (7)$$

$$[Rh_2(O_2CMe)_4Br]^0 + Br^- \rightleftharpoons [Rh_2(O_2CMe)_4Br_2]^- \quad (8)$$

$$[BrRh_2(O_2CMe)_4Br]^- \rightleftharpoons [Rh_2(O_2CMe)_4Br \cdots Br]^- \quad (9)$$

$$[Rh_2(O_2CMe)_4Br \cdots Br]^- \rightarrow [Rh_2(O_2CMe)_4] + Br_2^- \quad (10)$$

$$[Rh_2(O_2CMe)_4]^+ + Br_2^- \rightarrow [Rh_2(O_2CMe)_4] + Br_2 \quad (11)$$

The "vacant" axial coordination sites on the rhodium atoms are probably occupied by water. Steps (7) and (8) are anation of $[Rh_2(O_2CMe)_4]^+$ by Br^- and are analogous to anation by Cl^-. Step (10) is rate determining.

Scheme 5. Oxidation of $[Rh_2(O_2CMe)_4]$

$$[Rh_2(O_2CMe)_4] + Cl_2 \rightarrow [Rh_2(O_2CMe)_4]^+ + Cl_2^- \quad (12)$$

$$[Rh_2(O_2CMe)_4] + Cl_2^- \rightarrow [Rh_2(O_2CMe)_4Cl \cdots Cl]^- \quad (13)$$

$$[Rh_2(O_2CMe)_4Cl \cdots Cl]^- \rightarrow [Rh_2(O_2CMe)_4Cl] + Cl^- \quad (14)$$

Step (12) is rate limiting.
Alternatively an inner sphere mechanism has been proposed

$$[Rh_2(O_2CMe)_4] + Cl_2 \rightarrow [Rh_2(O_2CMe)_4Cl_2] \quad (15)$$

$$[Rh_2(O_2CMe)_4Cl_2] \rightarrow [Rh_2(O_2CMe)_4Cl] + Cl \quad (16)$$

$$Cl + Cl^- \rightarrow Cl_2^- \quad (17)$$

M. APPLICATIONS

Rhodium(II) carboxylates have a number of practical applications, the most promising being their anti-tumour activity (see next section). They have also found use as catalysts in organic reactions and as a stationary phase in gas chromatography.

Rhodium(II) carboxylates catalyse the decomposition of α-diazoesters giving rise to stereoselective insertion yielding *cis*-enoates [157,158]. The high efficiency of rhodium(II) carboxylates as catalysts in the cyclopropanation of substituted ethylenes [17a] and dienes [17b] is dependent on their solubilities, with the soluble butanoate and pivalate proving most efficient (Eqn. 18).

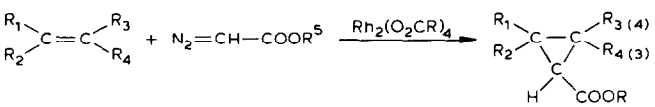

(18)

However, the solubility of the reagents and catalyst are not the sole factors responsible for the observed efficiency, since rhodium(II) trifluoroacetate, a very soluble complex, is not particularly effective (yield of products is 10–15%). Steric hindrance at the carboxylate group does not affect the yield, but the electronegativity of this group may be a determining factor. The high efficiency of rhodium(II) carboxylates in promoting the cycloaddition of carbenes generated from diazoesters to acetylenes [159,160], carbodiimides [161,162] and aromatic molecules including benzene, toluene, xylenes, trimethyl benzene and indan [163] has also been observed. The insertion of these carbenes into the hydroxylic bond of alcohols [164], or more generally into the polar X–H bonds of phenol, thiophenol, isomeric butyl mercaptans, aniline and acetylacetone [165a] are also catalysed by rhodium(II) carboxylates, giving high yields in specific reactions under relatively mild conditions. The rhodium carboxylate catalysed insertion of carbenes into C–H bonds of alkanes has also been reported [165b].

Rhodium(II) carboxylate catalysed reactions of benzhydryl 6-diazopenicillanate and other diazo compounds with alcohols [166], thiophene [167a,167b],

aromatics [168] and furan [169] have also been studied. Reaction of diazopenicillanate (**a**) in ethanol, t-butyl alcohol and benzyl alcohol containing $Rh_2(O_2CMe)_4(H_2O)_2$ gave thiazepines (**b**) (R = Et, ^{t}Bu, $PhCH_2$) as the main products [166].

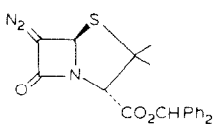

(a)

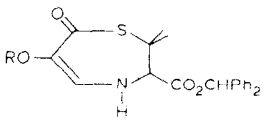

(b)

A reaction scheme for the carbenoid ring expansion of thiophene to 2H-thiopyran, in its rhodium(II) carboxylate catalysed reaction with benzhydryl 6-diazopenicillanate (**a**) has been proposed [167a,b]. It is postulated that the thiophene attacks the upper face of the β-lactam but the stability of the thiophenium ylide allows time for inversion through to the lower face as the reaction proceeds (Scheme 6).

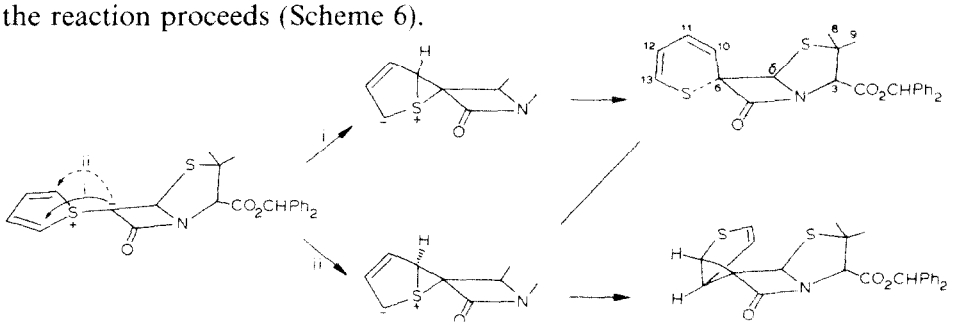

Scheme 6. Carbenoid ring expansion of thiophene to 2H-thiopyran.

The ring expansion of thiophene mentioned above, is the heterocyclic analogue of the Buchner reaction. For comparison the Buchner reaction was carried out between benzhydryl 6-diazopenicillanate (**a**) and anisole, using $[Rh_2(O_2CMe)_4(H_2O)_2]$ as a catalyst [167a] (Scheme 7). The anisole (*o* or *p*) attacks the upper face of the rhodium-complexed carbenoid to give the dipolar species (**c**) and (**d**). Collapse of each of these can take place to give the two possible norcaradienes (**e**, **e′**) and (**f**, **f′**) respectively, but subsequent ring opening of each pair of stereoisomers leads to a single cycloheptatriene. The observed specificity in the formation of the products (**g**) and (**h**) stems from the initial attack of anisole from the β-face of the penicillanate. It is thought that the bulky rhodium catalyst is complexed at the less hindered α-face of the β-lactam ring, preventing attack from this side, and that collapse of the intermediate dipolar species (**c**) and (**d**) is faster than inversion at C_6. This is in contrast to the thiophene reaction, where inversion does occur.

Rhodium(II) carboxylates have been employed as catalysts in the synthe-

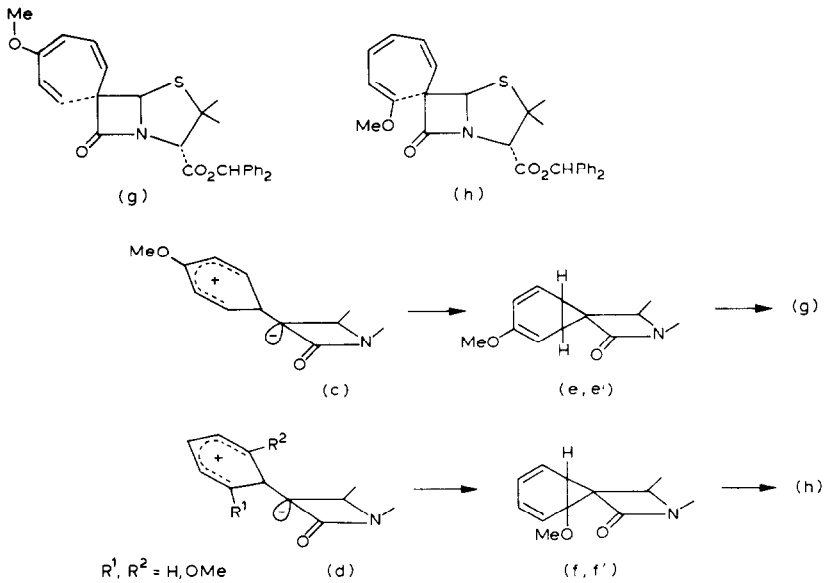

Scheme 7. The Buchner reaction between benzhydryl 6-diazopenicillanate (**a**) and anisole.

sis of various antibiotics (via cyclisation of diazo compounds) [170a] and in the synthesis of natural products (via conversion of α-diazo-β-hydroxyketo compounds to the corresponding β-diketones) [170b].

Rhodium(II) carboxylates act as homogeneous catalysts in the hydrogenation of olefins in a wide variety of solvents [16a]. A mechanism involving heterolytic cleavage of dihydrogen has been proposed [16b] (Scheme 8).

$$Rh_2(O_2CMe)_4 + H_2 \underset{k-1}{\overset{k_1}{\rightleftharpoons}} HRh_2(O_2CMe)_3 + H^+ + O_2CMe^- \tag{19}$$

$$HRh_2(O_2CMe)_3 + \text{olefin} \xrightarrow{k_2} HRh_2(O_2CMe)_3(\text{olefin}) \tag{20}$$

$$HRh_2(O_2CMe)_3(\text{olefin}) \rightleftharpoons Rh_2(O_2CMe)_3(\text{alkyl}) \tag{21}$$

$$Rh_2(O_2CMe)_3(\text{alkyl}) \xrightarrow{H^+ + O_2CMe^-} Rh_2(O_2CMe)_4 + \text{paraffin} \tag{22}$$

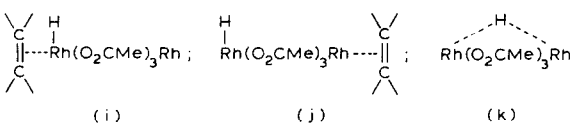

Scheme 8. Catalysis of hydrogenation of olefins [16]

The proton activation step [eqn. (19)] is supported by the observed inverse dependence on added acid. Hui et al. [16] speculated that the most facile

route to hydrogenation would be obtained when the olefin is π-bonded to the rhodium hydride as shown in intermediate (**i**), since coordination of the olefin to the nonhydridic rhodium site as shown in intermediate (**j**) would probably involve transfer of the hydride through a considerable distance rather than an olefin insertion into the Rh–H bond. Alternatively, a bridged hydride species (**k**) may be involved. Insertion of the olefin into the metal–hydride bond is followed by proton attack on the intermediate metal alkyl, which completes the catalytic cycle (eqns. 21 and 22). $[Rh_2(O_2CH)_2(N{-}N)_2Cl_2]$ (N–N = phenanthroline) also catalyzes the hydrogenation of olefins, but has been reported to be less effective [48].

The oxidation of cyclohexene using catalytic mixtures of $[Rh_2(O_2CR)_4]$ and vanadium or molybdenum epoxidation catalysts has been investigated. The proposed reaction mechanism involves rhodium(II) carboxylate promoted autooxidation of the olefin to yield cyclohexenyl hydroperoxide, followed by epoxidation to 2-cyclohexen-1-ol. The selectivity of the system seems to be controlled by the nature of R [171a]. Rhodium(II) carboxylates also catalyze hydrosilylation of terminal olefins, dienes, cyclic ketones and terminal acetylenes [171b]. The catalytic hydrogenation of 1-hexene by methanolic solutions of $[Rh_2(O_2CCH_3)_{4-x}]^{x+}$ ($x = 1, 2$) intercalated into a swelling mica-type silicate (hectorite) has also been observed [171c,d].

Rhodium(II) carboxylates suspended in squalene act as a stationary phase for gas chromatography [172]. The observed "inverse" steric effect (olefin coordination strengthens as alkyl substitution at the double bond increases) has been attributed to an increase in the donor capacity of the π orbital which more than offsets the steric hindrance caused by the alkyl substituents. The low steric effect is in accord with the open nature of the axial site.

N. ANTI-TUMOUR ACTIVITY

Prior to 1960 there was very little systematic work on the anti-tumour activity of complexes of the platinum group metals. Rosenberg's accidental discovery in 1965 that "inert Pt electrodes" cause the filamentous growth of bacteria [173a] led to the recognition and subsequent clinical application of cisplatin, *cis*-$Pt(NH_3)_2Cl_2$ [173b] and prompted investigation of the reactivity of other platinum metal complexes with biological systems, and in particular with tumour cells. There are several general articles which discuss the antitumour activities of cisplatin and other metal complexes [174–176].

Amongst the most promising of the second generation platinum metal anti-cancer compounds are the rhodium(II) carboxylates, the activity of which was first reported by Bear and co-workers in 1972 [13]. These compounds were shown to increase the life span of mice bearing Ehrlich

ascites [15], and leukaemia P388 tumours [180] and in favourable cases to produce complete regression [178]. This discovery has prompted investigations into the chemical properties and biological effects of the rhodium(II) carboxylates, which have shown that species containing unprotonated amino groups, including adenine, nucleotides and polynucleotides, single stranded DNA, RNase A, bovine serum albumin and certain amino acids (notably histidine and methionine), bind tightly but reversibly in the axial position [131,177]. In contrast to these N- and O-donors which form labile axial adducts with rhodium(II) carboxylates, sulphydryl compounds such as cysteine and glutathione react to liberate carboxylate ions and bind irreversibly with the rhodium [179]. It has not been determined with certainty which, if either of these two reactions is responsible for the observed anti-tumour or other biological activity. Bear and co-workers investigated the effects of rhodium(II) carboxylates on the activity of seventeen enzymes; all those having essential sulphydryl groups in or near their active site were found to be irreversibly inhibited, while the enzymes without essential sulphydryl groups were not affected. The reaction of the carboxylates with –SH enzymes closely parallels the toxicity and anti-tumour activity displayed by these compounds. A close "numerical" correlation has been observed be-

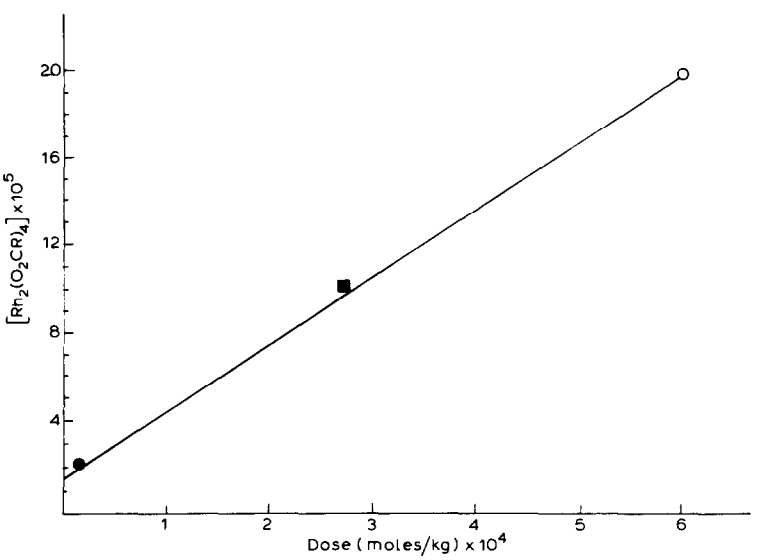

Fig. 38. Correlation between concentration of rhodium(II) carboxylate required to inactivate the sulphydryl enzyme LDH 50% in 1 min (y axis) and the therapeutic dose of rhodium(II) carboxylate which results in maximum survival rate of mice bearing Ehrlich ascites tumour cells (x axis): ○ rhodium(II) methoxyacetate; ■ rhodium(II) acetate; ● rhodium(II) propionate (with permission from ref. 179).

tween the concentration of a particular rhodium(II) carboxylate necessary to cause 95% deactivation of a sulphydryl enzyme (relative to control) in a specified time interval, and the dose of a rhodium(II) carboxylate which results in maximum survival rate in tumour bearing mice (Fig. 38). The above correlation is much better than that with the binding strength of amino group ligands [179]. Thus in vitro studies suggest the interaction with the sulphydryl group to be related to anti-tumour activity. However, whether appreciable inactivation occurs for the same enzymes in vivo has yet to be determined [178a,179].

In vivo studies have shown rhodium(II) carboxylates to inhibit DNA and protein synthesis but minimal inhibition of RNA synthesis has been observed [177,178a]. The inhibitory effect of rhodium(II) propionate and butyrate on DNA synthesis involving Ehrlich cells in vivo at different times after drug administration has been studied (Fig. 39). Cytosine arabinoside (15 mg kg^{-1}) was used as a positive control in the study. This drug inhibited thymidine incorporation into DNA by more than 90% at 1 h after administration; activity subsequently declined to ca. 10% after 24 h. In contrast, neither rhodium(II) propionate (2 mg kg^{-1}) nor butyrate (0.6 mg kg^{-1}) showed appreciable inhibition of DNA synthesis 1 h after the drug was

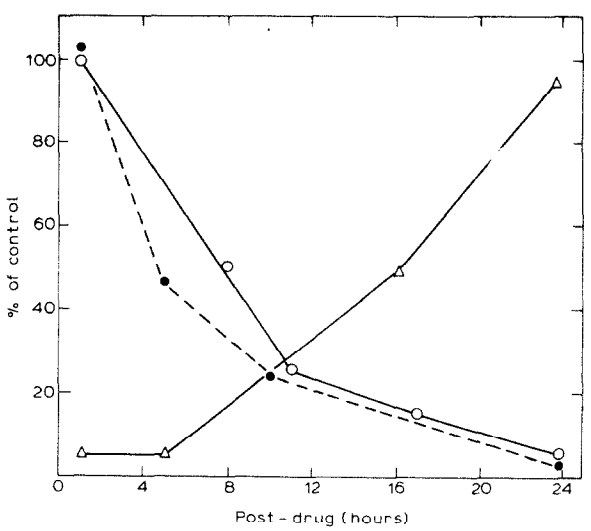

Fig. 39. In vivo inhibition of DNA synthesis by rhodium(II) carboxylates: O–O–O = rhodium(II) butyrate (0.6 mg kg^{-1}); ●···●···● = rhodium(II) propionate (2 mg kg^{-1}); —△—△—△ = cytosine arabinoside (15 mg kg^{-1}). A 30 min labelling time of thymidine-5-methyl-^{3}H (specific activity, 10 microcuries $mmol^{-1}$) was not included in post-drug intervals. Each point represents the average of three mice per group (with permission from ref. 177).

given. However, the degree of inhibition increased as a function of time to greater than 90% at 24 h [177].

Initial investigations indicated that rhodium(II) carboxylates were potent inhibitors of RNA polymerase from *Escherichia coli* in vitro [15,177]. However, studies on intact tumour cells have shown that rhodium(II) complexes have a slight stimulatory effect on the incorporation of uridine into RNA [14,177]. RNA synthesis studies yielded the results shown in Fig. 40. Rhodium(II) propionate and butyrate both exhibited a slight inhibition of RNA synthesis as measured by uridine-5-^{3}H incorporation, 1 h after the drug was given. However, after 1 h there was a continuous increase in uridine-5-^{3}H incorporation in the drug treated groups which was up to 1.5 times that noted in the controls approximately 11 h after the drug was given. After this time there was a gradual decrease in the incorporation; however, the amount was still greater than in the control group 24 h later. It has been conjectured that either rhodium(II) carboxylates actually stimulate the RNA synthesis of Ehrlich tumour cells in vivo, or they may interfere with the uridine precursor pools so that more uridine-5-^{3}H is incorporated in the acid-insoluble nucleic acid [177].

Rhodium(II) carboxylates appear to play an indirect role in the inhibition

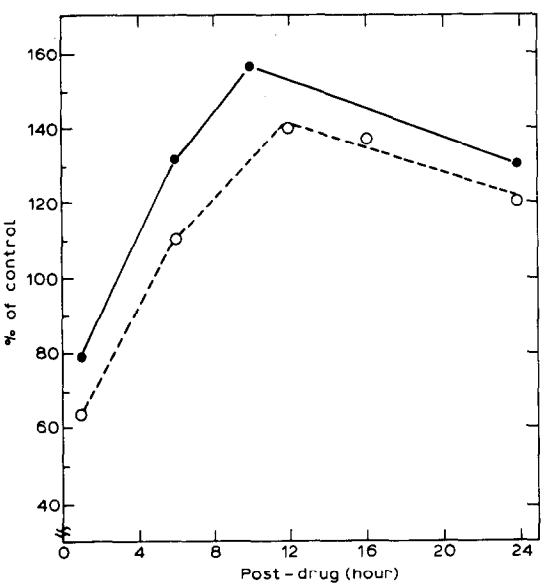

Fig. 40. In vivo inhibition of RNA synthesis by rhodium(II) carboxylates; ●–●–● = rhodium(II) butyrate (0.6 mg kg^{-1}); ○ · · · ○ · · · ○ = rhodium(II) propionate (2 mg kg^{-1}). A 30 min labelling time of uridine-5-^{3}H (specific activity, 10 microcuries mmol^{-1}) was not included in post drug intervals. Each point represents the average of separate determinations on three mice (with permission from ref. 177).

of DNA synthesis, possibly by inhibition of enzyme(s) essential for its synthesis [178a]; DNA polymerase α which is particularly active in copying "activated" double stranded DNA is strongly inhibited by reagents which block sulphydryl groups, while DNA polymerase β is resistant to such reagents and DNA polymerase γ requires sulphydryl containing compounds for maximum activity. Stabilization of rhodium(II) carboxylate toward the –SH reaction has been achieved by introduction of polyadenylic acid (poly(A)) [180] which binds the rhodium axial site more strongly than –SH groups and also stabilises the rhodium(II) carboxylate by chelate effect. Administration of rhodium(II) carboxylate/poly(A) mixtures gave an increase in the life span of treated mice (relative to those treated by complex alone). The survival study involved 8 groups of 10 Swiss mice, each implanted intraperitoneally with 6.7×10^6 Ehrlich cells. The LD_{10} of 1.5 mg kg^{-1} of rhodium(II) propionate, mixed with various concentrations of poly(A), was administered 24 h after tumour implantation and continued once daily for 6 days; results appear in Table 16. For an adenine : rhodium(II) propionate ratio of 10 : 1 or 20 : 1, the percent increase in life span (ILS%) increased from 190 for rhodium(II) propionate alone, to 280 for the poly(A) complex, while the number of 50-day survivors increased from two to five. The poly(A) is thought to slow down the extracellular deactivation of the rhodium(II) complex by the –SH reaction, which makes the drug available over a longer time period for tumour kill [180].

The inhibition of DNA synthesis in vitro follows an order of methoxyacetate < acetate < propionate < butyrate [15,177]. The time- and concentration-dependent inhibition of the proliferation of exponentially

TABLE 16

Rhodium(II) propionate–poly(A) survival data against Ehrlich ascites [a]

Ratio of adenine moiety of poly(A) to rhodium(II) propionate	Mean survival time (days)	ILS %	No. of 50 day survivors
0 : 1	37.0	190	2
10 : 1	45.1	279	5
20 : 1	45.2	280	5
40 : 1	39.7	212	1
60 : 1	38.3	201	2
Saline controls	12.9		0
Saline–poly(A) controls	12.7		0

[a] With permission from ref. 180.

TABLE 17

Proliferation of L1210 cells in suspension culture [a]

Rhodium(II) carboxylate		Cells/ml $\times 10^{-5}$					
		6 h	12 h	18 h	24 h	48 h	72 h
Control		2.8	3.4	4.4	5.7	16.0	32.0
Methoxyacetate	140 μM	2.2	2.7	3.3	4.0	8.3	17.0
	210 μM	1.9	2.2	2.7	3.2	3.8	7.7
	270 μM	1.8	1.9	2.0	2.1	1.3	1.0
Acetate	19 μM	2.2	2.8	3.5	4.2	10.0	23.0
	32 μM	2.1	2.4	2.7	2.9	2.6	4.2
	48 μM	2.0	2.1	2.0	1.9	1.3	1.1
Propionate	1.0 μM	2.3	2.7	3.4	3.8	7.0	17.0
	1.4 μM	2.2	2.3	2.4	2.4	1.9	3.4
	1.9 μM	2.1	2.1	2.0	1.9	1.2	1.5
Butyrate	0.31 μM	2.4	2.6	2.6	2.6	2.2	4.2
	0.60 μM	2.1	2.1	1.8	1.4	0.75	0.75
	1.23 μM	2.0	2.0	1.5	1.2	0.58	0.57

[a] With permission from ref. 14.

growing L1210 cells by the rhodium(II) carboxylates is shown in Table 17. The lipophilicity (partition coefficient) which increases with increasing carbon chain length of the rhodium(II) carboxylates correlates well with the anti-tumour activity and toxicity [181]. The thermodynamic stability of the rhodium(II) carboxylate adducts follow the same order as above; thus the increased stability of rhodium(II) propionate adducts over those of rhodium(II) acetate may have some bearing on biological activity [129]. The order of stability of these complexes could not be interpreted in terms of an electronic effect, since the expected increase of strength of the axial bonds between rhodium(II) methoxyacetate and biological molecules over that of the acetate or propionate, is not realised [131]. Bear and co-workers measured the enthalpies and entropies of formation of 1 : 1 and 1 : 2 adducts of rhodium(II) carboxylates with imidazole and found that the difference in the stability of the imidazole adducts was not large enough to account for the observed variation in their biological activity [129,130]. Results indicate that the more lipophilic drugs are absorbed by the cells to a greater extent. However, the simple extension of the carboxylate R chain beyond pentanoate is not effective in increasing the therapeutic effects of the drug. The observed decrease in the anti-tumour activity, toxicity and therapeutic efficacy of the hexanoate suggests that either steric problems arise or that the

rhodium(II) compounds must exhibit some intermediate degree of water solubility to be effective [181].

When L1210 cells have been exposed to inhibitory concentrations of rhodium(II) carboxylates, the drug effects are not readily reversed [14]. These results suggest that reversible axial ligation is not responsible for the biological activity; however, recent work by Farrell [98] contradicts this view. He investigated the simple 1 : 1 adducts of rhodium(II) carboxylates with adenine and adenosine, and assigned the binding sites as N(7) of the purine ring. The similarity in the properties of these species with those of rhodium(II) acetate/DNA solutions were taken to indicate the same binding site for DNA, and the specificity of the reaction was interpreted as being due to the presence of favourable hydrogen bonding interaction of the exocyclic amino group of adenine and acetate ligand (see Section G). Farrell suggests that the reactivity of these compounds is dictated by the presence of intramolecular hydrogen bonding interactions, and that these results are important in the understanding of the mechanism of transition metal anti-tumour activity.

In an investigation by Bear et al. [177] the rates of exchange of the trifluoroacetate ion for one carboxylate ion of rhodium(II) acetate, propionate and butyrate were determined by NMR spectroscopy. The pseudo-first order rate constants at 20°C were 1.4, 1.5, and 1.3×10^{-4} s^{-1} for the acetate, propionate and butyrate, respectively. Since these experimental results indicate that all three exchange reactions occurred at essentially the same rate, the vast differences in biological activity of the rhodium(II) carboxylates cannot be accounted for in terms of the differences in exchange rates.

In view of the reaction of –SH groups with rhodium(II) carboxylates, addition of non-toxic sulphydryl compounds may allow detoxification of large doses of the drug. Survival studies against the ascites P388 tumour have shown that not only does detoxification occur when high doses of glutathione are injected intraperitoneally 15 min after the injection of a toxic rhodium(II) propionate dose, but that in addition, substantial enhancement in the anti-tumour activity results [180].

No definite relationship between the redox and anti-tumour activity of the rhodium(II) carboxylate complexes has been found [155]. However, the complexes $[Rh_2(O_2CR)_4]^+$ which contain rhodium in the formal oxidation state of 2.5, have properties which make them interesting in terms of their potential as anti-tumour agents. Survival studies using $[Rh_2(O_2CR)_4]^+$ do not show a marked increase in effectiveness (Table 18). These charged species are more hydrophilic than the parent rhodium(II) compound, to which they revert over a period of time or on reaction with sulphydryl groups [180].

Most anti-cancer drugs induce chromosome damage in treated cells;

TABLE 18

Survival times of BDF_1 mice implanted with 1×10^6 P388 cells: the complexes were administered twice daily on days 1–9 in 0.2 mls of normal saline [a]

Complex	Dose (mg kg^{-1} per day)	Mean survival time (days)	ILS %
$Rh_2(O_2CC_2H_5)_4$	2.0	Toxic	–
	1.6	Toxic	–
	1.2	15.2	69
	0.8	16.0	78
$[Rh_2(O_2CC_2H_5)_4]^+$	2.0	Toxic	–
	1.6	17.0	89
	1.2	16.8	87
	0.8	15.9	76
Control	–	9.0	–

[a] With permission from ref. 155.

cisplatin has been shown to induce the DNA–DNA and DNA-protein cross-linking which leads to chromosome lesions [182]. In contrast, rhodium(II) butyrate only slightly increased the incidence of chromatid gaps and breaks [178a].

Hall et al. [178b] have recently reported poor response of rhodium(II) carboxylates with leukaemia L1210 and melanoma B16 tumours in mice; both tumours are recognised as having some predictive value for possible human use, thus the success of rhodium(II) carboxylates as a rival of cisplatin has been called into question.

O. CONCLUSIONS

In the past two decades a vast amount of interest has been shown in the rhodium(II) carboxylates with respect to their reactivity, electronic properties and application. It is now generally agreed that the rhodium–rhodium bond order is unity, although no adequate explanation for the short Rh–Rh bond length and high ν(Rh–Rh) stretching frequency exists: some authors now feel that the formal bond order is not a useful index of the metal–metal interaction. The nature of the rhodium–axial ligand bond and the effect of removal of an electron from the Rh–Rh bond upon formation of $[Rh_2(O_2CR)_4]^+$ are still matters of controversy. Experimental and theoretical work in this area is still being pursued for carboxylates as well as for other binuclear rhodium(II) compounds containing a wide variety of bridging ligands including carbonate, sulphate, dihydrogen phosphate, oxy-pyridine anions etc. (continued on p. 199)

TABLE 19

Compendium of references for rhodium(II) carboxylates and adducts [d]

L	n	Prep.	Colour	Vibrational spectra	Electronic spectra	ESCA	Other physical measurements [c]
$[Rh_2(O_2CH)_4L_n]$							
–	–	2		72	9		
H_2O	1	1, 187	Green			112	
H_2O	2	2	Green	72			
D_2O	2	72		72			Low freq. IR + Raman 81
$(NH_2)_2CO$	2	188	Blue	72			
NH_3	2	1, 187	Dark red	72			
NH_2Me	2	72 [a]	Pink	72			
NH_2Ph	2	188	Pink				
C_5H_5N	2	1, 32, 144, 187	Dark pink	72		112	
Quinoline	2	188	Pink				
o-$C_6H_4(NH_2)CO_2H$	2	188	Violet-red			113	
$(Gun)_n \cdot xH_2O$	2 ($x = 0$)	187	Violet	39			
	2 ($x = 2$)	39, 189					
Gun·CN	2	39	Violet	39			TGA 39
$(GunNH_2)_n \cdot xH_2O$	1 ($x = 1$)	39	Red-violet	39			TGA 39
$SC(NH_2)_2$	2					112	
$MeCSNH_2$	2	188	Red-violet				
$NH_2CS \cdot NH \cdot NH_2$	2	188	Violet			113	
$(Me_2SO)_n(H_2O)_x$	1 ($x = 2$)	76	Green				
Me_2SO	1.5	76	Olive green	76			
Me_2SO	2	76	Brown	76		112	TGA 76
Me_2SO	3	76	Light brown	76			
Et_2SO	2	76	Brown	76			TGA 76
PhCOSH	2	136	Red-brown				
PPh_3	2	32	Orange				
CNC_6H_{11}	2	75	Orange				

$[Rh_2(O_2CMe)_4L_n]$							
–	–	27, 28, 31, 33	Green	72	88		Raman 74; IR theory 80; mag.s. 94
H_2O	2	26, 31, 69, 88	Green	72, 92	31, 35, 39–42 67, 89, 94	112, 113	Raman 74, 81; NMR 33; mag.s., TGA 71
MeOH	2	27, 28	Blue-green				Raman 74, 79
EtOH	2	29	Green	29	31		
Me_2CO	2	31	Dark green		31		
THF	2	31	Green		31		
$MeCO_2H$	2	31	Green		31		
$HCONH_2$	2	84	Violet	84			TGA 84
$HCONMe_2$	2	84	Dark blue	84			
$(NH_2COMe)\cdot xH_2O$	2 ($x = 2$)	69, 84	Light green	84			TGA 84
$(MeCONMe_2)\cdot xH_2O$	2 ($x = 2$)	84	Green	84			
$(NH_2)_2CO$	2	188	Blue	72			
$((NH_2)_2CO)\cdot xH_2O$	2 ($x = 2$)	84	Green	84			Mag. data 71; TGA 84
$PhCONH_2$	2	84	Violet	83, 84			TGA 84
$(NH_2NHCONH_2)$	2	84	Red	83, 84			
$(PhNHNH)_2CO$	2	84	Violet	84			
$(1\text{-}NH_2C_6H_4CO_2H)$	2	188	Red				
NH_3	2	31, 69, 88	Crimson		88	113	Mag. data, TGA 71; Thermal data 88
$(N_2H_4)_n\cdot(H_2O)_x$	1 ($x = 1$)	187	Red				
NH_2Me	2	88	Red		88		
$NHMe_2$	2	88	Red		88		Thermal data 88
$NHEt_2$	2	88	Red		88		Thermal data 88
NMe_3	2	31, 88	Pink-red		88		Thermal data 88
NEt_3	2	88	Purple		88		Thermal data 88
En	2	26, 31	Pink-red				
	1						

TABLE 19 (continued)

L	n	Prep.	Colour	Vibrational spectra	Electronic spectra	ESCA	Other physical measurements [c]
$(En)_n \cdot (H_2O)_x$	1 ($x = 1$)	26	Red				Mag. data 71
$PhNH_2$	2	82	Violet-red	82			TGA 82
$3\text{-}H_2NC_6H_4Cl$	2	82	Violet	82	82		
$3\text{-}H_2NC_6H_4Br$	2	82	Violet	82			TGA 82
$3\text{-}H_2NC_6H_4I$	2	82	Violet	82			
$3\text{-}H_2NC_6H_4NO_2$	2	82	Violet	82			
$3\text{-}H_2NC_6H_4Me$	2	82	Violet	82			TGA 82
$3\text{-}H_2NC_6H_4OMe$	2	82	Violet	82			
C_5H_5N	2	31, 32 69, 88	Red	72, 126	88, 89	110, 112, 113	Thermal data 88, 126 mag. data 71; thermo + kinetic data 128
$2\text{-}CH_3C_5H_4N$	2	126	Pink	126			Thermal data 126
$3\text{-}CH_3C_5H_4N$	2	126	Pink	126			Thermal data 126
$4\text{-}CH_3C_5H_4N$	2	126	Pink	126			Thermal data 126
$2,6\text{-}Me_2C_5H_3N$	2	126	Pink	126			Thermal data 126
$2,4,6\text{-}Me_3C_5H_2N$	2	126	Pink	126			Thermal data 126
Quinoline	2	126, 130	Pink	126			Thermal data 126
Acridine	2	126	Green	126			Thermal data 126
$2\text{-}NH_2C_5H_4N$	2	83	Pink	83			Thermal data 83
$3\text{-}NH_2C_5H_4N$	2	83	Pink	83			Thermal data 83
$4\text{-}NH_2C_5H_4N$	2	83	Pink	83			Thermal data 83
3-Nicotinamide	2	83	Pink	83			Thermal data 83
3-Diethyl nicotinamide	2	83	Pink	83			Thermal data 83
$4\text{-}CN\text{-}C_5H_4N$	1, 2	77				111	
1-Phenanthroline	1	31	Olive-green				
MeCN	2	31	Violet		31		
NO	2	31	Brown				
HO–N=CH–CH=N·OH polymer	1	50	Red				

HO–N=C(C_4H_3O)–C(C_4H_3O)=N–OH	Polymer	50	Red				
(Gun·NH_2)$_n$(H_2O)$_n$	1, 1	39	Red-violet	39			
(Gun·CN)$_n$(H_2O)$_n$	1, 1	39	Violet	39			*Thermal data* 39
(Adenine)$_n$(H_2O)$_n$	1, 1	40	Pink				
9-Methyladenine	1	40	Pink	40			^{1}H NMR 40, 190
Triacetyladenosine	1	40	Pink	40			^{1}H NMR 40, 98
Adenosine	1	40	Pink	40			^{1}H NMR 40
Tetraacetyladenosine	2	40	Pink	40			^{1}H NMR 40
Adenosine-5′-monophosphate	1	40	Pink	40			Thermo + kinetic data + stab. const. 128, 131
Adenosine-5′-diphosphate	1	40	Pink	40			Stab. const. 131
Adenosine-5′-*triphosphate*	1	40	Pink	40			^{1}H NMR 40; stab. const. 131
(Theophylline)$_n$·$x$$H_2O$	2 (x = 2)	59	Violet-red				
Caffeine	2	59	Violet				
Imidazole	2	130					Thermo + kinetic data 128, 129
Histidine	2	128 [a]					Thermo + kinetic data 128
($CH_3C_6H_4N$)$_2$NH	2	101c	Purple	101c			^{1}H NMR 101b
Et_2S	2	88	Burgundy		70, 88		TGA, Mag.s. 70; thermal data 88
Et_2S	1	70	Purple		70		TGA, Mag.s. 70
$(NH_2)_2CS$	2	73	Violet	72, 73		110	TGA 73
NH_2CSMe	2	73	Violet-brown	73			TGA 73
($NH_2NHCSNH_2$)$_n$·$x$$H_2O$	1 (x = 1)	73	Red-brown	73			
$MeCONHCSNH_2$	2	73	Red-brown or violet	73			
$PhCSNH_2$	2	73	Red-brown or violet	73			TGA 73

TABLE 19 (continued)

L	n	Prep.	Colour	Vibrational spectra	Electronic spectra	ESCA	Other physical measurements [c]
PhNHCSNHPh	2	73	Red-brown or violet	73			
Ph·NH·CS·Ph	2	73	Red-brown or violet	73			
C_4H_8S	2	60	Dark red				
Me_2SO	2	31, 60 76, 88	Orange	72, 76	31, 32, 88	110, 112	TGA 88, 125; Raman 88, 74
Et_2SO	2	76		76			
$NH_2NHCSNH_2·HCl$	2	188	Dark violet				
BTD	2	124	Brown	124			TGA 124
$MeSCH_2CH(NH_2)CO_2H$	2	90	Orange-violet		90		
$EtSCH_2CH(NH_2)CO_2H$	2	90	Orange-violet		90		
$MeSCH_2CH_2CH(NH_2)CO_2H$	2	90	Orange-violet		90		
PPh_3	2	32	Orange	72, 74		110	Raman 74
$AsPh_3$	2	153	Maroon				
2-SH-C_5H_4N	2	138	Purple-brown	138			
$(PPh_3)_n·xEtOH$	2 ($x = 2$)	32					Mag.s., TGA 43 NMR 101a
$P(OMe)_3$	2	8	Orange				
$P(OPh)_3$	2	8	Orange				
$PPh_2(CH_2)PPh_2$	Polymer	101c	Orange	101c			
$PPh_2(CH_2)_2PPh_2$	Polymer	101c	Orange	101c			
PF_3	2	8					
$AsEt_3$	2	88	Red		88		
CO	2	8					
CNC_6H_{11}	2	75	Orange	75			
$[Rh_2(O_2CCH_2NH_2)_4L_n]$ Et_2O	2	71	Pale green				Mag. data 71
$[Rh_2(O_2CCH_2OMe)_4L_n]$ –	–	181					

Niacin	2	121	Pink			Thermo + kinetic data 121
Isonicotinic acid		121	Pink			Thermo + kinetic data 121
Imidazole		128	Pink			Thermo + kinetic data 128, 129, 139
Pyridine		121	Pink			Thermo + kinetic data 121
L-histidine		129	Pink			Thermo + kinetic data 128, 139
5′-AMP		131	Pink			Thermo + kinetic data 128, 131, 139
5′-ADP		131	Pink			Thermo data 131
5′-ATP		131	Pink			Thermo data 131
$[Rh_2(O_2CCH_2OPh)_4L_n]$						
–	–	105	Green			Redox by polarography etc. 105
$[Rh_2(O_2CCH_2F)_4L_n]$						
H_2O	2	86 [a]		86		
C_5H_5N	2	86 [a]				
$[Rh_2(O_2CCF_3)_4L_n]$						
–	–	29	Blue-green	72		M.S., mag.s., 30; redox by polarography etc 105
		31, 32				
H_2O	2		Blue	72		
$(H_2O)_n(EtOH)_x$	1 ($x = 1$)	71				Mag. data 71
EtOH	2	29	Blue	29, 72	112	
TMPNO	1	109				ESR 109
Me_2SO	2	65		72	112	
C_5H_5N	2	30, 32	Red	72	112	
NEt_3	2	30 [a]	Rose red			

TABLE 19 (continued)

L	n	Prep.	Colour	Vibrational spectra	Electronic spectra	ESCA	Other physical measurements [c]
SEt_2	2	30 [a]	Rose red				
PPh_3	2	30 [a]	Yellow-orange				
Me_2SO_2	2	66	Dark-green				
$P(OPh)_3$	2	67	Orange				
$[Rh_2(O_2CC_6F_5)_4L_n]$							
–	–	163					
$[Rh_2(O_2CCH_2Cl)_4L_n]$							
H_2O	2		Green	86, 191			
EtOH	2		Green	29			Elemental analysis 71
$[Rh_2(O_2CCHCl_2)_4L_n]$							
–	–	29		29			
EtOH	2	29	Blue	29			
C_5H_5N	2	29	Red				^{1}H NMR 29
PPh_3	2	29	Brown				
$[Rh_2(O_2CCCl_3)_4L_n]$							
–	–	29	Green	29			
EtOH	2	29	Blue	29			
Me_2SO	2	30	Blue				^{1}H NMR 29
C_5H_5N	2	29	Rose-red	29	29		
NEt_3	2		Rose-red				^{1}H NMR 29
SEt_3	2		Burgundy				
PhSH	2			29			
PPh_3	2	29, 30	Orange brown	29			^{1}H NMR 29

$[Rh_2(O_2CCClF_2)_4L_n]$					
–	–	29	Green	29	
EtOH	2	29	Blue	29	
$[Rh_2(O_2CCH_2Br)_4L_n]$					
EtOH	2		Green	29	
$[Rh_2(O_2CCH_2Ph)_4L_n]$					
–	–	105			Redox by polarography etc. 105
$[Rh_2(O_2CC_6HCl_2(NO_2)_2)_4L_n]$					
–	–	163			
$[Rh_2(O_2CEt)_4L_n]$					
–	–	30, 32	Green		Raman 74; TGA 30, 125; redox 105
H_2O	2	30 [a]	Green	76	
NEt_3	2	30 [a]	Rose-red		
C_5H_5N	2	32	Rose-red		TGA 125; thermo + kinetic data 128
$C_5H_{11}N$	2	32	Dark red		
C_9H_7N	2	32	Dark red		
$C_{13}H_9N$	2	41	Dark red-green		
$C_7H_6N_2$	2	41	Dark red		
$C_{12}H_8N_2$	1 Polymer	41	Dark red		
$C_{10}H_{16}N_2$	1 Polymer	41	Red-violet		
$(Gun{\sim}CN)_n \cdot xH_2O$	1 ($x = 2$)	39	Violet	39	TGA 39
$(Gun \cdot NH_2)_n \cdot xH_2O$	1 ($x = 1$)	39	Red-violet	39	TGA 39
Imidazole	1/2				Thermo + kinetic data 128
L-Histidine	1/2				Thermo + kinetic data 128
Niacin	1/2				Thermo + kinetic data 121
Isonicotinic acid	1/2				Thermo + kinetic data 121
Me_2SO	2	65, 76 125	Orange	76	TGA 12
Et_2SO	2	76		76	Thermal data 76
SEt_2	2	30 [a]	Burgundy		

TABLE 19 (continued)

L	n	Prep.	Colour	Vibrational spectra	Electronic spectra	ESCA	Other physical measurements [c]
PPh_3	2	32	Yellow-orange				
CNC_6H_{11}	2	75	Orange	75			TGA 75
5′-AMP	2						Thermo + kinetic data 128, 131
$[Rh_2(O_2CCHClMe)_4L_n]$							
–	–	105					Redox by polarography etc. 105
$[Rh_2(O_2CCH\cdot NH_2\text{–}Me)_4L_n]$							
–	–	192					
C_5H_5N	2	192	Pink				
Me_2SO	2	192	Orange	192		192	
$[Rh_2(O_2C(CH_2)_3CO_2H)_4L_n]$							
–	–	192					
C_5H_5N	2	192		192			
Me_2SO	2	192		192			
$[Rh_2(O_2CCH_2CHCl_2)_4L_n]$							
EtOH	2	29	Blue	29			
$[Rh_2(O_2CC_3H_7)_4L_n]$							
–	–	125	Green	86		111	TGA 125; thermo data 106 119, 153
Me_2SO	2	125	Burgundy				TGA 125; thermo data 106 119
C_5H_5N	2	125	Dark-red				TGA 125; thermo data 106 119

D [b]	1	106 [a]					Thermo data 106, 119
	2	119 [a]					
$[Rh_2(O_2CC_4H_9)_4L_n]$							
–	–	181					
$[Rh_2(O_2CCMe_3)_4L_n]$							
H_2O	2	60, 105	Dark green				
EtOH	2	112				112	
C_5H_5N	2	112				112	
$[Rh_2(O_2CC_5H_{11})_4L_n]$							
–	–	181					
$[Rh_2(O_2CC_5H_9)_4L_n]$							
–	–	105 [a]					Redox by polarography etc. 105
$[Rh_2(O_2CPh)_4L_n]$							
–	–	30	Yellow-green			112	TGA 30 Gas chromatography 171
H_2O	2	78	Blue-green	78			
Me_2CO	2	30	Deep blue-green				TGA 193
Me_2SO	2	78	Orange	78		78	
$HCONMe_2$	2	78				78	
NEt_3	2	30 [a]	Rose-red				
C_5H_5N	2	27	Red	78		78	
$(NH_2)_2CS$	2	78		78		78	
SEt_2	2	30 [a]	Rose-red				
PPh_3	2	27,30	Yellow-orange	74			Raman 74
KCN, H_2O	1.5, 2.0	86	Grey-violet	86			
$[Rh_2(O_2CC_6H_4OH)_4L_n]$							
H_2O	2	55	Blue-green	55	55	55	
$HCONMe_2$	2	55	Blue-green		55		
NH_3	2	55	Pink	55	55	55	

TABLE 19 (continued)

L	n	Prep.	Colour	Vibrational spectra	Electronic spectra	ESCA	Other physical measurements [c]
N_2H_4	0.5	55	Cherry-red	55	55	55	
$H_2NCH_2CH_2NH_2$	2	55	Cherry-red		55	55	
$PhNH_2$	2	55	Pink		55	55	
C_5H_5N	2	55	Cherry-red		55	55	
$MeCSNH_2$	2	55	Violet-red			55	
$(NH_2)_2CS$	2	55	Violet-red	55		55	
$[Rh_2(O_2CC_6H_4SH)_4 x H_2O \cdot L_n]$							
–	($x = 6$)	194				113	
EtOH	1 ($x = 2$)	194	Orange			113	
$HO_2CC_6H_4SH$	1 ($x = 7$)	194	Dark-red			113	
NH_3	1 ($x = 4$)	195	Red				
$H_2NCH_2CH_2NH_2$	1 ($x = 6$)	195	Red			113	
$HO_2CC_6H_4SH$ / $H_2NCH_2CH_2NH_2$	1, 1 ($x = 4$)	195	Red				
HCl	1 ($x = 6$)	194	Red				
HBr	1 ($x = 2$)	195					
HBr	2	195					
$(NH_2)_2CS$	2 ($x = 3,4$)	195					
$[Rh_2(O_2C \cdot C_5H_3N \cdot CO_2)_4L_n]$							
H_2O	3	54	Light-green		54	54	
Py, H_2O	1, 1	54	Brown			54	
$[Rh_2(O_2CC_6H_5CH(OH))_4L_n]$							
H_2O	2	196					
NH_3	2	196					
N_2H_4	2	196					
$(NH_2)_2CS$	2	196					
Me_2SO	2	196					
en, H_2O	2, 2	196					

C_5H_5N, H_2O		2, 1	196					
C_5H_5N		3	196					
C_5H_5N		4	196					
$C_6H_5NH_2$		4	196					
$[Rh_2(O_2CH)_4L_n]^+$								
H_2O		2	9, 10			10		Magnetic data 9, 10
$[Rh_2(O_2CMe)_4L_n]^+X^-$								
L	X	n						
	–	–		Orange-violet		87		
H_2O	ClO_4	2	35	Brown-red	35			Polarography etc. 155
–	O_2CMe	–	87				35	
–	Cl	–	87			87		
–	Br	–	156					
$[Rh_2(O_2CCH_2OMe)_4L_n]^+X^-$								
	–	–	105					Polarography etc. 105
$[Rh_2(O_2CCH_2OPh)_4L_n]^+X^-$								
	–	–	105					Polarography etc. 105
$[Rh_2(O_2CCF_3)_4L_n]^+X^-$								
–	–	–	105					Polarography etc. 105
PPh_3	–	2	104					ESR 104
$P(OPh)_3$	–	2	104					ESR 104
$P(OCH_2)_3CEt$	–	2	104					ESR 104
$[Rh_2(O_2CEt)_4L_n]^+X^-$								
–	–	–	105, 155					Polarography etc. 105
PPh_3	–	2	104, 107	Red-purple				ESR 104
$P(OPh)_3$	–	2	104					ESR 104
$P(OCH_2)_3CEt$	–	2	104					ESR 104

TABLE 19 (continued)

L		n	Prep.	Colour	Vibrational spectra	Electronic spectra	ESCA	Other physical measurements [c]
$[Rh_2(O_2CC_3H_7)_4L_n]^+ X^-$								
MeCN		1, 2	106, 119					Polarography etc. 106
C_5H_5N	–	1, 2	106, 119					Polarography etc. 106
N-methyl imidazole	–	1, 2	106, 119					Polarography etc. 106
Piperidine	–	1, 2	106, 119					Polarography etc. 106
Et_2S	–	1, 2	106, 119					Polarography etc. 106
4-picoline *N*-oxide	–	1, 2	106, 119					Polarography etc. 106
Me_2SO	–	1, 2	106, 119					Polarography etc. 106
Caged phosphite	–	1, 2	106, 119					Polarography etc. 106

$[M_n(Rh_2(O_2CH)_4)X_n]\cdot z\ H_2O$

M	X	n	z					
K	NO_2	2	–	187	Dark orange	72	112	
K	NCO	2	2	191	Violet	191		Thermal data 191
K	NCS	1	2	191	Violet	191		Thermal data 191
K	NCSe	1	2	191	Violet			Thermal data 191
Gun H	Cl	2	0	187	Dark green	39		
Gun NH_2H	Cl	2	0	39	Green	39		Thermal data 39
Na	Cl	2	0/2/6	187	Green			
Cs	Cl	2	0	72 [a]		72	112, 113	
NH_4	Br	2	0	187	Dark green			
Gun H	Br	2	0	187	Bright green		112, 113	Molar conductance 187
Cs	Br	2	0	72 [a]		72	112, 113	

Cs	Br	1	0	113[a]					
	NO_2	1							
K	I	2	1	72[a]		72			
K	CN	1	1	86		86			
K	HSO_3	2	0	197					

$M_n[Rh_2(O_2CH)_2(Y\text{-}Y)_2]X_n$

M	Y–Y	X	n						
K	$-O_2CO-$	–	2	189[a]					
Cs	$-O_2CO-$	–	2	189[a]					
–	*o*-Phen	Cl	2	47, 48	Violet-red	47, 48	48		
–	*o*-Phen	Br	2	97	Dark brown	47	97		
–	Bipy	Cl	2	47		47	97		

$M_n[Rh_2(O_2CMe)_4X_n]\cdot zH_2O$

M	X	n	z						
K	NO_2	2	–	69, 72	Red			111–113	TGA 71
K	NCO	2	2	43, 191	Violet	43, 191			TGA 43, 191
K	NCS	2	2	43, 191	Violet-green	43, 191			TGA 43, 191
K	$HONMe_2$	1	–	191		191			Thermal stability data 191
	NCS	1							
K	NCSe	1	2	43, 191	Violet-grey	43, 191			TGA 43, 191
K	$HCONMe_2$	1	–	191		191			Thermal stability data 191
	NCSe	1							
NH_4	Cl	2	–	26					
$H_2N(CH_2)_2NH_3$	Cl	2	6	26	Green				
$H_2NCONHNH_3$	Cl	2	–	188	Blue-green				
GunH	Cl	2	–	39, 69	Green	72		112, 113	TGA 71
Gun NH_2H	Cl	2	–	39[a]	Green	39			Thermal stability data 39

TABLE 19 (continued)

L			n	Prep.	Colour	Vibrational spectra	Electronic spectra	ESCA	Other physical measurements [c]
K	Cl	2	–	69, 114	Green	72		113, 114	TGA 71
Cs	Cl	2	–	114				114	
NH_4	Cl	1	–	26					
K	Cl	1	–	26	Green				
N_2H_5	Cl	1	1	71					Mag.s. 71
NH_4	Br	2	–	26					Mag.s. 71
Gun H	Br	2	–	26		72		112, 113	Mag.s. 71
K	Br	2	–	26		72		112, 114	
Gun H	I	2	2	26					
Gun	CN	2	–	39	Orange	39			
K_4	$(SO_3)_2$	–	4	197					
$M_n[Rh_2(O_2CCH_2F)_4X_n]\cdot zH_2O$									
K	CN	2	0.5	86	Orange	86			
$M_n[Rh_2(O_2CCH_2Cl)_4X_n]\cdot zH_2O$									
K	NCO	2	1	191	Violet	191			Thermal decomp. data 191
K	NCS	1	2	191	Violet-green	191			Thermal decomp. data 191
K	NCSe	1	2	191		191			Thermal decomp. data 191
K	CN	2	2	86	Orange	86			
$M_n[Rh_2(O_2CEt)_4X_n]\cdot z\,H_2O$									
K	NCO	2	2	191	Violet	191			Thermal decomp. data 191
K	NCS	1	2	191	Violet-green	191			Thermal decomp. data 191

K	NCSe	1	2	191	Grey-violet	191				Thermal decomp. data 191
Gun H	Cl	2	–	39	Green	39				
Gun NH_2H	Cl	2	–	39	Green	39				
K	CN	2	–	86	Orange	86				

$M_n[Rh_2(O_2CBu)_4X_n]\cdot zH_2O$

K	CN	2	–	86	Orange	86				

$[Rh_2(O_2CCH_2CH_2NH_3)_4(H_2O)_2]ClO_4\cdot 2H_2O$

				68	Blue-green	–	68			^{1}H NMR 68

$M_n[Rh_2(O_2CC_6H_5CH(OH))_4]X_n$

M	X	n								
Cs	Cl	1	196							
K	NO_2	2	196							

$Rh_2(OSCMe)_4L_n$

L	n									
–	–	77		77		77				
H_2O	2	77	Dark green	77		77, 112				
C_5H_5N	2	77	Orange	77		77, 112				Raman 77
CH_3CN	2	77	Red	77		77, 112				Raman 77
NH_2NH_3Cl	2	77	Dark	77		77, 112				
		198	cherry-red							
Me_2SO	2	77	Yellow	77		77, 112				
$(NH_2)_2CS$	2	77	Cherry-red	77		77, 112				
MeCOSH	2	77	Red	77		77, 112				X-ray crystal 199, 200
		198								

$Rh_2(OSCC_6H_5)_4L_n$

–	–	78, 136	Green	78		78, 112				

TABLE 19 (continued)

L			n	Prep.	Colour	Vibrational spectra	Electronic spectra	ESCA	Other physical measurements [c]
$HCONMe_2$			2	78	Brown	78		78, 112	
C_5H_5N			2	78, 136	Orange	78		112	Thermal decomp. data 78
MeCN			2	–					
Me_2SO			2	78	Orange	78		112, 78	
$(NH_2)_2CS$			2	78	Dark red	78		78, 112	
C_6H_5COSH			2	78, 136	Dark-red	78		78, 112	
$M_n[Rh_2(OSCMe)_4X_n]\cdot z\ H_2O$									
M	X	n	z						
K	NCS	2	2	77	Red	77		77	
Cs	Cl	2	1	77	Blue	77		77, 112	

[a] Complex mentioned, but no preparative details given. [b] D = MeCN, C_5H_5N, *N*-methylimidazole, piperidine, Et_2S, 4-picoline *N*-oxide, Me_2SO, caged phosphite. [c] Ms = mass spectrometry; Mag.s. = magnetic susceptibility. Thermo = thermodynamic. [d] The following compounds $Rh_2(O_2CR)_4$ have been mentioned briefly in papers concerning application: R = Cl–C_6H_4–, 1 MeO–C_6H_4–, 2 MeO–C_6H_4–, 3 MeO–C_6H_4–, NO_2–C_6H_4–, 1,5-$Me_2C_6H_3$–, $CH_3(CH_2)_6$– [96]; R = Me_2CH–, $CF_3(CF_2)_2$–, $HOCH_2(CH_2)_2$–, $MeCONH(CH_2)_3$–, cyclo C_4H_7–, $NaO_2CCH(Et)$– [178b].

In contrast to rhodium, iridium does not appear to form dimeric carboxylate compounds at all readily; although numerous attempts have been made to prepare compounds of this type, none has been reported to date. A binuclear iridium(II) carboxylate might be expected to show a stronger metal–metal interaction than the rhodium(II) carboxylates. An experimental procedure similar to that first used to prepare rhodium(II) formate has been applied to iridium, i.e., treatment of $H_2[IrCl_6]$ with formic acid in ethanol containing HCl; however the product of this reaction has been formulated as an iridium(III) compound $H[Ir(O_2CH)_2Cl_2]$ [183]. An iridium(II) carboxylate $[Ir(O_2CR)_2(AsPh_3)_2(CNC_6H_4Me)]$ [184] has been prepared, but it appears to be a mononuclear paramagnetic complex with tetragonally distorted octahedral geometry.

Cobalt(II) is also reluctant to form binuclear carboxylate complexes; only one example $[Co_2(O_2CC_6H_5)_4(quinoline)_2]$ [185,186] has been properly characterised. An X-ray diffraction study has revealed a metal–metal separation larger than that found in the binuclear carboxylates of Cr(II), Cu(II) or Rh(II). The long Co–Co distance (2.832 Å) is consistent with the weaker metal–metal interaction which one would expect for a first row transition metal.

ADDENDUM

Since the completion of this article, several papers on rhodium(II) carboxylates and related complexes have appeared.

X-ray diffraction structural investigations on rhodium(II) carboxylate–nitroxide radical adducts $[Rh_2(O_2CCF_3)_4L_2]$ and $[Rh_2(O_2CCF_3)_4(H_2O)_2L'_2]$ (L = 2,2,6,6-tetramethyl-4-hydroxy-piperidinyl-1-oxy [TEMPOL] and L′ = di-*tert*-butyl nitroxide [DTBN]) have been reported [201]. Although the nitroxyl groups do not coordinate directly to the rhodium atoms, the nitroxyl oxygen atoms participate in hydrogen bonding to the most acidic proton in each structure. In the former structure the TEMPOL ligands coordinate axially to the lantern structure via the 4-hydroxyl oxygen atom. The nitroxyl oxygen atoms participate in intermolecular hydrogen bonding with the hydroxyl groups from adjacent dinuclear molecules, linking the $[Rh_2(O_2CCF_3)_4(TEMPOL)_2]$ molecules into zigzag chains through the crystal. The latter structure is comprised of $[Rh_2(O_2CCF_3)_4(H_2O)_2]$ and DTBN molecules. The two water hydrogen atoms participate in hydrogen bonding interactions with the nitroxyl oxygen atoms of the DTBN molecules. DTBN molecules are situated between neighbouring $[Rh_2(O_2CCF_3)_4(H_2O)_2]$ molecules. The structural parameters measured for these complexes in conjunction with data reported for other $Rh_2(O_2CCF_3)_4$ diadducts (Table 1) help to establish that the inductive effect of the CF_3

group is less effective than that of the axial ligands in perturbing the Rh–Rh ground state. X-ray diffraction crystallographic data has also been reported for $[Rh_2(O_2CPh)_4Py_2]$ [202] and $[Rh_2(O_2CH)_2Cl_2(bipy)_2]\cdot 2H_2O$ [203]. The latter compound has been further characterized by infrared and electron spectroscopy and conductivity measurements.

Drago et al. [204] have pursued their study of the thermodynamics of base binding in systems containing metal–metal bonds. Comparison of the butyrate and perfluorobutyrate complexes of rhodium(II) and molybdenum(II) indicate that the increase in the carboxylate group electronegativity, decreases the relative importance of π-back bonding in the dirhodium system, although such a change has little influence on the inductive transfer to the second metal resulting from coordination of base to the first metal. The inductive transfer of electrostatic properties of the base are less effective through the longer Rh–Rh bond than through the Mo–Mo bond. However the greater polarizability of the Rh–Rh bond produces a more marked difference in the covalency of the 2 : 1 and 1 : 1 adducts of rhodium carboxylates than that found for the corresponding dimolybdenum systems.

The novel rhodium(II) trifluoroacetamide dimer $[Rh_2\{O(NH)CCF_3\}_4]$ [205,206] has been characterised by electrochemical and spectroscopic means. Reversible one-electron oxidation was observed in all the solvents investigated, except for pyridine and acetonitrile/pyridine mixtures, where a rapid chemical reaction followed the oxidation. Reduction was observed only for the solutions in THF and was irreversible. The ease with which $[Rh_2\{O(NH)CCF_3\}_4]$ is oxidized suggests that the HOMO of the Rh–Rh bonding scheme is destabilized relative to that in the analogous trifluoroacetate dimer $[Rh_2(O_2CCF_3)_4]$, which has previously been shown to be resistant to oxidation. Bear et al. [207] also prepared the novel rhodium(II) *N*-phenylacetamide compounds $[Rh_2\{O(NMe)CPh\}_4(H_2O)]$ and $[Rh_2\{O(NMe)CPh\}_4]$. They used ^1H and ^{13}C NMR to establish that the former exists in a 2 : 2 configuration while the latter adopts a 3 : 1 configuration (cf. the 3 : 1 configuration reported by Cotton et al. for the *o*-oxypyridine dirhodium compounds [44–46]). Electrochemical oxidation proceeds in two steps without destroying the dimeric structure; characterization of the product of the second oxidation step by electronic spectroscopy is in progress.

The reactions of $[Rh_2(O_2CCH_3)_4(H_2O)_2]$ and $[Rh_2(O_2CH)_4]$ with K_2SO_3, $K_2S_2O_5$ and SO_2 have been investigated [208]. Adducts of the rhodium(II) carboxylates with the sulphur-containing ligands are initially formed, but when the solutions are heated or left to stand for a long time, the carboxylate groups are replaced by sulphite groups, leading to formation of polynuclear rhodium compounds which have been investigated by X-ray photoelectron spectroscopy, and assigned as rhodium(III) species.

Porai-Koshits and co-workers have reported an X-ray diffraction analysis

of the related compound $[Rh_2(H_2PO_4)_4(H_2O)_2]$ [209], which revealed a Rh–Rh distance of 2.487(1) Å. They feel that this result supports the former single Rh–Rh bond model, and suggests that the Rh–Rh bond length is mainly determined by steric conditions, such as the "bite" of the bridging group. (This view is contrary to that expressed by Christoph and Koh [8] and Norman and Kolari [9]; see Section J.)

A brief review on bimetallic rhodium(II) complexes containing details on Rh–Rh bond length, bond order, molecular vibrations and chemical behaviour has appeared [210].

Finally, further studies on the rhodium(II) carboxylates catalyzed synthesis of antibiotics have been reported. The reaction of 4-thiaazetidinones with diazomalonates in the presence of a catalytic amount of rhodium(II) acetate yields carbon-introduced products at the C_4 position of the β-lactams [211].

ACKNOWLEDGEMENTS

One of the authors (EBB) gratefully acknowledges financial support from the SERC.

REFERENCES

1 I.I. Chernyaev, E.V. Shenderetskaya and A.A. Karyagina, Zh. Neorg. Khim., 5 (1960) 1163; Russ. J. Inorg. Chem., 5 (1960) 559.
2 I.I. Chernyaev, E.V. Shenderetskaya, A.G. Maiorova and A.A. Karyagina, Zh. Neorg. Khim., 10 (1965) 537; Russ. J. Inorg. Chem., 10 (1965) 290.
3 I.I. Chernyaev, E.V. Shenderetskaya, L.A. Nazarova and A.S. Antsyskina, Theory and Structure of Complex Compounds, Warsaw, 1964, p. 27.
4 M.A. Porai-Koshits and A.S. Antsyskina, Dokl. Akad. Nauk SSSR., 146 (1962) 1102; Proc. Acad. Sci. USSR, 146 (1962) 902.
5 A.S. Antsyskina, Acta Crystallogr. Sect. A, 21 (1966) 135.
6 J.N. van Niekerk, F.R.L. Schoening and J.F. de Wet, Acta Crystallogr., 6 (1953) 501.
7 J.N. van Niekerk and F.R.L. Schoening, Acta Crystallogr., 6 (1953) 227.
8 G.G. Christoph and Y.B. Koh, J. Am. Chem. Soc., 101 (1979) 1422.
9 J.G. Norman, Jr. and H.J. Kolari, J. Am. Chem. Soc., 100 (1978) 791.
10 J.G. Norman, Jr., G.E. Renzoni and D.A. Case, J. Am. Chem. Soc., 101 (1979) 5256.
11 F.A. Cotton, B.G. DeBoer, M.D. LaPrade, J.R. Pipal and D.A. Ucko, Acta Crystallogr. Sect. B, 27 (1971) 1664.
12 M.J. Bennett, K.G. Caulton and F.A. Cotton, Inorg. Chem., 8 (1969) 1.
13 R.G. Hughes, J.L. Bear and A.P. Kimball, Proc. Am. Assoc. Cancer Res., 13 (1972) 120.
14 R.A. Howard, A.P. Kimball and J.L. Bear, Cancer Res., 39 (1979) 2568.
15 A. Erck, L. Rainen, J. Whileyman, I.M. Chang, A.P. Kimball and J.L. Bear, Proc. Soc. Exp. Biol. Med., 145 (1974) 1278.
16a. B.C.Y. Hui and G.L. Rempel, J. Chem. Soc. Chem. Commun., (1970) 1195.
16b. B.C.Y. Hui, W.K. Teo and G.L. Rempel, Inorg. Chem., 12 (1973) 757.
17a. A.J. Hubert, A.F. Noels, A.J. Anciaux and P. Teyssié, Synthesis, 8 (1976) 600.
17b. D. Holland and D.J. Milner, J. Chem. Res. M, (1979) 3734.

18 I.B. Baranovskii and R.N. Shchelokov, Zh. Neorg. Khim., 23 (1978) 3; Russ. J. Inorg. Chem., 23 (1978) 1.
19 D.J. Cole-Hamilton, Coord. Chem. Rev., 35 (1981) 113.
20 E.B. Boyar and S.D. Robinson, Platinum Met. Rev., 26 (1982) 65.
21 A. Dobson and S.D. Robinson, Platinum Met. Rev., 20 (1976) 56.
22 C. Oldham, Prog. Inorg. Chem., 10 (1968) 223.
23 M.A. Porai-Koshits, Zh. Strukt. Khim., 21 (1980) 146; J. Struct. Chem., 21 (1980) 369.
24 J. Catterick and P. Thornton, Adv. Inorg. Chem. Radiochem., 20 (1977) 291.
25 C.D. Garner and B. Hughes, Adv. Inorg. Chem. Radiochem., 17 (1975) 1.
26 L.A. Nazarova, I.I. Chernyaev and A.S. Morozova, Zh. Neorg. Khim., 11 (1966) 2583; Russ. J. Inorg. Chem., 11 (1966) 1387.
27 P. Legzdins, R.W. Mitchell, G.L. Rempel, J.D. Ruddick and G. Wilkinson, J. Chem. Soc. A, (1970) 3322.
28 G.A. Rempel, P. Legzdins, H. Smith and G. Wilkinson, Inorg. Syn., 13 (1972) 90.
29 G. Winkhaus and P. Ziegler, Z. Anorg. Allg. Chem., 350 (1967) 51.
30 J. Kitchens and J.L. Bear, Thermochim. Acta, 1 (1970) 537.
31 S.A. Johnson, H.R. Hunt and H.M. Neumann, Inorg. Chem., 2 (1963) 960.
32 T.A. Stephenson, S.M. Morehouse, A.R. Powell, J.P. Heffer and G. Wilkinson, J. Chem. Soc. (1965) 3632.
33 J.L. Bear, J. Kitchens and M.R. Willcott, J. Inorg. Nucl. Chem., 33 (1971) 3479.
34 F.A. Cotton, B.G. De Boer, M.D. LaPrade, J.R. Pipal and D.A. Ucko, J. Am. Chem. Soc., 92 (1970) 2926.
35 M. Moszner and J.J. Ziolkowski, Bull. Acad. Pol. Sci. Ser. Sci. Chim., 24 (1976) 433.
36 J.J. Ziolkowski, M. Moszner and T. Glowiak, J. Chem. Soc. Chem. Commun., (1977) 760.
37 F.A. Cotton and T.R. Felthouse, Inorg. Chem., 21 (1982) 431.
38 M.A. Porai-Koshits, L.M. Dikareva, G.G. Sadikov and I.B. Baranovskii, Zh. Neorg. Khim., 24 (1979) 1286; Russ. J. Inorg. Chem., 24 (1979) 716.
39 T.A. Veteva and V.N. Shafranskii, Zh. Obshch. Khim., 49 (1979) 488; J. Gen. Chem. USSR, 49 (1979) 428.
40 G. Pneumatikakis and N. Hadjiliadis, J. Chem. Soc., Dalton Trans., (1979) 596.
41 F.A. Cotton and T.R. Felthouse, Inorg. Chem., 20 (1981) 600.
42 V.N. Shafranskii, T.A. Mal'kova and Yu. Ya. Kharitonov, Koord. Khim., 1 (1975) 375; Soviet J. Coord. Chem., 1 (1975) 297.
43 V.N. Shafranskii, T.A. Mal'kova and Yu.Ya. Kharitonov, Zh. Strukt. Khim., 16 (1975) 212; J. Struct. Chem., 16 (1975) 195.
44 F.A. Cotton and T.R. Felthouse, Inorg. Chem., 20 (1981) 584.
45 M. Berry, C.D. Garner, I.H. Hillier, A.A. MacDowell and W. Clegg, J. Chem. Soc. Chem. Commun., (1980) 494.
46 W. Clegg, Acta Crystallogr. Sect. B, 36 (1980) 2437.
47 F. Pruchnik, M. Zuber, H. Pasternak and K. Wajda, Spectrochim. Acta, Part A, 34 (1978) 1111.
48 H. Pasternak and F. Pruchnik, Inorg. Nucl. Chem. Lett., 12 (1976) 591.
49 J. Halpern, E. Kimura, J. Molin-Case and C.S. Wong, J. Chem. Soc. Chem. Commun., (1971) 1207.
50 H.J. Keller and K. Seibold, Z. Naturforsch. Teil B, 25 (1970) 551.
51 S.A. Shchepinov, E.N. Sal'nikova and M.L. Khidekel, Izv. Akad. Nauk SSSR. Ser. Khim., (1967) 2128.
52 S. Cenini, R. Ugo and F. Bonati, Inorg. Chim. Acta, 1 (1967) 443.

53 G. Pannetier and J. Segall, J. Less-Common Met., 22 (1970) 305.
54 R.W. Matthews, A.D. Hamer, D.L. Hoof, D.G. Tisley and R.A. Walton, J. Chem. Soc. Dalton Trans., (1973) 1035.
55 R.N. Shchelokov, A.G. Maiorova, G.N. Kuznetsova, I.F. Golovaneva and O.N. Evstaf'eva, Zh. Neorg. Khim., 25 (1980) 1891; Russ. J. Inorg. Chem., 25 (1980) 1049.
56 S. Jagner, R.G. Hazell and K.P. Larsen, Acta Crystallogr. Sect. B, 32 (1976) 548.
57 G.G. Christoph and Y.B. Koh, Inorg. Chem., 18 (1979) 1122.
58 G.G. Christoph and Y.B. Koh, Inorg. Chem., 17 (1978) 2590.
59 K. Aoki and H. Yamazaki, J. Chem. Soc. Chem. Commun., (1980) 186.
60 F.A. Cotton and T.R. Felthouse, Inorg. Chem., 19 (1980) 323.
61 G.G. Christoph, J. Halpern, G.P. Khare, Y.B. Koh and C. Romanowski, Inorg. Chem., 20 (1981) 3029.
62 L.M. Dikareva, G.G. Sadikov, I.B. Baranovskii and M.A. Porai-Koshits, Zh. Neorg. Khim., 25 (1980) 3146; Russ. J. Inorg. Chem., 25 (1980) 1725.
63 L.M. Dikareva, Acta Crystallogr. Sect. A, 21 (1966) 140.
64 A. Dereigne, J.M. Manoli and J. Segall, J. Less-Common Met., 22 (1970) 314.
65 F.A. Cotton and T.R. Felthouse, Inorg. Chem., 19 (1980) 2347.
66 F.A. Cotton and T.R. Felthouse, Inorg. Chem., 20 (1981) 2703.
67 F.A. Cotton, T.R. Felthouse and S. Klein, Inorg. Chem., 20 (1981) 3037.
68 A.M. Dennis, R.A. Howard, J.L. Bear, J.D. Korp and I. Bernal, Inorg. Chim. Acta, 37 (1979) L561.
69 L.A. Nazarova, I.I. Chernyaev and A.S. Morozova, Zh. Neorg. Khim., 10 (1965) 539; Russ. J. Inorg. Chem., 10 (1965) 291.
70 J. Kitchens and J.L. Bear, J. Inorg. Nucl. Chem., 32 (1970) 49.
71 V.I. Belova and Z.S. Dergacheva, Zh. Neorg. Khim., 16 (1971) 3062; Russ. J. Inorg. Chem., 16 (1971) 1626.
72 G.Ya. Mazo, I.B. Baranovskii and R.N. Shchelokov, Zh. Neorg. Khim., 24 (1979) 3330; Russ. J. Inorg. Chem., 24 (1979) 1855.
73 T.A. Mal'kova and V.N. Shafranskii, Zh. Fiz. Khim., 49 (1975) 2805; Russ. J. Phys. Chem., 49 (1975) 1653.
74 A.P. Ketteringham and C. Oldham, J. Chem. Soc., Dalton Trans., (1973) 1067.
75 V.N. Shafranskii and T.A. Mal'kova, Zh. Obshch. Khim., 46 (1976) 1197; J. Gen. Chem. USSR, 46 (1976) 1181.
76 T.A. Mal'kova and V.N. Shafranskii, Zh. Obshch. Khim., 47 (1977) 2592; J. Gen. Chem. USSR, 47 (1977) 2365.
77 I.B. Baranovskii, M.A. Golubnichaya, G.Ya. Mazo, V.I. Nefedov, Ya.V. Salyn' and R.N. Shchelokov, Zh. Neorg. Khim., 21 (1976) 1085; Russ. J. Inorg. Chem., 21 (1976) 591.
78 I.B. Baranovskii, M.A. Golubnichaya, G.Ya. Mazo, V.I. Nefedov, Ya. V. Salyn' and R.N. Shchelokov, Koord. Khim., 3 (1977) 743; Soviet J. Coord. Chem., 3 (1977) 576.
79 J. San Filippo Jr. and H.J. Sniadoch, Inorg. Chem., 12 (1973) 2326.
80 I.K. Kireeva, G. Ya. Mazo and R.N. Shchelokov, Zh. Neorg. Khim., 24 (1979) 396; Russ. J. Inorg. Chem., 24 (1979) 220.
81 Yu.Ya. Kharitonov, G. Ya. Mazo and N.A. Knyazeva, Zh. Neorg. Khim., 15 (1970) 1440; Russ. J. Inorg. Chem., 15 (1970) 739.
82 T.A. Mal'kova and V.N. Shafranskii, Zh. Neorg. Khim., 20 (1975) 1308; Russ. J. Inorg. Chem., 20 (1975) 735.
83 T.A. Mal'kova and V.N. Shafranskii, Zh. Neorg. Khim., 19 (1974) 2501; Russ. J. Inorg. Chem., 19 (1974) 1366.

84 V.N. Shafranskii and T.A. Mal'kova, Zh. Obshch. Khim., 45 (1975) 1065; J. Gen. Chem. USSR, 45 (1975) 1051.
85 K.A. Bailey, S.L. Kozak, T.W. Michelsen and W.N. Mills, Coord. Chem. Rev., 6 (1971) 407.
86 T.A. Mal'kova, V.N. Shafranskii and Yu. Ya. Kharitonov, Koord. Khim., 3 (1977) 1747; Soviet J. Coord. Chem., 3 (1977) 1371.
87 R.D. Cannon, D.B. Powell, K. Sarawek and J.C. Stillman, J. Chem. Soc. Chem. Commun., (1976) 31.
88 J. Kitchens and J.L. Bear, J. Inorg. Nucl. Chem., 31 (1969) 2415.
89 L. Dubicki and R.L. Martin, Inorg. Chem., 9 (1970) 673.
90 G. Pneumatikakis and P. Psaroulis, Inorg. Chim. Acta, 46 (1980) 97.
91 C.R. Wilson and H. Taube, Inorg. Chem., 14 (1975) 2276.
92 D.S. Martin, Jr., T.R. Webb, G.A. Robbins and P.E. Fanwick, Inorg. Chem., 18 (1979) 475.
93 G. Bienek, W. Tuszynski and G. Gliemann, Z. Naturforsch. Teil B, 33 (1978) 1095.
94 C.R. Wilson and H. Taube, Inorg. Chem., 14 (1975) 405.
95 J.J. Ziolkowski, Bull. Acad. Pol. Sci. Ser. Sci. Chim., 21 (1973) 125.
96 E. Sinn, Inorg. Nucl. Chem. Lett., 11 (1975) 665.
97 F. Pruchnik and M. Zuber, Rocz. Chem., 51 (1977) 1813.
98 N. Farrell, J. Inorg. Biochem., 14 (1981) 261.
99 D.F. Evans, J. Chem. Soc., (1959) 2003.
100 R.A. Bailey, J. Chem. Educ., 49 (1972) 297.
101a. E.B. Boyar and S.D. Robinson, Inorg. Chim. Acta, 64 (1982) L193.
101b. E.B. Boyar and S.D. Robinson, Inorg. Chim. Acta, 76 (1983) L137.
101c. E.B. Boyar and S.D. Robinson, unpublished results.
102a. R.A. Jones and G. Wilkinson, J. Chem. Soc., Dalton Trans., (1979) 472.
102b. R.A. Jones, K.W. Chiu, G. Wilkinson, A.M.R. Galas and M.B. Hursthouse, J. Chem. Soc. Chem. Commun., (1980) 408.
103 G. Balimann and P.S. Pregosin, J. Magn. Resonance, 22 (1976) 235.
104 T. Kawamura, K. Fukamachi, S. Hayashida, T. Sowa and T. Yonezawa, J. Am. Chem. Soc., 103 (1981) 364.
105 K. Das, K.M. Kadish and J.L. Bear, Inorg. Chem., 17 (1978) 930.
106 R.S. Drago, S.P. Tanner, R.M. Richman and J.R. Long, J. Am. Chem. Soc., 101 (1979) 2897.
107 T. Kawamura, K. Fukamachi and S. Hayashida, J. Chem. Soc. Chem. Commun., (1979) 945.
108 B.A. Goodman and J.B. Raynor, Adv. Inorg. Chem. Radiochem., 13 (1970) 135.
109 R.M. Richman, T.C. Kuechler, S.P. Tanner and R.S. Drago, J. Am. Chem. Soc., 99 (1977) 1055.
110 A.D. Hamer, D.G. Tisley and R.A. Walton, J. Chem. Soc., Dalton Trans., (1973) 116.
111 A.M. Dennis, R.A. Howard, K.M. Kadish, J.L. Bear, J. Brace and N. Winograd, Inorg. Chim. Acta, 44 (1980) L139.
112 V.I. Nefedov, Ya.V. Salyn', I.B. Baranovskii and A.G. Maiorova, Zh. Neorg. Khim., 25 (1980) 216; Russ. J. Inorg. Chem., 25 (1980) 116.
113 V.I. Nefedov, Ya.V. Salyn', A.G. Maiorova, L.A. Nazarova and I.B. Baranovskii, Zh. Neorg. Khim., 19 (1974) 1353; Russ. J. Inorg. Chem., 19 (1974) 736.
114 V.I. Nefedov, Ya. V. Salyn', A.V. Shtemenko and A.S. Kotelnikova, Inorg. Chim. Acta, 45 (1980) L49.
115 V.I. Nefedov, Ya.V. Salyn' and A.P. Sadovskiy, J. Electron Spectrosc. Relat. Phenom., 16 (1979) 299.

116 V.I. Nefedov, A.P. Sadovskii and Ya. V. Salyn', Koord. Khim., 5 (1979) 1204; Sov. J. Coord. Chem., 5 (1979) 949.
117 K.G. Caulton and F.A. Cotton, J. Am. Chem. Soc., 93 (1971) 1914.
118 B.E. Bursten and F.A. Cotton, Inorg. Chem., 20 (1981) 3042.
119 R.S. Drago, J.R. Long and R. Cosmano, Inorg. Chem., 20 (1981) 2920.
120 R.S. Drago, Inorg. Chem., 21 (1982) 1697.
121 J.L. Bear, R.A. Howard and J.E. Korn, Inorg. Chim. Acta, 32 (1979) 123.
122 H. Nakatsuji, T. Ushio, K. Kanda, Y. Onishi, T. Kawamura and T. Yonezawa, Chem. Phys. Lett., 79 (1981) 299.
123 B.E. Bursten, F.A. Cotton and M.B. Hall, J. Am. Chem. Soc., 102 (1980) 6348.
124 Y.N. Kukushkin, S.A. Simanova, V.K. Krylov, S.I. Bakhireva and I.A. Belen'kaya, Zh. Obshch. Khim., 46 (1976) 888; J. Gen. Chem. USSR, 46 (1976) 885.
125 R.A. Howard, A.M. Wynne, J.L. Bear and W.W. Wendlandt, J. Inorg. Nucl. Chem., 38 (1976) 1015.
126 T.A. Mal'kova and V.N. Shafranskii, Zh. Obshch. Khim., 45 (1975) 631; J. Gen. Chem. USSR, 45 (1975) 618.
127 G.S. Girolami and R.A. Andersen, Inorg. Chem., 20 (1981) 2040.
128 K. Das, E.L. Simmons and J.L. Bear, Inorg. Chem., 16 (1977) 1268.
129 K. Das and J.L. Bear, Inorg. Chem., 15 (1976) 2093.
130 A.M. Dennis, R.A. Howard and J.L. Bear, Inorg. Chim. Acta, 66 (1982) L31.
131 L. Rainen, R.A. Howard, A.P. Kimball and J.L. Bear, Inorg. Chem., 14 (1975) 2752.
132 I.B. Baranovskii, N.N. Chalisova and G.Ya. Mazo, Zh. Neorg. Khim., 24 (1979) 3395; Russ. J. Inorg. Chem., 24 (1979) 1893.
133 I.B. Baranovskii, S.S. Abdullaev and R.N. Shchelokov, Zh. Neorg. Khim., 24 (1979) 3149; Russ. J. Inorg. Chem., 24 (1979) 1753.
134 L.M. Dikareva, G.G. Sadikov, M.A. Porai-Koshits, I.B. Baranovskii and S.S. Abdullaev, Zh. Neorg. Khim., 25 (1980) 875; Russ. J. Inorg. Chem., 25 (1980) 488.
135 I.B. Baranovskii, S.S. Abdullaev, G.Ya. Mazo, I.F. Golovaneva, Ya.V. Salyn' and R.N. Shchelokov, Zh. Neorg. Khim., 26 (1981) 1715; Russ. J. Inorg. Chem., 26 (1981) 925.
136 I.B. Baranovskii, M.A. Golubnichaya, G.Ya. Mazo and R.N. Shchelokov, Koord. Khim., 1 (1975) 1573; Soviet J. Coord. Chem., 1 (1975) 1299.
137 J.S. Dwivedi and U. Agarwala, Z. Anorg. Allg. Chem., 397 (1973) 74.
138 I.P. Evans and G. Wilkinson, J. Chem. Soc. Dalton Trans., (1974) 946.
139 R.A. Howard, T.G. Spring and J.L. Bear, J. Clin. Hematol. Oncol., 7 (1977) 391.
140 A. Erck, E. Sherwood, J.L. Bear and A.P. Kimball, Cancer Res., 36 (1976) 2204.
141 E. Billig, S.I. Shupack, J.H. Waters, R. Williams and H.B. Gray, J. Am. Chem. Soc., 86 (1964) 926.
142 G.P. Mezharaush, Izv. Akad. Nauk. Latv. SSR, Ser. Khim., (1965) 263.
143 T.T. Pinnovaia, R. Raythatha, J.G.S. Lee, L.J. Halloran and J.F. Hoffman, J. Am. Chem. Soc., 101 (1979) 6891.
144 L.A. Nazarova and A.G. Maiorova, Zh. Neorg. Khim., 18 (1973) 1710; Russ. J. Inorg. Chem., 18 (1973) 904.
145 F. Maspero and H. Taube, J. Am. Chem. Soc., 90 (1968) 7361.
146 J.J. Ziolkowski, Bull. Acad. Pol. Sci. Ser. Chim., 21 (1973) 119.
147 H.D. Glicksman, A.D. Hamer, T.J. Smith and R.A. Walton, Inorg. Chem., 15 (1976) 2205.
148 H.D. Glicksman and R.A. Walton, Inorg. Chim. Acta, 33 (1979) 255.
149 S. Uemura, A. Spencer and G. Wilkinson, J. Chem. Soc., Dalton Trans., (1973) 2565.
150 J.G. Norman and E.O. Fey, J. Chem. Soc. Dalton Trans., (1976) 765.

151 I.B. Baranovskii, M.A. Golubnichaya, G. Ya. Mazo and R.N. Shchelokov, Zh. Neorg. Khim., 22 (1977) 555; Russ. J. Inorg. Chem., 22 (1977) 308.
152 R.A. Andersen, R.A. Jones, G. Wilkinson, M.B. Hursthouse and K.M.A. Malik, J. Chem. Soc. Chem. Commun., (1977) 283.
153 R.W. Mitchell, J.D. Ruddick and G. Wilkinson, J. Chem. Soc. A, (1971) 3224.
154a. B.R. James, G.L. Rempel and W.K. Teo, Inorg. Synth., 16 (1976) 49.
154b. R.B. King, A.D. King Jr. and M.Z. Iqbal, J. Am. Chem. Soc., 101 (1979) 4893.
155 K.M. Kadish, K. Das, R. Howard, A. Dennis and J.L. Bear, Bioelectrochem. Bioenerg., 5 (1978) 741.
156 R.D. Cannon, D.B. Powell and K. Sarawek, Inorg. Chem., 20 (1981) 1470.
157 N. Ikota, N. Takamura, S.D. Young and B. Ganem, Tetrahedron Lett., 22 (1981) 4163.
158 R. Pellicciari, R. Fringuelli, P. Ceccherelli and E. Sisani, J. Chem. Soc. Chem. Commun., (1979) 959.
159 N. Petiniot, A.J. Anciaux, A.F. Noels, A.J. Hubert and P. Teyssié, Tetrahedron Lett., (1978) 1239.
160 A.J. Anciaux, A.J. Hubert, A.F. Noels, N. Petiniot and P. Teyssié, J. Org. Chem., 45 (1980) 695.
161 J. Drapier, A. Feron, R. Warin, A.J. Hubert and P. Teyssié, Tetrahedron Lett., (1979) 559.
162 A.J. Hubert, A. Feron, R. Warin and P. Teyssié, Tetrahedron Lett., (1976) 1317.
163 A.J. Anciaux, A. Demonceau, A.F. Noels, A.J. Hubert, R. Warin and P. Teyssié, J. Org. Chem., 46 (1981) 873.
164 R. Paulissen, H. Reimlinger, E. Hayez, A.J. Hubert and P. Teyssié, Tetrahedron Lett., (1973) 2233.
165a. R. Paulissen, E. Hayez, A.J. Hubert and P. Teyssié, Tetrahedron Lett., 7 (1974) 607.
165b. A. Demonceau, A.F. Noels, A.J. Hubert and P. Teyssié, J. Chem. Soc. Chem. Commun., (1981) 688.
166 S.A. Matlin and Lam Chan, J. Chem. Soc. Chem. Commun., (1980) 798.
167a. S.A. Matlin and Lam Chan, Tetrahedron Lett., 22 (1981) 4025.
167b. R.J. Gillespie, J. Murray-Rust, P. Murray-Rust and A.E.A. Porter, J. Chem. Soc. Chem. Commun., (1978) 83.
168 A.J. Anciaux, A. Demonceau, A.J. Hubert, A.F. Noels, N. Petiniot and P. Teyssié, J. Chem. Soc. Chem. Commun., (1980) 765.
169 S.A. Matlin and Lam Chan, J. Chem. Soc. Chem. Commun., (1981) 10.
170a. R.J. Ponsford and R. Southgate, J. Chem. Soc. Chem. Commun., (1979) 846.
170b. R. Pellicciari, E. Sisani and R. Fringuelli, Tetrahedron Lett., 21 (1980) 4039.
171a. A.F. Noels, A.J. Hubert and P. Teyssié, J. Organomet. Chem., 166 (1979) 79.
171b. A.J. Cornish, M.F. Lappert, G.L. Filatovs and T.A. Nile, J. Organomet. Chem., 172 (1979) 153.
171c. T.J. Pinnavaia and P.K. Welty, J. Am. Chem. Soc., 97 (1975) 3819.
171d. T.J. Pinnavaia, R. Raythatha, J.G.-Shuh Lee, L.J. Halloran and J.F. Hoffman, J. Am. Chem. Soc., 101 (1979) 6891.
172 V. Schurig, J.L. Bear and A. Zlatkis, Chromatographia, 5 (1972) 301.
173a. B. Rosenberg, L. Van Camp and T. Krigas, Nature (London), 205 (1965) 698.
173b. B. Rosenberg, L. Van Camp, J.E. Trosko and V.H. Mansour, Nature (London), 222 (1969) 385.
174 P.J. Sadler, Chem. Br., 18 (1982) 182.
175 A.I. Stentsenko, M.A. Presnov and A.L. Konovalova, Usp. Khim., 50 (1981) 665; Russ. Chem. Rev., 50 (1981) 353.

176 M.J. Cleare, Coord. Chem. Rev., 12 (1974) 349.
177 J.L. Bear, H.B. Gray, Jr., L. Rainen, I.M. Chang, R. Howard, G. Serio and A.P. Kimball, Cancer Chemother. Rep., 59 (1975) 611.
178a. P.N. Rao, M.L. Smith, S. Pathak, R.A. Howard and J.L. Bear, J. Nat. Cancer Inst., 64 (1980) 905.
178b. L.M. Hall, R.J. Speer and H.J. Ridgway, J. Clin. Hematol. Oncol., 10 (1980) 25.
179 R.A. Howard, T.G. Spring and J.L. Bear, Cancer Res., 36 (1976) 4402 and references therein.
180 J.L. Bear, R.A. Howard and A.M. Dennis, Curr. Chemother., (1978) 1321.
181 R.A. Howard, E. Sherwood, A. Erck, A.P. Kimball and J.L. Bear, J. Med. Chem., 20 (1977) 943.
182 L.A. Zwelling, T. Andersen and K.W. Kohn, Cancer Res., 39 (1979) 365.
183 I.I. Chernyaev and Z.M. Novozhenyuk, Zh. Neorg. Khim., 11 (1966) 1880; Russ. J. Inorg. Chem., 11 (1966) 1004.
184 A. Aràneo, F. Morazzoni and T. Napoletano, J. Chem. Soc., Dalton Trans., (1975) 2039.
185 J. Drew, M.B. Hursthouse, P. Thornton and A.J. Welch, J. Chem. Soc. Chem. Commun., (1973) 52.
186 J. Catterick, M.B. Hursthouse, P. Thornton and A.J. Welch, J. Chem. Soc., Dalton Trans., (1977) 223.
187 I.I. Chernyaev, E.V. Shenderetskaya, A.G. Maiorova and A.A. Karyagina, Zh. Neorg. Khim., 11 (1966) 2575; Russ. J. Inorg. Chem., 11 (1966) 1383.
188 L.A. Nazarova and A.G. Maiorova, Zh. Neorg. Khim., 21 (1976) 1070; Russ. J. Inorg. Chem., 21 (1976) 583.
189 R.N. Shchelokov, A.G. Maiorova, O.M. Evstaf'eva and G.N. Emel'yanova, Zh. Neorg. Khim., 22 (1977) 1414; Russ. J. Inorg. Chem., 22 (1977) 770.
190 N. Farrell, J. Chem. Soc. Chem. Commun., (1980) 1014.
191 T.A. Mal'kova, V.N. Shafranskii and Yu. Ya. Kharitonov, Koord. Khim., 1 (1975) 375; Soviet J. Coord. Chem., 1 (1975) 297.
192 M.A. Golubnichaya, I.B. Baranovskii, G. Ya. Mazo and R.N. Shchelokov, Zh. Neorg. Khim., 26 (1981) 2868; Russ. J. Inorg. Chem., 26 (1981) 1534.
193 G.A. Barclay, R.F. Broadbent, J.V. Kingston and G.R. Scollary, Thermochim. Acta, 10 (1974) 73.
194 A.G. Maiorova, L.A. Nazarova and G.N. Emel'yanova, Zh. Neorg. Khim., 18 (1973) 1866; Russ. J. Inorg. Chem., 18 (1973) 986.
195 A.G. Maiorova, L.A. Nazarova and G.N. Emel'yanova, Zh. Neorg. Khim., 18 (1973) 1871; Russ. J. Inorg. Chem., 18 (1973) 989.
196 R.N. Shchelokov, A.G. Maiorova, S.S. Abdullaev, O.N. Evstaf'eva, I.F. Golovaneva and G.N. Emel'yanova, Zh. Neorg. Khim., 26 (1981) 3308; Russ. J. Inorg. Chem., 26 (1981) 1774.
197 I.B. Baranovskii, S.S. Abdullaev, G. Ya. Mazo and R.N. Shchelokov, Zh. Neorg. Khim., 27 (1982) 536; Russ. J. Inorg. Chem., 27 (1982) 305.
198 I.B. Baranovskii, M.A. Golubnichaya, G. Ya. Mazo and R.N. Shchelokov, Zh. Neorg. Khim., 20 (1975) 844; Russ. J. Inorg. Chem., 20 (1975) 475.
199 L.M. Dikareva, M.A. Porai-Koshits, G.G. Sadikov, I.B. Baranovskii, M.A. Golubnichaya and R.N. Shchelokov, Zh. Neorg. Khim., 23 (1978) 1044; Russ. J. Inorg. Chem., 23 (1978) 578.
200 L.M. Dikareva, G.G. Sadikov, M.A. Porai-Koshits, M.A. Golubnichaya, I.B. Baranovskii and R.N. Shchelokov, Zh. Neorg. Khim., 22 (1977) 2013; Russ. J. Inorg. Chem., 22 (1977) 1093.

201 F.A. Cotton and T.R. Felthouse, Inorg. Chem., 21 (1982) 2667.
202 G. Li and Y. Sun, Huaxue Xuebao 39 (1981) 945, Chem. Abstr., 97 (1982) 102117P.
203 A.P. Kochetkova, L.B. Sveshnikova, V.M. Stepanovich and V.I. Sokol, Koord. Khim., 8 (1982) 529, Chem. Abstr., 96 (1982) 228000t.
204 R.S. Drago, J.R. Long and R. Cosmano, Inorg. Chem., 21 (1982) 2196.
205 A.M. Dennis, R.A. Howard, D. Lançon, K.M. Kadish and J.L. Bear, J. Chem. Soc., Chem. Commun., (1982) 399.
206 K.M. Kadish, D. Lançon, A.M. Dennis and J.L. Bear, Inorg. Chem., 21 (1982) 2987.
207 J. Duncan, T. Malinski, T.P. Zhu, Z.S. Hu, K.M. Kadish and J.L. Bear, J. Am. Chem. Soc., 104 (1982) 5507.
208 I.B. Baranovskii, S.S. Abdullaev, G. Ya. Mazo and R.N. Shchelekov, Zh. Neorg. Khim., 27 (1982) 536; Russ. J. Inorg. Chem., 27 (1982) 305.
209 L.M. Dikareva, G.G. Sadikov, M.A. Porai-Koshits, I.B. Baranovskii, S.S. Abdullaev and R.N. Shchelokov, Zh. Neorg. Khim., 27 (1982) 417; Russ. J. Inorg. Chem., 27 (1982) 236.
210 I.B. Baranovskii, Zh. Neorg. Khim., 27 (1982) 1347, Chem. Abstr., 97 (1982) 115413g.
211 T. Kametani, N. Kanaya, T. Mochizuki and T. Honda, Heterocycles, 19 (1982) 1023.